Study on performance of Cement Paste Backfill (CPB) with different binder under various situation

by

Yue Zhao

Thesis submitted in fulfilment of the requirement for the Degree of Doctor of Philosophy

The University of Adelaide

Faculty of Engineering, Computer and Mathematical Sciences

School of Civil, Environmental and Mining Engineering

January 2020

Table of Contents

Chapter 6— The influence of saturation condition on the strength of Cement Paste Backfill 143

Abstract

The mining process involves the removal and recovery of economically valuable minerals from the earth's crust. The resulting excavations are commonly revived by a process referred to as backfill. The fill performs as both a support system and a working platform; its different roles determine the requirements of its mechanical properties. Cemented Paste Backfill (CPB) is a high-density slurry composed of dewatered tailings, a cementitious binder and processed mine water, which is thickened to obtain a non-settling character for facile pumping into mined cavities resulted from underground mine operations. Over the past few decades, CPB technology has increasingly been used to revive mined cavities in underground mine operations, owing to its low operating cost. It minimises the adversities associated with tailings disposal, and it has higher mechanical performance compared with other backfilling methods. The present study intends to examine various factors influencing CPB mechanical and rheological properties to get a better understanding of backfill design.

The experimental program consisted of the combined capacity of ordinary Portland cement (PC), a newly developed slag-blended cement (Minecem, MC), the binder, and fly ash (FA), the additive, as a sustainable solution towards improving the mechanical performance of a copper-gold underground mine CPB system. A series of unconfined compression tests were carried out on various binder and binder + additive mix designs to evaluate the effect of binder and additive contents and curing time on strength, toughness and stiffness of the CPB system. For some PC + FA mix designs, the failure patterns of the tested samples were also investigated using the three-dimensional DIC technique. Furthermore, the rheological properties of CPB slurry are studied with different concentrations Minecem (MC), Portland cement (PC) and fly ash (FA), under various water and temperature condition using the same tailings material as well. A series of rheometer tests (for yield stress) were carried out on different MC + FA and PC + FA designs for evaluating the effects of binder and additive contents, as well as water content, water type and temperature on the rheological properties of CPB slurry.

After placing the CPB material in the stope, and during the setting and hardening processes, the weight of CPB stope applies an axial load over the CPB paste, from the upper layer to the bottom layer of the stope, may result in a consolidation of early-aged backfill material in the lower layers which is called self-consolidation. This self-applied load leads to the

strength of CPB specimens obtained by coring from in situ backfill stope are 50% to 200% higher than CPB specimens prepared by using conventional plastic molds over the same curing period. The present study intends to investigate the impact of axial applied stress (A_s) during curing, which represents the various self-consolidation condition, on the mechanical properties of CPB material. Also, the complicated underground situation may lead to delayed drainage or re-saturation by external water after backfilling. The unsaturated condition will happen due to the irrigation and drain down of backfill material over time. A series of triaxial compression test for CPB consist of MC only were carried out on various saturation condition and confining pressure to evaluate the effect of saturation condition on the mechanical properties of the CPB system.

Statement of Originality

I, **Yue Zhao**, certify that this work contains no material which has been accepted for the award of any other degree or diploma in my name in any university or other tertiary institution and, to the best of my knowledge and belief, contains no material previously published or written by another person, except where due reference has been made in the text. In addition, I certify that no part of this work will, in the future, be used in a submission in my name for any other degree or diploma in any university or other tertiary institution without the prior approval of the University of Adelaide and where applicable, any partner institution responsible for the joint award of this degree.

The author acknowledges that the copyright of published works contained within this thesis resides with the copyright holder(s) of those works.

I give permission for the digital version of my thesis to be made available on the web, via the University's digital research repository, the Library Search and also through web search engines, unless permission has been granted by the University to restrict access for a period of time.

Date: 10/01/2020

Yue Zhao

List of Publication

Zhao, Y., Soltani, A., Taheri, A., Karakus, M., & Deng, A. (2018). Application of Slag–Cement and Fly Ash for Strength Development in Cemented Paste Backfills. *Minerals*, *9*(1), 22. doi:10.3390/min9010022

Zhao, Y., Taheri, A., Soltani, A., Karakus, M., & Deng, A. (2019). Strength Development and Strain Localization Behaviour of Cemented Paste Backfills Using Portland Cement and Fly Ash. *Materials (Basel), 12*(20). doi:10.3390/ma12203282

Zhao, Y., Taheri, A., Karakus, M., Cheng, Z., & Deng, A. (2019). Effects of water content, water type and temperature on the rheological behaviour of Slag-Cement and Fly Ash-cement Paste backfill. *International Journal of Mining Science and Technology*. (Accepted)

Zhao, Y., Taheri, A., Karakus, M., & Deng, A. (2020). The effect of curing under applied stress on the strength of Cement Paste Backfill. *Journal of Rock Mechanics and Geotechnical Engineering*. (Submitted)

Zhao, Y., Taheri, A., Karakus, M., & Deng, A. (2020). The influence of saturation condition on the strength of Cement Paste Backfill. (Unpublished and Unsubmitted work in manuscript)

Acknowledgements

I gratefully acknowledge my supervisors Dr Abbas Taheri, A/Prof. Murat Karakus and Dr An Deng, of the School of Civil, Environmental and Mining Engineering. Their time, patience, guidance and continual support help me finish this thesis. Moreover, I am honoured to be supervised by them.

I would like to give my sincere thanks to Dr Zhongwei Cheng, the University of Queensland, and Dr Amin Soltani, The University of Melbourne, for their help and contribution to my scientific publications.

I would also like to thank our laboratory staffs of the School of Civil, Environmental and Mining Engineering, especially Mr Adam Ryntjes and Mr Simon Golding, for their great supports and help to this research.

Finally, I would like to thank my families and friends for their support and advice which motivated me and helped me to overcome obstacles.

Chapter 1— Thesis Overview

1. Background

Mine tailings, deposited after minerals been extracted, are the largest source of waste in mine processing. Approximately 14 billion tons of tailings were produced globally by the mining industry in 2010 (Jones and Boger 2012; Öhlander et al. 2012). Given the high-volume generation of tailings every year throughout the world, a significant concern hitherto has been the space required for storing and transporting these waste materials, and the resulting environmental hazards and costs (Öhlander et al. 2012, Aldhafeeri et al. 2016; Davies and Rice, 2001). Tailings have been traditionally deposited into tailings storage facilities such as embankments, dams and other types of surface impoundments (Xu et al. 2018). These conventional disposal methods, though commonly practised, are often associated with serious environmental, geotechnical (or structural failure) and economic concerns (Dold 2014; Franks et al. 2011; Liu et al. 2016).

The mining process involves the removal and recovery of economically valuable minerals from the earth's crust. The resulting excavations are commonly revived by a process referred to as backfilling (Kesimal et al. 2004 & 2005; Bloss 2014). Backfilling first provides ground support for the mine structures and mitigates the risk of surface subsidence associated with the underground stopes (Bloss 2014). Backfilling then replace the original supporting pillars, therefore, increase the ore dilution. It also provides a disposal site for waste rocks or milled tailings which are causing significant environmental problems including the formation of acid mine drainage and pollution of water, air and soil resources. Backfilling techniques can be categorised into three groups; namely, rock fills, hydraulic fills and paste fills, which can be implemented in cemented or uncemented forms (Sivakugan et al. 2015).

Cement Paste Backfill (CPB) is a relatively new backfilling method originating in the 1980s using a mixture of mine tailings, water and binder agents (mainly cement) to fill mined underground voids. Cement paste backfill (CPB) has increasingly been used to fill the mined cavities in underground mine operations, to re-use tailings in underground mines (Dold 2014; Franks et al. 2011; Liu et al. 2016; Kesimal et al. 2004). Cemented Paste Backfill recycles processed tailings into underground mined voids, which reduces the volume that needs to be surface-disposed. Using CPB thus mitigates the potential environmental impacts associated with tailings disposal and assists waste management (Kesimal et al. 2005; Bloss 2014;

Sivakugan et al. 2015). These refilled CPB can then performs as both the support system and working platform for further ore extraction.

CPB is a high-density slurry composed of dewatered tailings, a cementitious binder and processed mine water, which is thickened to obtain a non-settling character for facile pumping into mined cavities resulted from underground mine operations. The desired rheological behaviour, the non-settling character, often emerges at a solids content (by total mass) ranging between 70% and 85% (Sivakugan et al. 2015; Rankine and Sivakugan 2007; Orejarena and Fall 2010). CPB technology recycles tailings into underground mine excavations, and as such, reduces the volume of surface-disposed tailings, mitigates the burden on the environment, and assists waste management (Sivakugan 2006; Belem and Benzaazoua 2007; Huang et al. 2011; Zhang et al. 2018).

2. Research Gaps and Aims

Over the past few decades, CPB technology has been increasingly applied to reviving mined cavities in underground mine operations, owing to its low operating costs as well as its superior mechanical performance compared with other backfilling methods, i.e., rock fills and hydraulic fills. The following research gaps are identified in this research:

1. Strength performance of CPBs is governed by physicochemical and mineralogical properties of the tailings, chemical composition of the mixing water, binder type (and its content), the adopted mix design (or solids content), and in situ stress and curing conditions. Ordinary Portland cement is often implemented as the cementitious binder; its application for strength development of CPBs has been well documented in the literature. Some reports indicate that the cost of CPB implementation tends to vary from 10% to 20% of the mine's total operating cost, and the cementitious binder represents up to 75% of the total CPB cost. A review of the literature indicates in an attempt to minimise costs while maintaining the strength performance at its required level, the use of alternative binders and/or additives should be sought. Although the effects of these variables have been well understood and documented in the research literature, the reported results are still not consistent, as the physical properties, chemical composition and mineralogical background of the tailings often vary from mine to mine. In this thesis, a newly developed slag-blended cement referred to Mincem (MC) specifically developed for underground mine backfilling applications were introduced as well.

2. The complete stress-strain characteristics of CPB (for both pre-peak and post-peak stress-strain regimes) under uniaxial loading conditions with mapping the strain field development of the CPB specimen has not been done. Quite clearly, a comprehensive understanding of the strain localization behaviour of CPBs will be beneficial towards evaluating its damage evolution and failure mechanism under real-life loading regimes. To the authors' knowledge, no studies have been undertaken to investigate the strain localization behaviour of CPBs, and as such, further research is urgently required.

3. Other than basic mechanical performance of CPB, the pumpability and placement performance of fresh Cemented Paste Backfill (CPB) is an essential parameter in paste design. As after the mix of CPB slurry, fresh CPB is transported to underground voids by gravity or is pumped through pipelines and boreholes. Optimizing the CPB flowability in mines will help to behaviour the energy consumed by pumping, and reduce the risk of pipe clogging. Several studies have been conducted in past years to understand CPB's rheological behaviour better, and it is affecting factors. These studies show that the rheological behaviour is affected by external (e.g. temperature, time) and internal (e.g., cement content, the addition of slag, fly ash or superplasticizers, water type and content) factors. Although the effects of these variables have been widely documented in the literature, the reported results are not consistent as the physical, chemical and mineralogical properties of the tailings varies from mine to mine.

4. Furthermore, numerous researchers have indicated that laboratory studies using conventional molds, which are typically used to determine mine backfill design values, tend to underestimate the mechanical strength of a given CPB mixture when assessed over the same curing period as field-acquired data. Some studies show the laboratory-made CPB samples are underestimating 50% to 200% of the strength of CPB specimens obtained by coring from in situ backfill stope.

Self-weight consolidation of the backfill material after placement is one major factor which may contribute to the in situ strength of CPB. In an in situ condition, mine fills are on an enormous scale with at least 20m height. After placing the CPB material in the stope, and during the setting and hardening processes, the weight of CPB stope applies an axial load over the CPB paste, from the upper layer to the bottom layer of the stope, may result in a consolidation of early-aged backfill material in the lower layers. In this study, this consolidation is called self-consolidation. With the increase of backfill depth,

because of the weight of CPB in the stope, the lower layers of CPB are cured under pressure. In order to determine the effect of self-consolidation on the behaviour of backfill material, Belem et al. (2002) and Yilmaz et al. (2009) developed a system called CUAPS (Curing under Applied Pressure System). Using this system, the CPB samples in the lab were cured under specific applied pressures to imitate in situ curing conditions and a strength increase of 20% to 50% was found (Belem et al. 2002; Yilmaz et al. 2011 & 2015). However, the maximum applied pressure during curing was limited to 300 kPa (equivalent axial stress to 10 m CPB underground). Also, the passive lateral pressure that is applied to the CPB sample during curing has not been investigated in the literature. Moreover, previous studies on the under-pressure cured sample were only limited to uniaxial compressive testing. The behaviour of this material under confined loading has not been investigated before.

5. Finally, in realistic conditions, the drainage of initially saturated backfill and the interference of surrounding underground water may lead to the variation of backfill saturation condition. The mechanical properties of CPB varies under various saturation condition. Under the influence of cementitious binder, the hydraulic conductivity of CPB is highly time-dependent. The hydraulic conductivity decreases as the curing time increase, especially at early ages (0- 14 days) (Cao et al. 2018; Belem et al. 2002; El Mkadmi et al. 2014; Fall et al. 2009). It leads to massive difficulty on the study of CPB mechanical performance under different saturation as it is time-consuming to change the saturation condition of CPB as well. Hence the effect of saturation condition on the mechanical properties of CPB is limited in the literature.

Therefore, the following research aims are addressed in this thesis work:

1. To study the combined capacity of a newly developed slag-blended cement, the binder, and fly ash, the additive, as a sustainable solution towards improving the mechanical performance of CPB.

2. To investigate localized behaviour of CPB under uniaxial compression. It is aimed to visualize the effect of binder type, binder content and curing period on failure pattern and CPB strain field in the pre-peak and the post-peak stress-strain regimes.

3. To study the effects of water content, water type and temperature on the rheological behaviour of CPB.

4. To investigate the effect of curing under pressure on the mechanical behaviour of CPB under uniaxial and triaxial compressive loading. Behaviour of backfill material in terms of strength, deformability and ductility will be studied for the samples that undergo different curing period.

5. To investigate the influence of saturation condition on the mechanical performance of cement paste backfill under different loading conditions.

3. Thesis Layout

The present thesis consists of six chapters and is in the format of a thesis by publication. Chapter 1 presents an introduction of this research and including the background introduction, research gaps and research objectives and a conclusion of the present thesis. Chapter 2 to 6 include, five published and submitted journal papers which intended to address the five research gaps outlined in the previous section.

Chapter 2 contains a journal paper published in ***Minerals***. This paper presents the study investigates the combined capacity of a newly developed slag-blended cement (MC) and fly ash (FA) as a sustainable solution towards improving the mechanical performance of the cemented paste backfill (CPB) system of a copper-gold underground mine. A series of unconfined compression (UC) tests on various binder and binder + additive mix designs to evaluate the effect of binder and additive contents and curing time on strength, toughness and stiffness of the CPB system. Scanning electron microscopy (SEM) studies were also carried out to observe the evolution of fabric in response to MC and MC + FA amendments.

Chapter 3 contains a journal paper published in ***Materials***. This paper examines the combined performance of Portland cement (PC), the binder, and fly ash (FA), the additive, towards improving the mechanical performance of the South Australian copper-gold underground mine cemented paste backfill (CPB) system. A series of unconfined compressive strength (UCS) tests results on various PC + FA mix designs to evaluate the effects of binder and additive contents, as well as curing time, on the strength, stiffness and toughness of the CPB system. An accurate non-contact strain measurement scheme — using the three-dimensional digital image correlation (DIC) technique — was implemented to (i) measure the full-field of strain development on the surface of CPB samples, and (ii) characterize the deformations and strains of CPB samples with and without strain

localization. Making use of several virtual extensometers, the state of strain localization was also investigated in both the axial and lateral directions.

Chapter 4 contains a journal paper which is in the publication in the ***International Journal of Mining Science and Technology***. This paper presents an experimental study investigating the effects of binder type, content, water chemical properties and content, and temperature, on the rheological properties of CPB material prepared using the tailings of a copper mine in South Australia. A series of rheometer tests (for yield stress) were carried out on various MC + FA and PC + FA designs for evaluating the effects of binder and additive contents, as well as water content, water type and temperature on the rheological properties of CPB slurry. The coupled effect of binder type, water content, water type and temperature are discussed as well. The paper is accepted and is not in publication.

Chapter 5 contains a journal paper submitted to ***Journal of Rock Mechanics and Geotechnical Engendering***. This paper presents an experimental study of investigating the effects of axial applied stress (As) during curing, which represents the various self-consolidation condition and curing time on the mechanical properties of CPB material prepared using the tailings of a copper mine in South Australia and a newly released commercially manufactured cement called Minecem (MC). A novel curing under pressure equipment is designed and manufactured to cure CPB samples under pressure. The equipment is capable of applying and measuring axial load during curing and then measure the passive pressure that is applied laterally to the sample. Using this equipment, the samples were cured under different weights in environmentally-controlled curing room. A series of uniaxial and triaxial compression tests were carried out on various applied stress during curing and curing time to evaluate the effect of self-weight curing on pressure, curing time and confining pressure on the strength, brittleness and stiffness of the CPB system samples that are cured for a different period under different confining pressures.

Chapter 6 contains an ***Unsubmitted work write in manuscript style***. This manuscript presents an experimental study of investigating the influence of saturation condition on the mechanical performance of cement paste backfill under different loading condition. A series of confined compression tests for compacted CPB sample with different binder content and curing time and various unsaturated confined compression tests for compacted tailing material were carried out by providing four different matric suction using a back pressure shear box to study the effect of saturation condition on the strength of CPB.

4. Conclusions

The following general conclusions can be drawn from the present research work:

- As a result of MC inclusion and increase of curing period, the greater the MC content or, the longer the curing period, the higher the developed strength, toughness and stiffness, with the former, the MC content, portraying a more significant role. The exhibited improvements; however, were only notable up to 56 days of curing, beyond of which the effect of curing was found to be marginal. The axial strain at failure, an indication of the material's ductility, demonstrated a trend similar to that observed for the strength, toughness and stiffness; however, in an adverse manner. (see in Chapter 2)
- The use of FA alongside MC improved the bonding/connection interface generated between the tailings aggregates and thus led to improved mechanical performance compared with similar MC inclusions containing no FA. For any given MC content, the greater the FA content and/or the longer the curing period, the higher the developed strength, toughness and stiffness up to 56 days of curing, beyond of which the effect of curing was found to be marginal. Similarly, for any given FA content, an increase in MC content promoted higher mechanical properties. However, in all cases, the material's ductility was adversely affected by the MC + FA content and/or curing time. (see in Chapter 2)
- The performance of 4% PC was found to be similar to that of 1.5% MC, while the higher MC inclusions of 2.5% and 3%, though lower in terms of binder content, consistently outperformed 4% PC in terms of both strength and stiffness. As such, the newly introduced binder, MC, can be regarded as a sustainable alternative for conventional PC. (see in Chapter 2)
- As opposed to external measurement devices, the DIC technique was found to provide strain measurements free from bedding errors. The developed field of axial and lateral strains indicated that strain localization initiates in the pre-peak regime at around 80% of the UCS. The greater the PC (or PC + FA) content, and more importantly the longer the curing period, the closer the axial stress level required to initiate localization to the UCS, thus emulating the failure mechanism of quasi-brittle materials such as rock and concrete — the failure process changed from "multiple fractures parallel and perpendicular to the axial loading direction" to "sample disintegration" where a single major failure plane became noticeable. Finally, with an increase in curing time, the

difference between strain values at the localized and non-localized zones became less significant in the pre-peak regime and more pronounced in the post-peak regime. (see in Chapter 3)

- Regardless of binder type, the yield stress decreases with an increase in water content. However, the MC-CPB showed a more significant increase in fluidity after an increase in water content. Hence, the variations of MC-CPB viscosity appears to be more sensitive to water-content change. With regards to the UCS performance, the replacement of 4% PC-CPB (28 days UCS 425 kPa) to 3% MC-CPB (28 days UCS 519 kPa), reduced the slurry yield stress from 210.7 Pa to 178.5 Pa. (see in Chapter 4)
- Overall regardless of binder type, the yield stress increase with an increase in temperature; however, the increase in temperature influences the two components of CPB yield stress in different ways. The results indicate that the influence of temperature on yield stress for MC-CPB are much more sensitive than that for PC-CPB, while the water content is equal to or less than 23%. Thus, when using MC as an alternative for conventional PC, a better regulatory system might be required for both in situ water content and temperature condition. (see in Chapter 4)
- The introduce of applied axial pressure during curing improved the bonding/connection interface generated between the tailings aggregates, and thus led to improved mechanical performance compared with CPB inclusions with less or no applied axial pressure during curing. The greater applied axial pressure during curing, and the longer the curing period, the higher the developed strength, stiffness and toughness whit the CPB sample under both uniaxial and triaxial compression test. With regards to the UCS performance, A CPB sample that is cured under 3.6 MPa axial load for in 28 days curing, the difference of CPB at As = 0 (UCS 719.3 kPa) to CPB at As = 3.6 MPa (UCS 1862.1 kPa), is 390.7%demonstrates a UCS five times more than a sample that is cured under atmospheric curing condition. (see in Chapter 5)
- The passive lateral stress measures during curing by CPA apparatus were found at about 20% of the applied axial pressure during curing. The passive lateral stress that is measured with a newly developed equipment may represent the stress that is applied to the barricade in an underground mine. (see in Chapter 5)
- As the confining stress increases the maximum deviator stress increases regardless of the state of specimens. The greater the MC content and/or the longer the curing period, the higher the friction angle of failure envelope. However, the difference between the friction angles obtained from MC-treated mixtures is considerably small (4.4 °) compare

to the difference between the friction angles obtained from pure tailing specimen under various saturation condition (9.6 °). (see in Chapter 6)

- The tailing material shows a peak value followed by a softening behaviour at high matric suction and a strain hardening behaviour at zero matric suction. For any given applied confining pressure, the wetted pure tailings specimens had a lower peak deviator stress than dry specimens. The friction angles show a linear relationship concerning the matric suction. The increase in peak deviator stress shows a non-linear increment trend concerning the matric suction. (see in Chapter 6)

References

Aldhafeeri, Z., Fall, M., Pokharel, M., & Pouramini, Z. (2016). Temperature dependence of the reactivity of cemented paste backfill. *Applied Geochemistry, 72*, 10-19. doi:10.1016/j.apgeochem.2016.06.005

Belem, T., Benzaazoua, M., Bussière, B., Dagenais, A.-M. (2002). Effects of settlement and drainage on strength development within mine paste backfill. *Tailings and Mine Waste'02*, 27-30 January 2002, Fort Collins, Colorado, Balkema, Rotterdam, 139-148.

Belem, T., & Benzaazoua, M. (2007). Design and Application of Underground Mine Paste Backfill Technology. *Geotechnical and Geological Engineering, 26*(2), 175-175. doi:10.1007/s10706-007-9167-y

Bloss, M.L. (2014). An Operational Perspective of Mine Backfill. *In Proceedings of the 11th International Symposium on Mining with Backfill, Mine Fill 2014*, Australian Centre for Geomechanics, Perth, WA, Australia, 15–30.

Cao, S., Song, W., & Yilmaz, E. (2018). Influence of structural factors on uniaxial compressive strength of cemented tailings backfill. *Construction and Building Materials, 174*, 190-201. doi:10.1016/j.conbuildmat.2018.04.126

Davies, M.P., Rice, S. (2001). An alternative to conventional tailings management-dry-stack filtered tailings. *In Proceedings Tailings and Mine Waste '01*. Fort Collins, CO, USA, 16–19 January, 411-420.

Dold, B. (2014). Submarine Tailings Disposal (STD)—A Review. *Minerals, 4*(3), 642-666. doi:10.3390/min4030642

El Mkadmi, N., Aubertin, M., & Li, L. (2014). Effect of drainage and sequential filling on the behaviour of backfill in mine stopes. *Canadian Geotechnical Journal, 51*(1), 1-15. doi:10.1139/cgj-2012-0462

Fall, M., Adrien, D., Célestin, J. C., Pokharel, M., & Touré, M. (2009). Saturated hydraulic conductivity of cemented paste backfill. *Minerals Engineering, 22*(15), 1307-1317. doi:10.1016/j.mineng.2009.08.002

Franks, D. M., Boger, D. V., Côte, C. M., & Mulligan, D. R. (2011). Sustainable development principles for the disposal of mining and mineral processing wastes. *Resources Policy, 36*(2), 114-122. doi:10.1016/j.resourpol.2010.12.001

Huang, S., Xia, K., & Qiao, L. (2011). Dynamic tests of cemented paste backfill: effects of strain rate, curing time, and cement content on compressive strength. *Journal of Materials Science, 46*(15), 5165-5170. doi:10.1007/s10853-011-5449-0

Jones, H., & Boger, D. V. (2012). Sustainability and Waste Management in the Resource Industries. *Industrial & Engineering Chemistry Research, 51*(30), 10057-10065. doi:10.1021/ie202963z

Kesimal, A., Yilmaz, E., & Ercikdi, B. (2004). Evaluation of paste backfill mixtures consisting of sulphide-rich mill tailings and varying cement contents. *Cement and Concrete Research, 34*(10), 1817-1822. doi:10.1016/j.cemconres.2004.01.018

Kesimal, A., Yilmaz, E., Ercikdi, B., Alp, I., & Deveci, H. (2005). Effect of properties of tailings and binder on the short-and long-term strength and stability of cemented paste backfill. *Materials Letters, 59*(28), 3703-3709. doi:10.1016/j.matlet.2005.06.042

Liu, Q., Liu, D., Liu, X., Gao, F., & Li, S. (2016). Research and application of surface paste disposal for clay-sized tailings in tropical rainy climate. *International Journal of Mineral Processing, 157*, 227-235. doi:10.1016/j.minpro.2016.11.014

Öhlander, B., Chatwin, T., & Alakangas, L. (2012). Management of Sulfide-Bearing Waste, a Challenge for the Mining Industry. *Minerals, 2*(1), 1-10. doi:10.3390/min2010001

Orejarena, L., & Fall, M. (2010). The use of artificial neural networks to predict the effect of sulphate attack on the strength of cemented paste backfill. *Bulletin of Engineering Geology and the Environment, 69*(4), 659-670. doi:10.1007/s10064-010-0326-7

Rankine, R. M., & Sivakugan, N. (2007). Geotechnical properties of cemented paste backfill from Cannington Mine, Australia. Geotechnical and Geological Engineering, 25(4), 383-393. doi:10.1007/s10706-006-9104-5

Sivakugan, N., Rankine, R. M., Rankine, K. J., & Rankine, K. S. (2006). Geotechnical considerations in mine backfilling in Australia. *Journal of Cleaner Production, 14*(12-13), 1168-1175. doi:10.1016/j.jclepro.2004.06.007

Sivakugan, N., Veenstra, R., & Naguleswaran, N. (2015). Underground Mine Backfilling in Australia Using Paste Fills and Hydraulic Fills. *International Journal of Geosynthetics and Ground Engineering, 1*(2). doi:10.1007/s40891-015-0020-8

Xu, W., Cao, P., & Tian, M. (2018). Strength Development and Microstructure Evolution of Cemented Tailings Backfill Containing Different Binder Types and Contents. Minerals, 8(4). doi:10.3390/min8040167

Yilmaz, E., Belem, T., Bussière, B., & Benzaazoua, M. (2011). Relationships between microstructural properties and compressive strength of consolidated and unconsolidated cemented paste backfills. *Cement and Concrete Composites, 33*(6), 702-715. doi:10.1016/j.cemconcomp.2011.03.013

Yilmaz, E., Belem, T., Bussière, B., Mbonimpa, M., & Benzaazoua, M. (2015). Curing time effect on consolidation behaviour of cemented paste backfill containing different cement types and contents. *Construction and Building Materials, 75*, 99-111. doi:10.1016/j.conbuildmat.2014.11.008

Yilmaz, E., Benzaazoua, M., Belem, T., & Bussière, B. (2009). Effect of curing under pressure on compressive strength development of cemented paste backfill. *Minerals Engineering, 22*(9-10), 772-785. doi:10.1016/j.mineng.2009.02.002

Zhang, J., Deng, H., Taheri, A., Deng, J., & Ke, B. (2018). Effects of Superplasticizer on the Hydration, Consistency, and Strength Development of Cemented Paste Backfill. *Minerals, 8*(9), 381. doi:10.3390/min8090381

Chapter 2—Application of Slag-Cement and Fly Ash for Strength Development in Cemented Paste Backfills

Statement of Authorship

Yue Zhao[a] , Amin Soltani[b]*, Abbas Taheri [c]*, Murat Karakus[d] and An Deng[e]

[a] **PhD Student** - School of Civil, Environmental and Mining Engineering, The University of Adelaide, Adelaide 5005, Australia (Email: Yue.Zhao@adelaide.edu.au)

[b] **Research Fellow** - Geotechnical Engineering, Infrastructure Engineering, The University of Melbourne, Melbourne 3010, Australia (Email: amin.soltani@outlook.com.au)

[c] **Senior Lecturer** - School of Civil, Environmental and Mining Engineering, The University of Adelaide, Adelaide 5005, Australia (Email: Abbas.Taheri@adelaide.edu.au)

[d] **Associate Professor** - School of Civil, Environmental and Mining Engineering, The University of Adelaide, Adelaide 5005, Australia (Email: Murat.Karakus@adelaide.edu.au)

[e] **Senior Lecturer** - School of Civil, Environmental and Mining Engineering, The University of Adelaide, Adelaide 5005, Australia (Email: An.Deng@adelaide.edu.au)

***Correspondence:** Amin Soltani, Abbas Taheri

Publication Details:

Zhao, Y., Soltani, A., Taheri, A., Karakus, M., & Deng, A. (2018). Application of Slag–Cement and Fly Ash for Strength Development in Cemented Paste Backfills. *Minerals*, *9*(1), 22. doi:10.3390/min9010022

Statement of Authorship

Title of Paper	Application of Slag–Cement and Fly Ash for Strength Development in Cemented Paste Backfills
Publication Status	☑ Published ☐ Accepted for Publication ☐ Submitted for Publication ☐ Unpublished and Unsubmitted work written in manuscript style
Publication Details	Zhao, Y., Soltani, A., Taheri, A., Karakus, M., & Deng, A. (2018). Application of Slag–Cement and Fly Ash for Strength Development in Cemented Paste Backfills. *Minerals, 9*(1), 22. doi:10.3390/min9010022

Principal Author

Name of Principal Author (Candidate)	Yue Zhao		
Contribution to the Paper	Overall paper preparation		
Overall percentage (%)	60%		
Certification:	This paper reports on original research I conducted during the period of my Higher Degree by Research candidature and is not subject to any obligations or contractual agreements with a third party that would constrain its inclusion in this thesis. I am the primary author of this paper.		
Signature		Date	10/01/2020

Co-Author Contributions

By signing the Statement of Authorship, each author certifies that:

i. the candidate's stated contribution to the publication is accurate (as detailed above);

ii. permission is granted for the candidate in include the publication in the thesis; and

iii. the sum of all co-author contributions is equal to 100% less the candidate's stated contribution.

Name of Co-Author	Amin Soltani Research Fellow In Geotechnical Engineering, Infrastructure Engineering, The University of Melbourne		
Contribution to the Paper	Involved with analysis of results and writing up the original draft		
Signature		Date	07/01/2020

Name of Co-Author	Abbas Taheri Senior Lecturer, School of Civil, Environmental and Mining Engineering, The University of Adelaide		
Contribution to the Paper	Development of research idea, Supervised research, review and revision for the paper		
Signature		Date	06/01/2020

Name of Co-Author	Murat Karakus Associate Professor, School of Civil, Environmental and Mining Engineering, The University of Adelaide		
Contribution to the Paper	Development of research idea, Paper review and revision		
Signature		Date	06/01/2020

Name of Co-Author	An Deng Senior Lecturer, School of Civil, Environmental and Mining Engineering, The University of Adelaide		
Contribution to the Paper	Development of research idea, Paper review and revision		
Signature		Date	10/01/20

Please cut and paste additional co-author panels here as required.

Abstract

The present study investigates the combined capacity of a newly developed slag-blended cement (MC) and fly ash (FA) as a sustainable solution towards improving the mechanical performance of the cemented paste backfill (CPB) system of a copper-gold underground mine. A total of thirteen mix designs consisting of three MC-treated and ten MC + FA-treated blends were examined. Samples were prepared with a solids content of 77% (by total mass) and were allowed to cure for 7, 14, 28, 56 and 128 days prior to unconfined compression testing. Scanning electron microscopy (SEM) studies were also carried out to observe the evolution of fabric in response to MC and MC + FA amendments. The greater the MC content and/or the longer the curing period, the higher the developed strength, toughness and stiffness. The exhibited improvements, however, were only notable up to 56 days of curing, beyond which the effect of curing was marginal. The performance of 4% Portland cement or PC (by total dry mass) was found to be similar to that of 1.5% MC, while the higher MC inclusions of 2.5% and 3%, though lower in terms of binder content, unanimously outperformed 4% PC. The use of FA alongside MC improved the bonding/connection interface generated between the tailing aggregates and thus led to improved mechanical performance compared with similar MC inclusions containing no FA. Common strength criteria for CPBs were considered to assess the applicability of the newly introduced MC and MC + FA mix designs. The mix designs "3% MC" and "2.5% MC + 2–2.5% FA" satisfied the 700 kPa strength threshold required for stope stability, and thus were deemed as optimum design choices.

Keywords: cemented paste backfill; slag; fly ash; portland cement; unconfined compressive strength; stiffness; scanning electron microscopy

1. Introduction

Mine tailings, a by-product of the ore beneficiation process, are among the largest and most problematic sources of solid waste. Approximately 14 billion tons of tailings were produced globally by the mining industry in 2010 (Jones and Boger 2012). Given the high-volume generation of tailings every year throughout the world, a significant concern hitherto has been the space required for storing and transporting these waste materials, and the resulting environmental hazards and costs (Öhlander et al. 2012; Aldhafeeri et al. 2016). Tailings have been traditionally deposited into tailings storage facilities such as embankments, dams and other types of surface impoundments (Davies and Rice 2001; Xu et al. 2018). These conventional disposal methods, though commonly practised, are often associated with serious environmental, geotechnical (or structural failure) and economic concerns (Dold 2014; Franks et al. 2011; Liu et al. 2016).

The mining process involves the removal and recovery of economically valuable minerals from the earth's crust. The resulting excavations are commonly revived by a process referred to as backfilling (Kesimal et al. 2004 & 2005; Bloss 2014). The fill performs as both a support system and a working platform; its different roles determine the requirements of its mechanical properties. Backfilling techniques can be categorised into three groups, namely, rock fills, hydraulic fills and paste fills, which can be implemented in cemented or uncemented forms (Sivakugan et al. 2015). Cemented Paste Backfill (CPB) is a high-density slurry composed of dewatered tailings, a cementitious binder and processed mine water, which is thickened to obtain a non-settling character for facile pumping into mined cavities resulted from underground mine operations. The desired rheological behaviour, the non-settling character, often emerges at a solids content (by total mass) ranging between 70% and 85% (Sivakugan et al. 2015; Rankine and Sivakugan 2007; Orejarena and Fall 2010). CPB technology recycles tailings into underground mine excavations, and as such, reduces the volume of surface-disposed tailings, mitigates the burden on the environment, and assists waste management (Sivakugan et al. 2006; Belem and Benzaazoua 2007; Huang et al. 2011; Zhang et al. 2018).

Over the past few decades, CPB technology has been increasingly applied to reviving mined cavities in underground mine operations, owing to its low operating costs as well as its superior mechanical performance compared with other backfilling methods, i.e., rock fills and hydraulic fills (Brackebusch 1994; Landriault 1995; Fall et al. 2010; Ouattara et al.

2017). Strength performance of CPBs is governed by physicochemical and mineralogical properties of the tailings, chemical composition of the mixing water, binder type (and its content), the adopted mix design (or solids content), and in situ stress and curing conditions (Xu et al. 2018; Benzaazoua et al. 2004; Fall and Samb 2008; Taheri and Tatsuoka 2012 & 2015; Cao et al. 2018; Wu et al. 2018). Ordinary Portland cement is often implemented as the cementitious binder; its application for strength development of CPBs has been well documented in the literature. Some reports indicate that the cost of CPB implementation tends to vary from 10% to 20% of the mine's total operating cost, and the cementitious binder represents up to 75% of the total CPB cost (Bloss 2014). In an attempt to minimise costs while maintaining the strength performance at its required level, the use of alternative binders and/or additives should be sought. In this context, several studies have examined the efficiency of newly developed cement blends, fly ashes, nano-silica particles and superplasticizers (Xu et al. 2018; Zhang et al. 2018; Klein and Simon 2006; Mishra and Karanam 2006; Fall et al. 2007; Ercikdi et al. 2009; Koohestani et al. 2016). Though promising, the reported results are not consistent in defining an ad hoc alternative for Portland cement, and as such, further research is urgently required.

The present study examines the combined capacity of a newly developed slag-blended cement, the binder, and fly ash, the additive, as a sustainable solution towards improving the mechanical performance of a copper-gold underground mine CPB system. A series of unconfined compression tests were carried out on various binder and binder + additive mix designs to evaluate the effect of binder and/or additive contents and curing time on strength, toughness and stiffness of the CPB system. Additional tests were also carried out on samples prepared with ordinary Portland cement for comparison. Finally, scanning electron microscopy (SEM) studies were carried out to observe the evolution of fabric in response to the binder and binder + additive amendments.

2. Materials

2.1.Mine Tailings

A large quantity of processed tailings was sourced from a copper-gold underground mine and was used in the present study. The physical and mechanical properties of the tailings, determined as per relevant ASTM and Australian (AS) standards, are summarised in Table 1. The conventional grain-size analysis, carried out in accordance with ASTM D422–07, indicated a fines fraction (<75 μm) of 38.6%, along with 55.2% fine sand (0.075–0.425 mm)

and 6.2% medium sand (0.425–2 mm). The liquid limit and plasticity index were, respectively, measured as w_L = 19.2% and I_P = 6.1%, of which the fines fraction of the tailings was characterized as clay-silt with low plasticity (i.e., CL-ML) in accordance with the Unified Soil Classification System (USCS). The standard Proctor compaction test, carried out in accordance with ASTM D698–12, indicated an optimum water content of w_{opt} = 8.7% and a maximum dry unit weight of γ_{dmax} = 20.2 kN/m^3, which are both on par with that reported for natural CL-ML soils (Blotz et al. 1998; Nagaraj et al. 2015).

The chemical composition of the tailings, as supplied by the distributor, is provided in Table 2. The chemical composition is mainly dominated by silicon dioxide (SiO_2) and ferric oxide (Fe_2O_3), with mass fractions of 38.27% and 37.70%, respectively.

2.2.Binders and Additives

A commercially manufactured cementitious agent, commonly traded as Mine Cement in Australia (and hereafter referred to as MC), was used as the binder. MC is a slag-blended cement specifically developed for underground mine backfilling applications. The chemical composition of MC, as supplied by the manufacturer, consists of ground-granulated blast-furnace slag (50%), Portland cement clinker (20%), cement kiln dust (<15%), natural gypsum (5–7%), limestone (<7%), and other mineral additives (see Table 3). As stated by the manufacturer, an MC content of 3% (by total dry mass) is anticipated to satisfy common strength criteria for cemented paste backfills adopted in mining applications. Class C Fly Ash, hereafter referred to as FA, was adopted as the siliceous-aluminous (or pozzolan) additive to partially replace (by mass) the main cementitious binder (or MC).

2.3.Mine Water

A large quantity of processed mine water was sourced from the underground copper-gold mine and was used for the experimental program (see Section 3.1). The chemical composition of the processed mine water, as supplied by the distributor, is presented in Table 4. The pH was found to be 7.5, based on which the water was characterized as a neutral substance.

3. Experimental Program

3.1.Mix Designs and Sample Preparations

In this study, a total of thirteen mix designs consisting of three MC-treated and ten MC + FA-treated blends were examined (see Table 5). Hereafter, the following coding system is used to designate the various mix designs:

$$M_x F_y T_z \tag{1}$$

where M_x = x% MC; F_y = y% FA; and T_z = z days of curing.

The binder or binder + additive (MC or MC + FA), solids and water contents were, respectively, defined as:

$$B_c = \frac{m_B}{m_B + m_T} \times 100 \tag{2}$$

$$S_c = \frac{m_B + m_T}{m_B + m_T + m_W} \times 100 \tag{3}$$

$$W_c = \frac{m_W}{m_B + m_T} \times 100 \tag{4}$$

where B_c = binder or binder + additive content (in %); S_c = solids content (in %); W_c = water content (in %); m_B = mass of binder or binder + additive; m_T = mass of dry tailings; and m_W = mass of processed mine water.

The tailings and binder (or binder + additive) were mixed in dry form in accordance with the adopted MC and MC + FA contents summarised in Table 5. The required amount of processed mine water corresponding to a water content of W_c = 30% (or a solids content of S_c = 77%) was added to each blend, and thoroughly mixed by a mechanical mixer for approximately 5 minutes to obtain slurries of uniform consistency. The choice of W_c = 30% (or S_c = 77%) was selected as per the mine's requirements; this provides the rheological behaviour required to accommodate facile pumping of the paste into mined cavities. The resultant slurries were poured into cylindrical molds (measuring 42 mm in diameter and 100 mm in height) in one-third length increments, each layer being tamped approximately 25 times with a small metal rod to remove entrapped air. The molds were then transferred to a

humidity chamber, maintained at 70% relative humidity and a temperature of 25 ℃, where curing was allowed for periods of 7, 14, 28, 56 and 128 days. Upon demolding, the two ends of the samples were covered with a thin layer of dental paste, targeting surface homogeneity, and hence uniform load distribution, during unconfined compression testing (see Section 3.2).

3.2.Unconfined Compression Test

Unconfined compression (UC) tests were carried out in accordance with ASTM C39–18. The prepared samples (see Section 3.1) were axially compressed at a constant displacement rate of 0.1 mm/min. Axial strains and the corresponding axial stresses were recorded at various time intervals to a point at which the maximum axial stress required for sample failure, denoted as the peak UC strength, and its corresponding axial strain could be achieved. To ensure sufficient accuracy, triplicate samples were tested for each mix design and the median value was considered for further analyses. On account of the five curing times and the three replicates adopted, a total of 195 UC tests, i.e., 45 for MC and 150 for MC + FA, were conducted to address the thirteen mix designs outlined in Table 5. The standard deviation (SD) and the coefficient of variation (CV) for the triplicate peak UC strength data were found to range between SD = 2.0 kPa and 4.9 kPa, and CV = 0.4% and 0.8%, thus corroborating the sufficient accuracy and, hence, the repeatability of the adopted sample preparation technique and the implemented testing procedure.

3.3.Microstructure Analysis

Scanning electron microscopy (SEM) studies were carried out to investigate the evolution of fabric in response to MC and MC + FA amendments. The Philips XL20 scanning electron microscope (PHILIPS, Amsterdam, The Netherlands), with a resolution of 4 μm and a maximum magnification ratio of 50,000×, was employed for SEM imaging. A total of five mix designs consisting of $M_0F_0T_7$ (pure tailings), $M_{2.5}F_0T_7$, $M_{2.5}F_0T_{28}$, $M_{2.5}F_{1.5}T_7$ and $M_{2.5}F_{1.5}T_{28}$ were examined. The middle sections of the desired samples (prepared as per Section 3.1) were carefully fractured into small cubic–shaped pieces, measuring approximately 1 cm^3 in volume, as suggested in the literature (Estabragh et al. 2016; Soltani et al. 2018), and were further scanned over various magnification ratios ranging from 250× to 20,000×. The pure tailings sample (or $M_0F_0T_7$) was prepared in a similar fashion to that described for various MC and MC + FA blends (see Section 3.1). In this case, however, the

molded tailings slurry was allowed to desiccate under room temperature conditions (for 7 days) to gain rigidity for SEM testing.

4. Results and Discussions

4.1.Effect of MC on UC Strength

Stress-strain curves, obtained from the UC tests, for various MC-treated mixtures—$M_xF_yT_z$ where x = {1.5, 2.5, 3.0}, y = {0} and z = {7, 14, 28, 56, 128}—are provided in Figure A1 in the Appendix section. The stress-strain locus for all MC-treated mixtures exhibited a rise–fall behaviour with visually detectable peak points, thus signifying a strain-softening character accompanied by brittle sample failures. In general, the greater the MC content and/or the longer the curing period, the more pronounced the strain-softening effect, and hence, the more dramatic the sample failures.

Figure 1a illustrates the variations of peak UC strength against MC content for the samples tested at various curing times. At any given curing time, the greater the MC content the higher the peak UC strength, following a monotonically increasing trend. The sample $M_{1.5}F_0T_7$, for instance, exhibited a peak UC strength of q_u = 272.1 kPa, while the inclusion of M_c = 2.5% and 3%, with the same 7-day curing condition, resulted in q_u = 375.5 kPa and 476.5 kPa, respectively. Similarly, for any given MC content, an increase in curing time promoted a major increase in the peak UC strength up to T_c = 56 days, beyond of which the effect of curing was found to be rather marginal. The inclusion of 3% MC at T_c = 7 days, for instance, resulted in q_u = 476.5 kPa, while higher values of 619.5 kPa, 719.3 kPa, 800.6 kPa and 812.6 kPa were noted for the same 3% MC inclusion at 14, 28, 56 and 128 days of curing, respectively.

The axial strain at failure, denoted as ε_u, is an indication of the material's ductility, with higher values manifesting a more ductile/less brittle character (Estabragh et al. 2012; Soltani et al. 2017[b]). Figure 1b illustrates the variations of axial strain at failure against MC content for the samples tested at various curing times. The axial strain at failure demonstrated a trend similar to that observed for the peak UC strength; however, in an adverse manner. In general, the greater the MC content and/or the longer the curing period, the lower the sample's ductility. As typical cases, the samples $M_{1.5}F_0T_7$, $M_{1.5}F_0T_{128}$, $M_{3.0}F_0T_7$ and $M_{3.0}F_0T_{128}$ resulted in ε_u = 4.74%, 2.58%, 3.81% and 1.80%, respectively.

The area under a typical stress-strain curve up to the failure point, defined as peak strain energy (or energy adsorption capacity) and denoted as E_u, serves as a measure of the material's toughness (Maher and Ho 1994; Yadav and Tiwari 2018). Figure 2a illustrates the variations of peak strain energy against MC content for the samples tested at various curing times. The variations of peak strain energy followed a trend similar to that observed for the peak UC strength, thus indicating that the greater the MC content and/or the longer the curing period, the higher the sample's degree of toughness. An increase in peak strain energy signifies an increase in the peak UC strength and/or the axial strain at failure, thereby indicating a balance between the material's strength and ductility (Mirzababaei et al. 2013 & 2018; Soltani et al. 2019). As demonstrated in Figure 1b, the axial strain at failure was adversely affected by MC inclusion and/or curing time, and thus should lead to lower peak strain energy values. On the contrary, the peak UC strength was in favour of greater MC contents and/or longer curing times (see Figure 1a), which in turn should give rise to higher degrees of toughness. As such, the increase in peak strain energy, as demonstrated in Figure 2a, indicates that the improvement in q_u for all MC-treated mixtures outweighs the exhibited reduction in ε_u. As typical cases, the samples $M_{1.5}F_0T_7$, $M_{1.5}F_0T_{128}$, $M_{3.0}F_0T_7$ and $M_{3.0}F_0T_{128}$ resulted in E_u = 7.4 kJ/m^3, 12.3 kJ/m^3, 13.9 kJ/m^3 and 18.7 kJ/m^3, respectively.

The elastic stiffness modulus, defined as the secant modulus at 50% of the peak UC strength and denoted as E_{50} (Soltani et al. 2019; Taheri and Tani 2008), was also measured for various MC-treated mixtures, and the results are provided in Figure 2b. Similar to the peak UC strength and the peak strain energy, the development of stiffness was in favour of a greater MC content and/or a longer curing time. The samples $M_{1.5}F_0T_7$ and $M_{1.5}F_0T_{128}$, for instance, resulted in E_{50} = 17.7 MPa and 32.6 MPa, respectively. With the inclusion of 3% MC; however, higher values of 29.3 MPa and 74.6 MPa were observed at 7 and 128 days of curing, respectively.

Figures 3a and 3b illustrate the variations of E_u and E_{50} against q_u for various MC-treated mixtures, respectively. The variations of E_u lies within the $0.022q_u < E_u < 0.033q_u$ domain (E_u in kJ/m^3, and q_u in kPa). For E_{50}, however, a wider domain in the form of $0.056q_u < E_{50} < 0.092q_u$ (E_{50} in MPa, and q_u in kPa) can be observed. Both E_u and E_{50} exhibited good correlations with q_u. In this case, simple correlative models in the forms of $E_u = 0.025q_u$ (with R^2 = 0.742) and $E_{50} = 0.073q_u$ (with R^2 = 0.833) can be obtained, and hence implemented for indirect estimations.

Table 6 presents common strength criteria for cemented paste backfills adopted in mining applications. As is evident from the data outlined in Figure 1a, the peak UC strength for various MC-treated mixtures ranges between 272.1 kPa (for $M_{1.5}F_0T_7$) and 812.6 kPa (for $M_{3.0}F_0T_{128}$), and thus satisfies the requirement for eliminating liquefaction in underground disposal applications. However, none of the tested samples meets the prerequisite for roof support applications, i.e., $q_u > 4000$ kPa, and hence alternative mix designs should be sought. The inclusion of $M_c = 3\%$ resulted in $q_u = 719.3$ kPa at 28 days of curing, and thus satisfies the minimum 700 kPa threshold suggested for stope stability. With regard to surface disposal applications, all MC-treated mixtures, excluding $M_{1.5}F_0T_7$ and $M_{1.5}F_0T_{14}$, well meet the $q_u >$ 345 kPa criterion. Moreover, the ASTM D4609–08 standard suggests a minimum increase of 345 kPa in the peak UC strength as a criterion for characterizing an effective stabilization scheme for general/non-mining construction practices (Soltani et al. 2017[a]). Conservatively, assuming that the non-cemented tailings in high-moisture environments would have a low to negligible peak UC strength, all MC-treated mixtures, excluding $M_{1.5}F_0T_7$ and $M_{1.5}F_0T_{14}$, well meet with the aforementioned criterion and hence are deemed to be optimum design choices for general construction practices.

Portland Cement (PC) often serves as a benchmark binder with respect to underground mine backfilling applications. The performance of any newly introduced binder, such as MC, should hence be cross-checked with that of PC to further justify its applicability. In this regard, Figures 4a and 4b illustrate the variations of peak UC strength and elastic stiffness modulus against curing time for the samples treated with 1.5%, 2.5% and 3% MC alongside 4% PC, respectively. It should be noted that all PC-treated samples were prepared in a similar fashion to that described for various MC-treated blends (see Section 3.1). The performance of 4% PC was found to be on par with that of 1.5% MC, while the higher MC inclusions of 2.5% and 3% unanimously outperformed 4% PC in terms of both strength and stiffness. Interestingly, the effect of curing time, i.e., $T_c = 14$–56 days, was found to be rather marginal for PC-treated mixtures, while the development of strength and particularly stiffness were evidently monotonic for various MC-treated blends (compare the trendlines 3% MC and 4% PC in Figure 4). As a typical case, 4% PC resulted in $q_u = 352.8$ kPa ($E_{50} = 26.7$ MPa) at 28 days of curing, while the inclusion of $M_c = 1.5\%$, 2.5% and 3% (at $T_c = 28$ days), though lower in terms of binder content, resulted in similar to higher values of $q_u = 325.2$ kPa, 510.6 kPa and 719.3 kPa ($E_{50} = 27.6$ MPa, 37.8 MPa and 41.9 MPa), respectively.

4.2.Effect of MC + FA on UC Strength

Stress-strain curves, obtained from the UC tests, for various MC + FA-treated mixtures—$M_xF_yT_z$ where x = {1.5, 2.5}, y = {0.5, 1.0, 1.5, 2.0, 2.5}, and z = {7, 14, 28, 56, 128}—are provided in Figure A2 of the Appendix section. Similar to the mixtures treated with MC alone (see Figure A1), the stress-strain response for all MC + FA-treated mixtures exhibited a strain-softening behaviour with visually detectable peak points, thus indicating brittle sample failures. In general, for any given MC content, the greater the FA content and/or the longer the curing period, the more pronounced the strain-softening effect, with M_c = 2.5% displaying a more pronounced strain-softening character (and hence more dramatic sample failures) compared with similar cases treated with M_c = 1.5%.

Figure 5a,b illustrates the variations of peak UC strength against FA content for the samples treated with M_c = 1.5% and 2.5% and tested at various curing times, respectively. At any given curing time, the greater the FA content the higher the peak UC strength, following a monotonically increasing trend, with all M_c = 2.5% blends holding a notable advantage over their M_c = 1.5% counterparts. The samples $M_{1.5}F_0T_7$ and $M_{2.5}F_0T_7$, for instance, exhibited peak UC strengths of q_u = 272.1 kPa and 375.5 kPa, respectively. For M_c = 1.5% and the same 7-day curing condition, the inclusion of 0.5%, 1%, 1.5%, 2% and 2.5% FA resulted in q_u = 282.8 kPa, 292.8 kPa, 305.4 kPa, 313.9 kPa and 320.7 kPa, respectively. Similar mix designs treated with M_c = 2.5%, however, promoted a higher peak UC strength, as the aforementioned values increased to 384.4 kPa, 404.8 kPa, 425.1 kPa, 429.3 kPa and 429.6 kPa, respectively. Moreover, for any given MC+FA content, an increase in curing time promoted a significant increase in the peak UC strength up to T_c = 56 days, beyond which marginal improvements were noted. The inclusions of M_c = 2.5% and F_c = 1.5% at T_c = 7 days, for instance, resulted in q_u = 425.1 kPa, while higher values of 584.3 kPa, 653.6 kPa, 671.7 kPa and 695.1 kPa were obtained for the same MC + FA inclusion at 14, 28, 56 and 128 days of curing, respectively.

Figures 6a and 6b illustrate the variations of axial strain at failure against FA content for the samples treated with M_c = 1.5% and 2.5% and tested at various curing times, respectively. The axial strain at failure, an indication of the material's ductility, exhibited a trend similar to that observed for the peak UC strength; however, in an adverse manner. In general, the greater the FA content and/or the longer the curing period, the lower the sample's ductility, with all M_c = 1.5% blends holding a notable advantage over similar cases treated with M_c =

2.5%. The samples $M_{1.5}F_0T_7$ and $M_{2.5}F_0T_7$ displayed failure axial strains of ε_u = 4.74% and 3.14%, respectively. As typical cases, these values, respectively, dropped to 4.25% and 2.62% for $M_{1.5}F_{1.5}T_7$ and $M_{2.5}F_{1.5}T_7$, and 2.05% and 0.91% for $M_{1.5}F_{1.5}T_{128}$ and $M_{2.5}F_{1.5}T_{128}$.

The peak strain energy, a measure of the material's toughness, was also calculated for various MC + FA-treated mixtures, and the results are provided in Figure 7. Similar to the peak UC strength, the improvement in toughness was in favour of both the FA content and the curing time, with all M_c = 2.5% blends (see Figure 7b) holding a notable advantage over similar cases treated with M_c = 1.5% (see Figure 7a). As discussed in Section 4.1, the improvement in toughness with respect to an increase in binder content and/or curing time can be attributed to an increase in the peak UC strength and/or the axial strain at failure. The rise in peak strain energy, which, as demonstrated in Figure 7 was in favour of a greater MC + FA content and/or a longer curing period, indicates that the improvement in q_u dominates the exhibited reduction in ε_u for all MC + FA mix designs. The samples $M_{1.5}F_0T_7$ and $M_{2.5}F_0T_7$ resulted in peak strain energies of E_u = 7.4 kJ/m^3 and 10.1 kJ/m^3, respectively. As typical cases, these values, respectively, increased to 8.9 kJ/m^3 and 12.2 kJ/m^3 for $M_{1.5}F_{1.5}T_7$ and $M_{2.5}F_{1.5}T_7$, and 15.6 kJ/m^3 and 16.8 kJ/m^3 for $M_{1.5}F_{1.5}T_{128}$ and $M_{2.5}F_{1.5}T_{128}$.

Figures 8a and 8b illustrate the variations of elastic stiffness modulus E_{50} against FA content for the samples treated with M_c = 1.5% and 2.5% and tested at various curing times, respectively. In general, the elastic stiffness modulus demonstrated a trend similar to that observed for the peak UC strength and the peak strain energy. The greater the FA content and/or the longer the curing period, the higher the developed stiffness, with all M_c = 2.5% blends outperforming similar cases treated with M_c = 1.5%. The samples $M_{1.5}F_0T_7$ and $M_{2.5}F_0T_7$ resulted in E_{50} = 17.7 MPa and 25.1 MPa, respectively. As typical cases, these values, respectively, increased to 24.5 MPa and 28.4 MPa for $M_{1.5}F_{1.5}T_7$ and $M_{2.5}F_{1.5}T_7$, and 44.1 MPa and 66.4 MPa for $M_{1.5}F_{1.5}T_{128}$ and $M_{2.5}F_{1.5}T_{128}$.

Figure 9a,b illustrates the variations of E_u and E_{50} against q_u for various MC + FA-treated mixtures, respectively. The variations of E_u lies within the $0.027q_u < E_u < 0.039q_u$ and $0.021q_u < E_u < 0.030q_u$ domains (E_u in kJ/m^3, and q_u in kPa) for the samples treated with M_c = 1.5% and 2.5%, respectively. For E_{50}, however, wider domains in the forms of $0.056q_u < E_{50} < 0.111q_u$ and $0.064q_u < E_{50} < 0.095q_u$ (E_{50} in MPa, and q_u in kPa) can be observed, respectively. For any given MC content, the variations of E_u and E_{50} both exhibited good correlations with q_u. In this case, simple correlative models in the forms of $E_u = 0.033q_u$

(with $R^2 = 0.814$) and $E_{50} = 0.085q_u$ (with $R^2 = 0.641$) can be obtained for $M_c = 1.5\%$. For the samples treated with $M_c = 2.5\%$, the correlations changed to $E_u = 0.024q_u$ (with $R^2 = 0.708$) and $E_{50} = 0.078q_u$ (with $R^2 = 0.667$), which strongly indicate a lower rate of increase in both E_u and E_{50} with respect to an increase in q_u.

As is evident with the data outlined in Figure 5, the peak UC strength for various MC + FA-treated mixtures—$M_xF_yT_z$ where $x = \{1.5, 2.5\}$, $y = \{0.5, 1.0, 1.5, 2.0, 2.5\}$, and $z = \{7, 14, 28, 56, 128\}$—ranges between 282.8 kPa (for $M_{1.5}F_{0.5}T_7$) and 743.4 kPa (for $M_{2.5}F_{2.5}T_{128}$), and thus unanimously satisfies the requirement for eliminating liquefaction, i.e., $150 < q_u$ (kPa) < 300. Similar to the samples treated with MC alone, none of the tested MC + FA mix designs meet the prerequisite for roof support applications, i.e., $q_u > 4000$ kPa. With regard to stope stability, the samples $M_{2.5}F_{2.0}T_{28}$ ($q_u = 701.6$ kPa) and $M_{2.5}F_{2.5}T_{28}$ ($q_u = 714.4$ kPa) well comply with the minimum 700 kPa (at $T_c = 28$ days) requirement, and thus are deemed to be sustainable alternatives for $M_{3.0}F_0T_{28}$ ($q_u = 719.3$ kPa). As for surface disposal applications and general construction practices (ASTM D4609–08), all MC + FA-treated mixtures, excluding $M_{1.5}F_yT_7$ where $y = \{0.5, 1.0, 1.5, 2.0, 2.5\}$, well satisfy the $q_u > 345$ kPa criterion.

4.3.Amending Mechanisms and Fabric Evolution

In the presence of water, calcium-rich binders such as MC act as a precursor agent, initiating a series of short/immediate- and long-term chemical reactions in the tailings-binder medium, thereby amending the tailings fabric into a unitary mass of enhanced mechanical performance. Short-term chemical reactions include cation exchange and flocculation-agglomeration, the amending roles of which are often limited with respect to neutrally charged particles such as sands, silts and tailings. For fine-grained soils containing notable fractions of negatively charged clay particles; however, short-term reactions lead to notable improvements in soil plasticity, workability, early age strength and swell-consolidation capacity (Soltani et al. 2017[b]; Locat et al. 1990; Sivapullaiah et al. 1996; Mallela et al. 2004). Long-term chemical reactions consist of pozzolanic reactions, which are strongly time- and often temperature-dependent; their commencement and evolution require a specific and often long period of curing. During pozzolanic reactions, calcium cations (Ca^{2+}) and hydroxide anions (OH^-), both released from the cementitious binder, or in this case MC, gradually react with silicate (SiO_2) and aluminate (Al_2O_3) units from the tailings, thereby resulting in the formation of cementation products/gels, i.e., Calcium–Silicate–Hydrates (C–

S–H), Calcium–Aluminate–Hydrates (C–A–H) and Calcium–Aluminate–Silicate–Hydrates (C–A–S–H), which encourage solidification and flocculation of the tailings particles and hence the development of a uniform, dense matrix coupled with enhanced strength performance (Soltani et al. 2017[b]; Mallela et al. 2004; Sharma and Sivapullaiah 2016). Quite clearly, the commencement and evolution of pozzolanic reactions are strongly dependent on the amount of available silicate and aluminate units (or pozzolan materials) in the matrix. In general, the greater the number of available silicate and aluminate units, the greater the number of developed cementation products and hence the higher the developed peak UC strength.

As demonstrated in Figure 4, the performance of 4% PC was found to be on par with that of 1.5% MC, while the higher MC inclusions of 2.5% and 3% unanimously outperformed 4% PC in terms of both strength and stiffness. Such observations can be attributed to the more dominant self–hardening features exhibited by MC compared with that of PC. Calcium hydroxide or $Ca(OH)_2$ is a by-product of PC hydration during the pozzolanic reactions stage; however, it does not contribute to further strength development, owing to the lack of any remaining silicate and aluminate units in the medium which are normally exhausted during PC hydration. When slag-blended cement or MC is used as the main cementitious binder, the additional silicate and aluminate units in slag particles gradually react with $Ca(OH)_2$ and water, thereby resulting in the formation of additional cementation products as part of secondary pozzolanic reactions which further densify the matrix and hence enhance the peak UC strength.

Common fly ash additives, or in this case FA, often contain a low content of calcium oxide (CaO), and as such, possess limited self-hardening features; such additives require activation by a calcium-rich binder, e.g., PC or MC, to encourage pozzolanic reactions (Sharma and Sivapullaiah 2016). Unlike tailings, which are rather poor in terms of aluminate (see Table 2), FA is dominated by large fractions of silicate and, particularly, aluminate. As such, the addition of FA, alongside MC as its activator, induces the development of pozzolanic reactions (or cementation products) in the matrix, which in turn leads to an improved peak UC strength compared with similar MC inclusions containing no FA.

Figure 10a–c illustrates SEM micrographs for the samples $M_0F_0T_7$ (pure tailings), $M_{2.5}F_0T_7$ and $M_{2.5}F_0T_{28}$, respectively. The micro-fabric of the pure tailings sample displayed a partly loose matrix, along with a notable number of large inter- and intra-assemblage pore-spaces,

respectively, formed between and within the tailings aggregates, thereby corroborating the existence of an edge-to-edge dispersed structure (see Figure 10a). For the sample $M_{2.5}F_0T_7$, as shown in Figure 10b, the micro-fabric became more uniform in nature, indicating aggregation of the tailings particles and hence the development of a dense matrix with an edge-to-face flocculated structure. Prevalent cementation products, i.e., C–S–H, C–A–H and C–A–S–H, were clearly visible between and within the tailings aggregates, which portrayed a major role in reducing the number of inter- and intra-assemblage pore-spaces in the matrix. The same 2.5% MC inclusion at 28 days of curing (or sample $M_{2.5}F_0T_{28}$) exhibited a micro-fabric similar to that observed for $M_{2.5}F_0T_7$ (compare Figures 10b and 10c). In this case, however, a more pronounced cementation bonding was evident, which in turn promoted a slightly denser matrix with fewer pore-spaces followed by a higher developed strength and stiffness, i.e., the peak UC strength increased from 375.5 kPa for $M_{2.5}F_0T_7$ to 510.6 kPa for $M_{2.5}F_0T_{28}$. SEM micrographs for the samples $M_{2.5}F_{1.5}T_7$ and $M_{2.5}F_{1.5}T_{28}$ are provided in Figure 10d,e, respectively. In general, the samples $M_{2.5}F_{1.5}T_7$ and $M_{2.5}F_{1.5}T_{28}$ displayed micro-fabric features similar to that observed for their $F_c = 0$ counterparts, i.e., $M_{2.5}F_0T_7$ and $M_{2.5}F_0T_{28}$. However, as a result of FA inclusion, the bonding/connection interface generated between the tailings aggregates was markedly improved. Moreover, the inter- and intra-assemblage pore-spaces displayed a notable decrease in both number and size, which all in all justify the increase in strength and stiffness compared with similar cases containing no FA, e.g., the peak UC strength increased from 510.6 kPa for $M_{2.5}F_0T_{28}$ to 653.6 kPa for $M_{2.5}F_{1.5}T_{28}$.

5. Conclusions

The following conclusions can be drawn from this study:

- The greater the MC content and/or the longer the curing period, the higher the developed strength, toughness and stiffness, with the former, the MC content, portraying a more significant role. The exhibited improvements; however, were only notable up to 56 days of curing, beyond of which the effect of curing was found to be marginal. The axial strain at failure, an indication of the material's ductility, demonstrated a trend similar to that observed for the strength, toughness and stiffness; however, in an adverse manner.
- The performance of 4% PC was found to be similar to that of 1.5% MC, while the higher MC inclusions of 2.5% and 3%, though lower in terms of binder content, consistently

outperformed 4% PC in terms of both strength and stiffness. As such, the newly introduced binder, MC, can be regarded as a sustainable alternative for conventional PC.

- The use of FA alongside MC improved the bonding/connection interface generated between the tailings aggregates, and thus led to improved mechanical performance compared with similar MC inclusions containing no FA. For any given MC content, the greater the FA content and/or the longer the curing period, the higher the developed strength, toughness and stiffness up to 56 days of curing, beyond of which the effect of curing was found to be marginal. Similarly, for any given FA content, an increase in MC content promoted higher mechanical properties. However, in all cases, the material's ductility was adversely affected by the MC + FA content and/or curing time.
- Common strength criteria for cemented paste backfills were considered to assess the applicability of the newly introduced MC and MC + FA mix designs. With regard to stope stability, for instance, the mix designs $M_{3.0}F_0T_{28}$, $M_{2.5}F_{2.0}T_{28}$ and $M_{2.5}F_{2.5}T_{28}$ satisfied the minimum 700 kPa threshold, and thus were deemed as optimum design choices.

References

Aldhafeeri, Z., Fall, M., Pokharel, M., & Pouramini, Z. (2016). Temperature dependence of the reactivity of cemented paste backfill. *Applied Geochemistry, 72*, 10-19. doi:10.1016/j.apgeochem.2016.06.005

Belem, T., & Benzaazoua, M. (2007). Design and Application of Underground Mine Paste Backfill Technology. *Geotechnical and Geological Engineering, 26*(2), 147-174. doi:10.1007/s10706-007-9154-3

Benzaazoua, M., Fall, M., & Belem, T. (2004). A contribution to understanding the hardening process of cemented pastefill. *Minerals Engineering, 17*(2), 141-152. doi:10.1016/j.mineng.2003.10.022

Bloss, M.L. (2014). An Operational Perspective of Mine Backfill. *In Proceedings of the 11th International Symposium on Mining with Backfill, Mine Fill 2014*, Australian Centre for Geomechanics, Perth, WA, Australia, 15–30.

Blotz, L. R., Benson, C. H., & Boutwell, G. P. (1998). Estimating optimum water content and maximum dry unit weight for compacted clays. *Journal of Geotechnical & Geoenvironmental Engineering*, *124*(9), 907. doi:10.1061/(ASCE)1090-0241(1998)124:9(907).

Brackebusch, F.W. (1994). Basics of paste backfill systems. *Mining Engineering*, 46(1), 1175–1178. doi:10.1016/0148-9062(95)90153-V

Cao, S., Yilmaz, E., & Song, W. (2018). Evaluation of Viscosity, Strength and Microstructural Properties of Cemented Tailings Backfill. *Minerals*, *8*(8). doi:10.3390/min8080352

Davies, M.P., & Rice, S. (2001). An alternative to conventional tailings management-dry-stack fi ltered tailings. *In Proceedings Tailings and Mine Waste '01*. Fort Collins, CO, USA, 16–19 January, 411-420.

Dold, B. (2014). Submarine Tailings Disposal (STD)—A Review. *Minerals, 4*(3), 642-666. doi:10.3390/min4030642

Ercikdi, B., Kesimal, A., Cihangir, F., Deveci, H., & Alp, İ. (2009). Cemented paste backfill of sulphide-rich tailings: Importance of binder type and dosage. *Cement and Concrete Composites, 31*(4), 268-274. doi:10.1016/j.cemconcomp.2009.01.008

Estabragh, A. R., Khatibi, M., & Javadi, A. A. (2016). Effect of Cement on Treatment of a Clay Soil Contaminated with Glycerol. *Journal of Materials in Civil Engineering, 28*(4). doi:10.1061/(asce)mt.1943-5533.0001443

Estabragh, A.R., Namdar, P., & Javadi, A.A. (2012). Behaviour of cement–stabilized clay reinforced with nylon fiber. *Geosynthetics International*. 19(85).

Fall, M., & Samb, S. S. (2008). Pore structure of cemented tailings materials under natural or accidental thermal loads. *Materials Characterization, 59*(5), 598-605. doi:10.1016/j.matchar.2007.05.003

Fall, M., Belem, T., Samb, S., & Benzaazoua, M. (2007). Experimental characterization of the stress–strain behaviour of cemented paste backfill in compression. *Journal of Materials Science, 42*(11), 3914-3922. doi:10.1007/s10853-006-0403-2

Fall, M., Célestin, J. C., Pokharel, M., & Touré, M. (2010). A contribution to understanding the effects of curing temperature on the mechanical properties of mine cemented tailings backfill. *Engineering Geology, 114*(3-4), 397-413. doi:10.1016/j.enggeo.2010.05.016

Franks, D. M., Boger, D. V., Côte, C. M., & Mulligan, D. R. (2011). Sustainable development principles for the disposal of mining and mineral processing wastes. *Resources Policy, 36*(2), 114-122. doi:10.1016/j.resourpol.2010.12.001

Grice, T. (1998). Underground Mining with Backfill. *In Proceedings of 2nd Annual Summit — Mine Tailings Disposal Systems*, Australasian Institute of Mining and Metallurgy: Carlton, Victoria, Australia, 234–239.

Huang, S., Xia, K., & Qiao, L. (2011). Dynamic tests of cemented paste backfill: effects of strain rate, curing time, and cement content on compressive strength. *Journal of Materials Science, 46*(15), 5165-5170. doi:10.1007/s10853-011-5449-0

Jewell, R. J., & Fourie, A. B. (2002). *Paste and Thickened Tailings — A Guide*, 1st ed. Australian Centre for Geomechanics: Perth, Western Australia, Australia, 103–126.

Jones, H., & Boger, D. V. (2012). Sustainability and Waste Management in the Resource Industries. *Industrial & Engineering Chemistry Research, 51*(30), 10057-10065. doi:10.1021/ie202963z

Kesimal, A., Yilmaz, E., & Ercikdi, B. (2004). Evaluation of paste backfill mixtures consisting of sulphide-rich mill tailings and varying cement contents. *Cement and Concrete Research, 34*(10), 1817-1822. doi:10.1016/j.cemconres.2004.01.018

Kesimal, A., Yilmaz, E., Ercikdi, B., Alp, I., & Deveci, H. (2005). Effect of properties of tailings and binder on the short-and long-term strength and stability of cemented paste backfill. *Materials Letters, 59*(28), 3703-3709. doi:10.1016/j.matlet.2005.06.042

Klein, K., & Simon, D. (2006). Effect of specimen composition on the strength development in cemented paste backfill. *Canadian Geotechnical Journal, 43*(3), 310-324. doi:10.1139/t06-005

Koohestani, B., Belem, T., Koubaa, A., & Bussière, B. (2016). Experimental investigation into the compressive strength development of cemented paste backfill containing Nano-silica. *Cement and Concrete Composites, 72*, 180-189. doi:10.1016/j.cemconcomp.2016.06.016

Landriault, D. (1995). Paste Backfill Mix Design for Canadian Underground Hard Rock Mining. *In Proceedings of the 97th Annual General Meeting of the CIM Rock Mechanics and Strata Control Session*, Canadian Institute of Mining, Metallurgy and Petroleum, Montreal, QC, Canada, 652–663.

Liu, Q., Liu, D., Liu, X., Gao, F., & Li, S. (2016). Research and application of surface paste disposal for clay-sized tailings in tropical rainy climate. *International Journal of Mineral Processing, 157*, 227-235. doi:10.1016/j.minpro.2016.11.014

Locat, J., Bérubé, M.-A., & Choquette, M. (1990). Laboratory investigations on the lime stabilization of sensitive clays: shear strength development. *Canadian Geotechnical Journal, 27*(3), 294-304. doi:10.1139/t90-040

Maher, A., & Ho, Y. C. (1994). Mechanical properties of kaolinite/fiber soil composite. *Journal of Geotechnical Engineering, 120*(8), 1381-1393. doi:10.1061/(ASCE)0733-9410(1994)120:8(1381)

Mallela, J., Von Quintus, H., & Smith, K.L. (2004). Consideration of Lime–Stabilized Layers in Mechanistic–Empirical Pavement Design, The National Lime Association: Arlington, VA, USA. Available online: http://lime.org/documents/other/MechEmpPavement.pdf (accessed on 2 December 2018).

Mirzababaei, M., Arulrajah, A., Horpibulsuk, S., Soltani, A., & Khayat, N. (2018). Stabilization of soft clay using short fibers and poly vinyl alcohol. *Geotextiles and Geomembranes, 46*(5), 646-655. doi:10.1016/j.geotexmem.2018.05.001

Mirzababaei, M., Miraftab, M., Mohamed, M., & McMahon, P. (2013). Unconfined Compression Strength of Reinforced Clays with Carpet Waste Fibers. *Journal of Geotechnical and Geoenvironmental Engineering, 139*(3), 483-493. doi:10.1061/(asce)gt.1943-5606.0000792

Mishra, M. K., & Karanam, U. M. R. (2006). Geotechnical characterization of fly ash composites for backfilling mine voids. *Geotechnical and Geological Engineering, 24*(6), 1749-1765. doi:10.1007/s10706-006-6805-8

Nagaraj, H. B., Reesha, B., Sravan, M. V., & Suresh, M. R. (2015). Correlation of compaction characteristics of natural soils with modified plastic limit. *Transportation Geotechnics, 2*, 65-77. doi:10.1016/j.trgeo.2014.09.002

Öhlander, B., Chatwin, T., & Alakangas, L. (2012). Management of Sulfide-Bearing Waste, a Challenge for the Mining Industry. *Minerals, 2*(1), 1-10. doi:10.3390/min2010001

Orejarena, L., & Fall, M. (2010). The use of artificial neural networks to predict the effect of sulphate attack on the strength of cemented paste backfill. *Bulletin of Engineering Geology and the Environment, 69*(4), 659-670. doi:10.1007/s10064-010-0326-7

Ouattara, D., Yahia, A., Mbonimpa, M., & Belem, T. (2017). Effects of superplasticizer on rheological properties of cemented paste backfills. International Journal of Mineral Processing, 161, 28-40. doi:10.1016/j.minpro.2017.02.003

Rankine, R. M., & Sivakugan, N. (2007). Geotechnical properties of cemented paste backfill from Cannington Mine, Australia. *Geotechnical and Geological Engineering, 25*(4), 383-393. doi:10.1007/s10706-006-9104-5

Sharma, A. K., & Sivapullaiah, P. V. (2016). Ground granulated blast furnace slag amended fly ash as an expansive soil stabilizer. *Soils and Foundations, 56*(2), 205-212. doi:10.1016/j.sandf.2016.02.004

Sivakugan, N., Rankine, R. M., Rankine, K. J., & Rankine, K. S. (2006). Geotechnical considerations in mine backfilling in Australia. *Journal of Cleaner Production, 14*(12-13), 1168-1175. doi:10.1016/j.jclepro.2004.06.007

Sivakugan, N., Veenstra, R., & Naguleswaran, N. (2015). Underground Mine Backfilling in Australia Using Paste Fills and Hydraulic Fills. *International Journal of Geosynthetics and Ground Engineering, 1*(2). doi:10.1007/s40891-015-0020-8

Sivapullaiah, P.V., Prashanth, J.P., & Sridharan, A. (1996). Effect of fly ash on the index properties of black cotton soil. *Soils Found*, 36, 97–103, doi:10.3208/sandf.36.97.

Soltani, A., Deng, A., Taheri, A., & Mirzababaei, M. (2017[a]). A sulphonated oil for stabilisation of expansive soils. *International Journal of Pavement Engineering, 20*(11), 1285-1298. doi:10.1080/10298436.2017.1408270

Soltani, A., Deng, A., Taheri, A., & Mirzababaei, M. (2018). Rubber powder–polymer combined stabilization of South Australian expansive soils. *Geosynthetics International, 25*(3), 304-321. doi:10.1680/jgein.18.00009

Soltani, A., Deng, A., Taheri, A., & Sridharan, A. (2019). Swell–Shrink–Consolidation Behaviour of Rubber–Reinforced Expansive Soils. *Geotechnical Testing Journal, 42*(3). doi:10.1520/gtj20170313

Soltani, A., Taheri, A., Khatibi, M., & Estabragh, A. R. (2017[b]). Swelling Potential of a Stabilized Expansive Soil: A Comparative Experimental Study. *Geotechnical and Geological Engineering, 35*(4), 1717-1744. doi:10.1007/s10706-017-0204-1

Taheri, A., & Tani, K. (2008). Use of down-hole triaxial apparatus to estimate the mechanical properties of heterogeneous mudstone. *International Journal of Rock Mechanics and Mining Sciences, 45*(8), 1390-1402. doi:10.1016/j.ijrmms.2008.01.017

Taheri, A., & Tatsuoka, F. (2012). Stress-strain relations of cement–mixed gravelly soil from multiple–step triaxial compression test results. *Soils Found*, 52, 748–766, doi:10.1016/j.sandf.2012.07.014

Taheri, A., & Tatsuoka, F. (2015). Small- and large-strain behaviour of a cement-treated soil during various loading histories and testing conditions. *Acta Geotech*, 10, 131–155, doi:10.1007/s11440-014-0339-7

Tariq, A. (2012). Synergistic and Environmental Benefits of Using Cement Kiln Dust with Slag and Fly Ash in Cemented Paste Tailings. PhD, The University of Western Ontario, London, Ontario, Canada, Available online: http://ir.lib.uwo.ca/etd/560 (accessed on 22 October 2018).

United States Environmental Protection Agency (USEPA). (1986). *Handbook for Stabilization/Solidification of Hazardous Waste*, Report EPA/540/2-86/001, Hazardous Waste Engineering Research Laboratory: Cincinnati, Ohio, USA.

Wu, J., Feng, M., Chen, Z., Mao, X., Han, G., & Wang, Y. (2018). Particle Size Distribution Effects on the Strength Characteristic of Cemented Paste Backfill. *Minerals, 8*(8). doi:10.3390/min8080322

Xu, W., Cao, P., & Tian, M. (2018). Strength Development and Microstructure Evolution of Cemented Tailings Backfill Containing Different Binder Types and Contents. Minerals, 8(4). doi:10.3390/min8040167

Yadav, J.S., & Tiwari, S.K. (2018). Evaluation of the strength characteristics of cement–stabilized clay–crumb rubber mixtures for its sustainable use in geotechnical applications. *Environ. Dev. Sustain*, 20 (5), 1961–1985, doi:10.1007/s10668-017-9972-2.

Zhang, J., Deng, H., Taheri, A., Deng, J., & Ke, B. (2018). Effects of Superplasticizer on the Hydration, Consistency, and Strength Development of Cemented Paste Backfill. *Minerals, 8*(9), 381. doi:10.3390/min8090381

List of Tables

Table 1. Physical and mechanical properties of the used tailings.

Properties	Value	Standard Designation
Specific gravity, G_s	2.4	ASTM D854–14
Natural water content, w_N (%)	40.2	ASTM D2216–10
Fines [<75 μm] (%)	38.6	ASTM D422–07
Fine sand [0.075–0.425 mm] (%)	55.2	ASTM D422–07
Medium sand [0.425–2 mm] (%)	6.2	ASTM D422–07
Coarse sand [2–4.75 mm] (%)	0	ASTM D422–07
Liquid limit, w_L (%)	19.2	AS 1289.3.9.1–15
Plastic limit, w_P (%)	13.1	AS 1289.3.2.1–09
Plasticity index, I_P (%)	6.1	AS 1289.3.3.1–09
USCS classification	CL–ML	ASTM D2487–11
Optimum water content, w_{opt} (%)	8.7	ASTM D698–12
Maximum dry unit weight, γ_{dmax} (kN/m^3)	20.2	ASTM D698–12
Unconfined compressive strength, q_u (kPa) [1]	143.6	ASTM D2166–16

[1] Tested at standard Proctor optimum condition.

Table 2. Chemical composition of the used tailings.

Component	SiO_2	Fe_2O_3	Al_2O_3	K_2O	CaO	MgO	TiO_2	Na_2O	Other
Mass percentage (%)	38.27	37.70	7.19	2.33	0.81	0.75	0.56	0.07	12.32

Table 3. Chemical composition of MC (as supplied by the manufacturer).

Component	Mass Percentage (%)
Ground–granulated blast–furnace slag	50
Portland cement clinker	20
Cement kiln dust	<15
Natural gypsum	5–7
Chloride, Cl^-	<8
Limestone	<7
Sulphur trioxide, SO_3	<4
Crystalline silica	<1

Table 4. Chemical composition of the processed mine water (as supplied by the distributor).

Component	CL^-	SO_4^{2-}	NO_3^-	Na^+	Ca^{2+}	K^+	Mg^{2+}
Value (mg/L)	5800	2400	6	3800	480	380	280

Table 5. Mix designs and their properties.

Designation	MC Content, M_c (%)	FA Content, F_c (%)	Solids Content, S_c (%)	Water Content, W_c (%)
$M_{1.5}F_0T_{7,14,28,56,128}$	1.5	0	77	30
$M_{2.5}F_0T_{7,14,28,56,128}$	2.5	0	77	30
$M_{3.0}F_0T_{7,14,28,56,128}$	3.0 [1]	0	77	30
$M_{1.5}F_{0.5}T_{7,14,28,56,128}$	1.5	0.5	77	30
$M_{1.5}F_{1.0}T_{7,14,28,56,128}$	1.5	1.0	77	30
$M_{1.5}F_{1.5}T_{7,14,28,56,128}$	1.5	1.5	77	30
$M_{1.5}F_{2.0}T_{7,14,28,56,128}$	1.5	2.0	77	30
$M_{1.5}F_{2.5}T_{7,14,28,56,128}$	1.5	2.5	77	30
$M_{2.5}F_{0.5}T_{7,14,28,56,128}$	2.5	0.5	77	30
$M_{2.5}F_{1.0}T_{7,14,28,56,128}$	2.5	1.0	77	30
$M_{2.5}F_{1.5}T_{7,14,28,56,128}$	2.5	1.5	77	30
$M_{2.5}F_{2.0}T_{7,14,28,56,128}$	2.5	2.0	77	30
$M_{2.5}F_{2.5}T_{7,14,28,56,128}$	2.5	2.5	77	30

[1] Manufacturer–recommended content.

Table 6. Common strength criteria for cemented paste backfills adopted in mining applications.

Application	Peak UC Strength, q_u (kPa)	Reference
Roof support	>4000	[Grice 1998; Tariq 2012]
Stope stability	700–2000 (at T_c = 28 days)	[Brackebusch 1994]
Surface disposal	>345	[USEPA 1986]
Eliminating liquefaction	150–300	[Tariq 2012; Jewell and Fourie 2002]

List of Figures

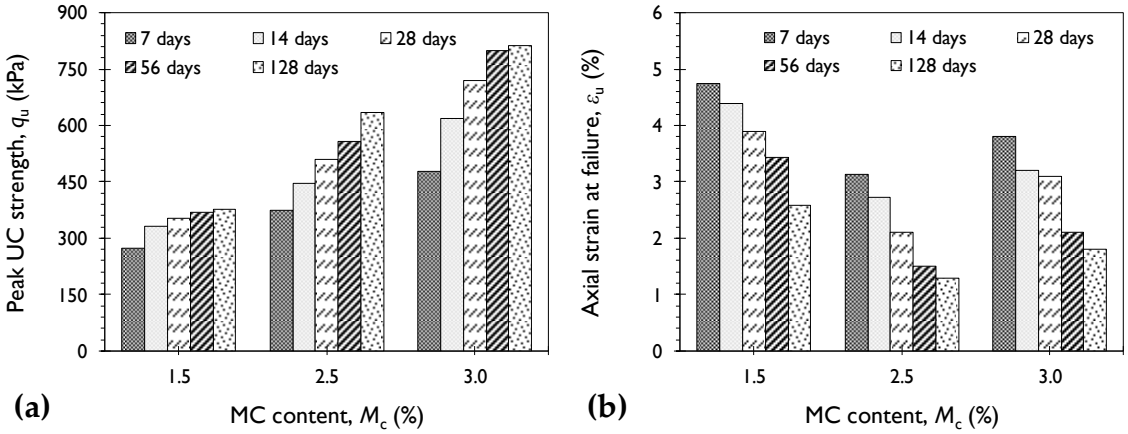

Figure 1. Variations of (a) peak UC strength q_u and (b) axial strain at failure ε_u against MC content for the samples tested at various curing times (i.e., $M_xF_yT_z$ where x = {1.5, 2.5, 3.0}, y = {0}, and z = {7, 14, 28, 56, 128}).

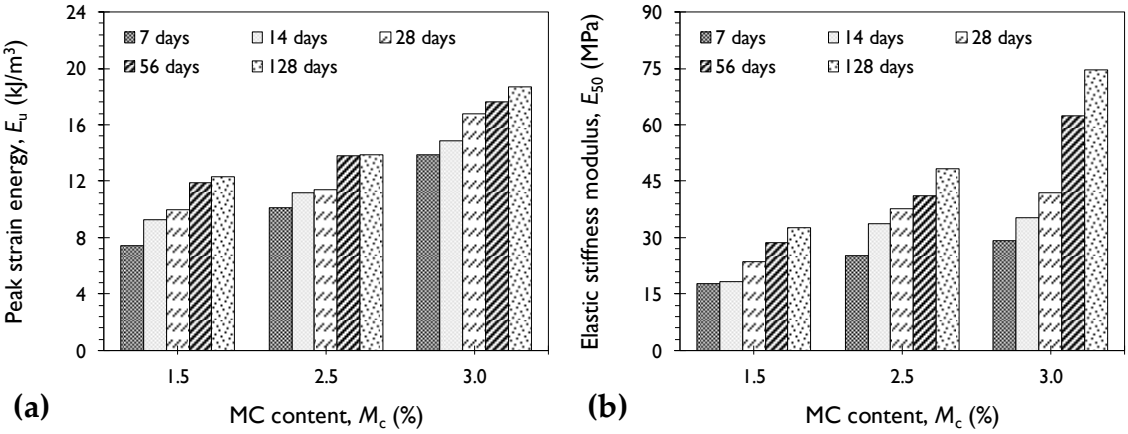

Figure 2. Variations of (a) peak strain energy E_u and (b) elastic stiffness modulus E_{50} against MC content for the samples tested at various curing times (i.e., $M_xF_yT_z$ where x = {1.5, 2.5, 3.0}, y = {0}, and z = {7, 14, 28, 56, 128}).

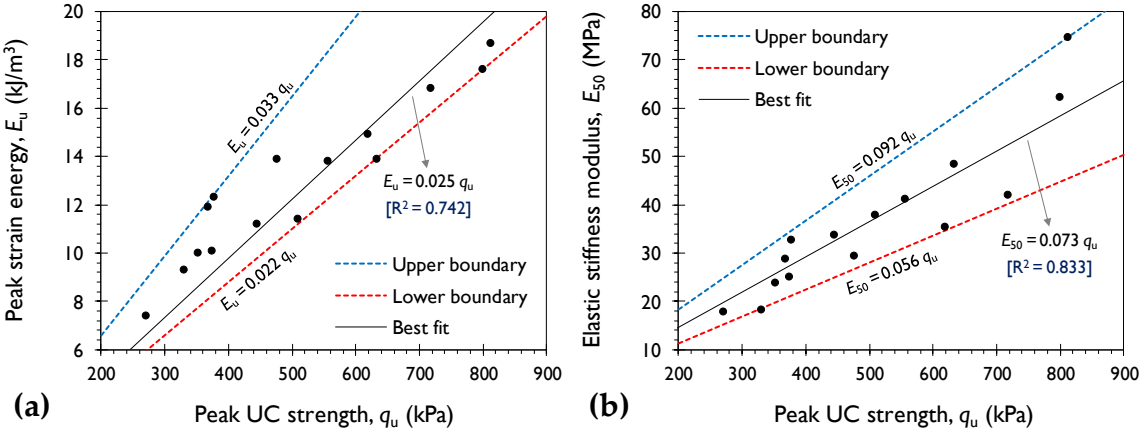

Figure 3. Variations of (a) peak strain energy E_u and (b) elastic stiffness modulus E_{50} against peak UC strength q_u for various MC-treated mixtures (i.e., $M_xF_yT_z$ where x = {1.5, 2.5, 3.0}, y = {0}, and z = {7, 14, 28, 56, 128}).

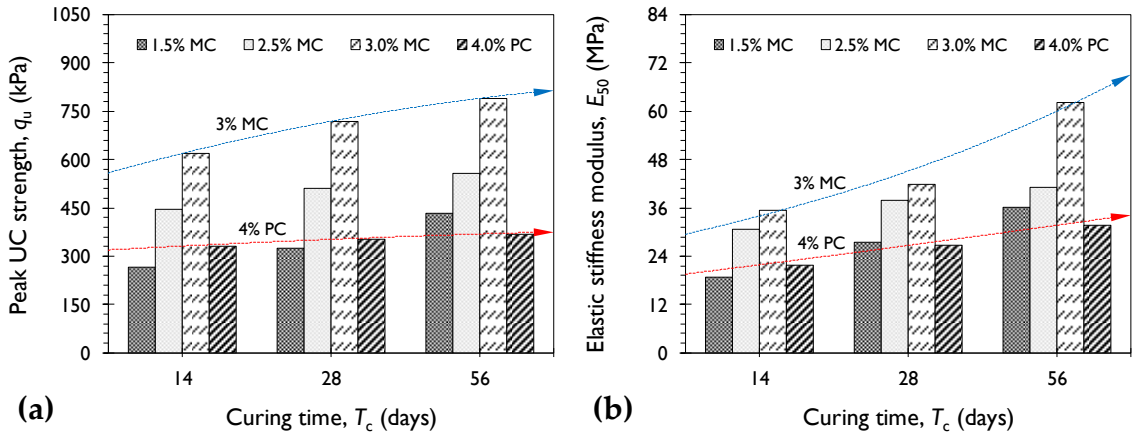

Figure 4. Variations of (a) peak UC strength q_u and (b) elastic stiffness modulus E_{50} against curing time for the samples treated with 1.5%, 2.5% and 3% MC and 4% PC.

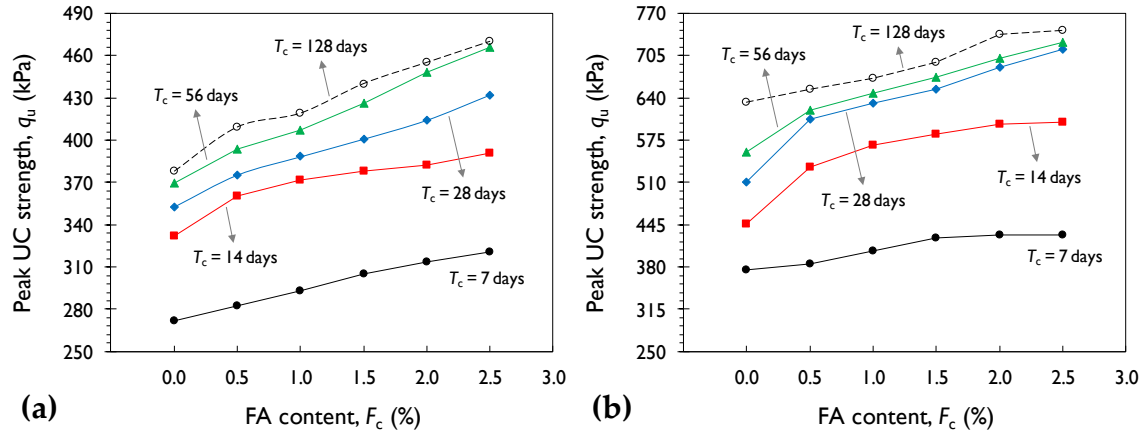

Figure 5. Variations of peak UC strength q_u against FA content for the samples tested at various curing times: (a) $M_{1.5}F_yT_z$; (b) $M_{2.5}F_yT_z$ (y = {0, 0.5, 1.0, 1.5, 2.0, 2.5}, and z = {7, 14, 28, 56, 128}).

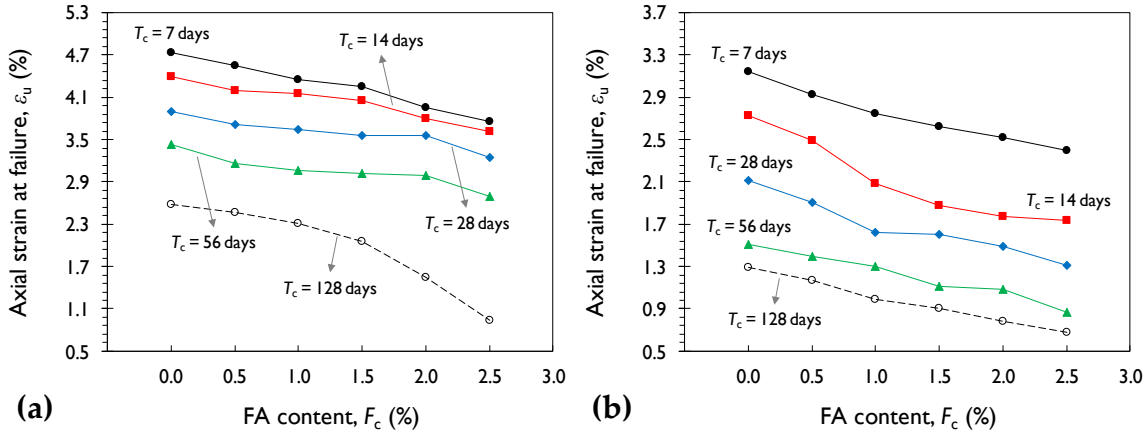

Figure 6. Variations of axial strain at failure ε_u against FA content for the samples tested at various curing times: (a) $M_{1.5}F_yT_z$; (b) $M_{2.5}F_yT_z$ (y = {0, 0.5, 1.0, 1.5, 2.0, 2.5}, and z = {7, 14, 28, 56, 128}).

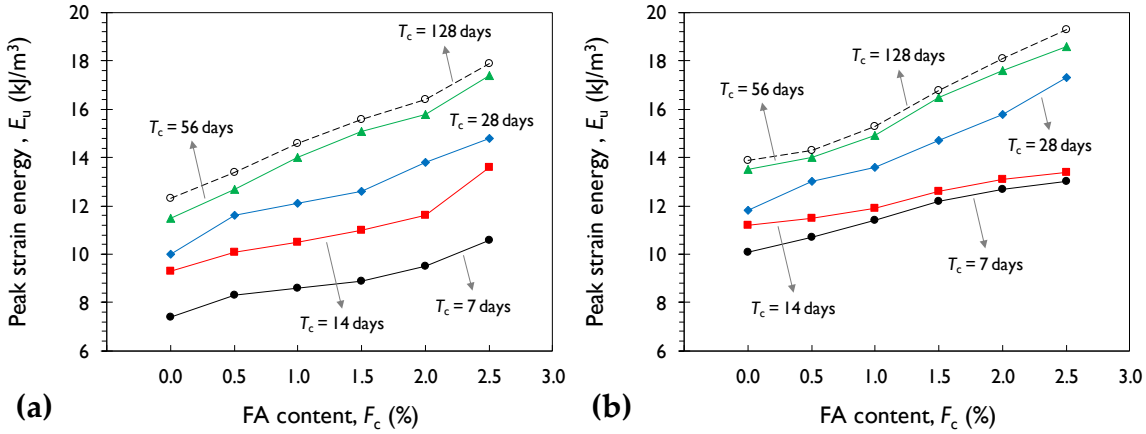

Figure 7. Variations of peak strain energy E_u against FA content for the samples tested at various curing times: (a) $M_{1.5}F_yT_z$; (b) $M_{2.5}F_yT_z$ (y = {0, 0.5, 1.0, 1.5, 2.0, 2.5}, and z = {7, 14, 28, 56, 128}).

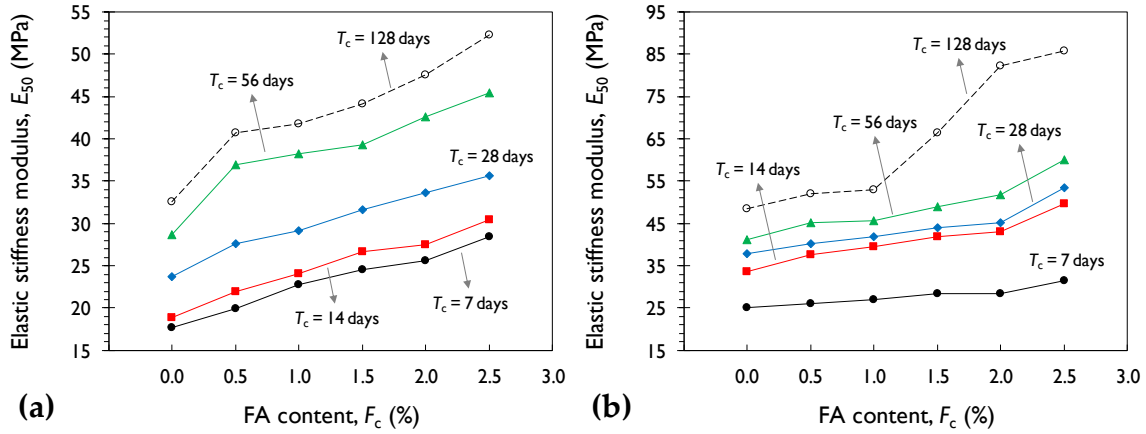

Figure 8. Variations of elastic stiffness modulus E_{50} against FA content for the samples tested at various curing times: (a) $M_{1.5}F_yT_z$; (b) $M_{2.5}F_yT_z$ (y = {0, 0.5, 1.0, 1.5, 2.0, 2.5}, and z = {7, 14, 28, 56, 128}).

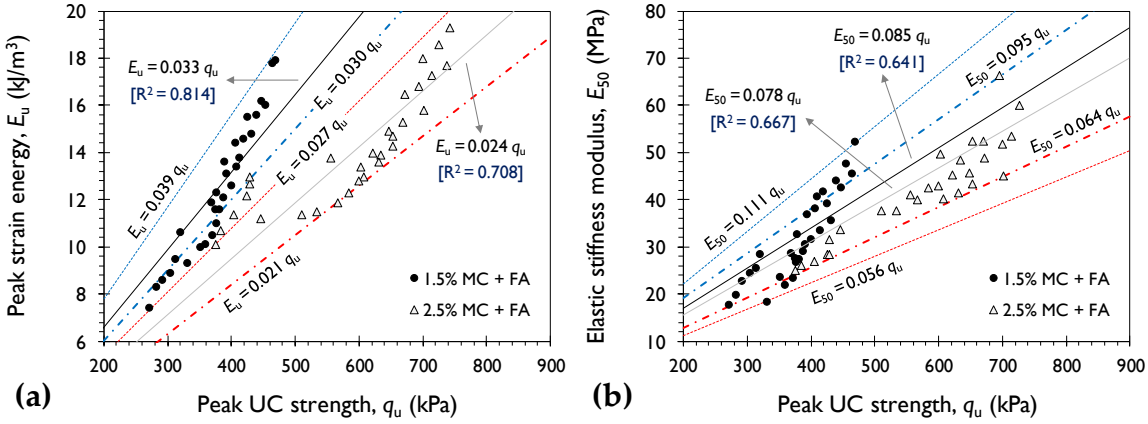

Figure 9. Variations of (a) peak strain energy E_u and (b) elastic stiffness modulus E_{50} against peak UC strength q_u for various MC + FA-treated mixtures (i.e., $M_xF_yT_z$ where x = {1.5, 2.5}, y = {0, 0.5, 1.0, 1.5, 2.0, 2.5}, and z = {7, 14, 28, 56, 128}).

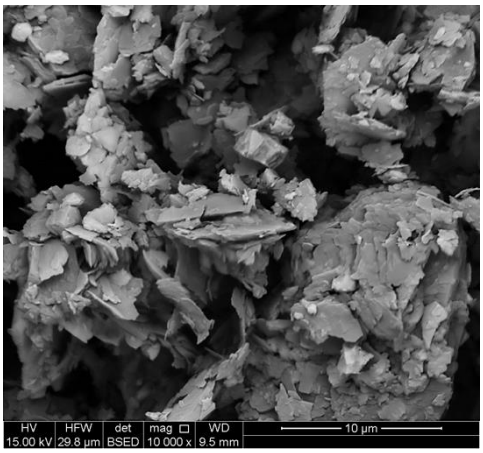

(**a**)

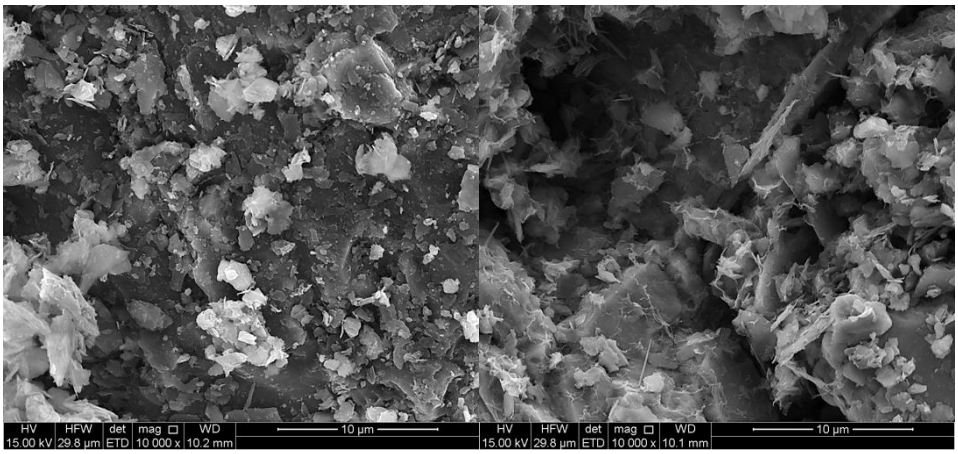

(**b**) (**c**)

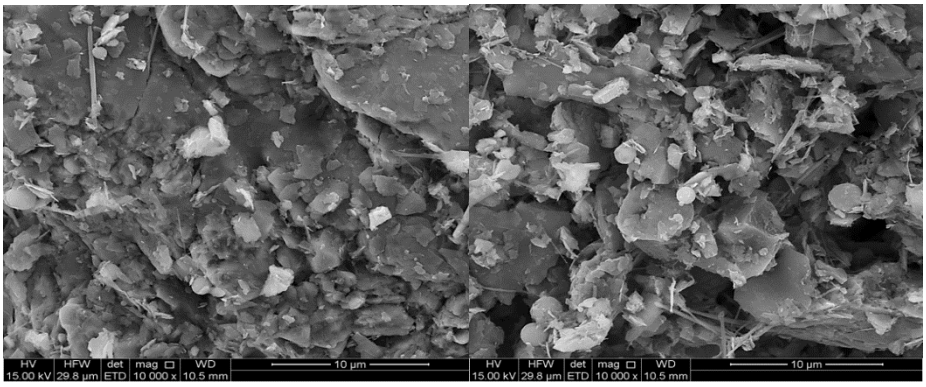

(**d**) (**e**)

Figure 10. SEM micrographs for the tested samples: (a) $M_0F_0T_7$ (pure tailings); (b) $M_{2.5}F_0T_7$; (c) $M_{2.5}F_0T_{28}$; (d) $M_{2.5}F_{1.5}T_7$; (e) $M_{2.5}F_{1.5}T_{28}$.

Appendix

Stress–strain curves, obtained from the UC tests, for various MC-treated mixtures—$M_xF_yT_z$ where x = {1.5, 2.5, 3.0}, y = {0}, and z = {7, 14, 28, 56, 128}—are provided in Figure A1.

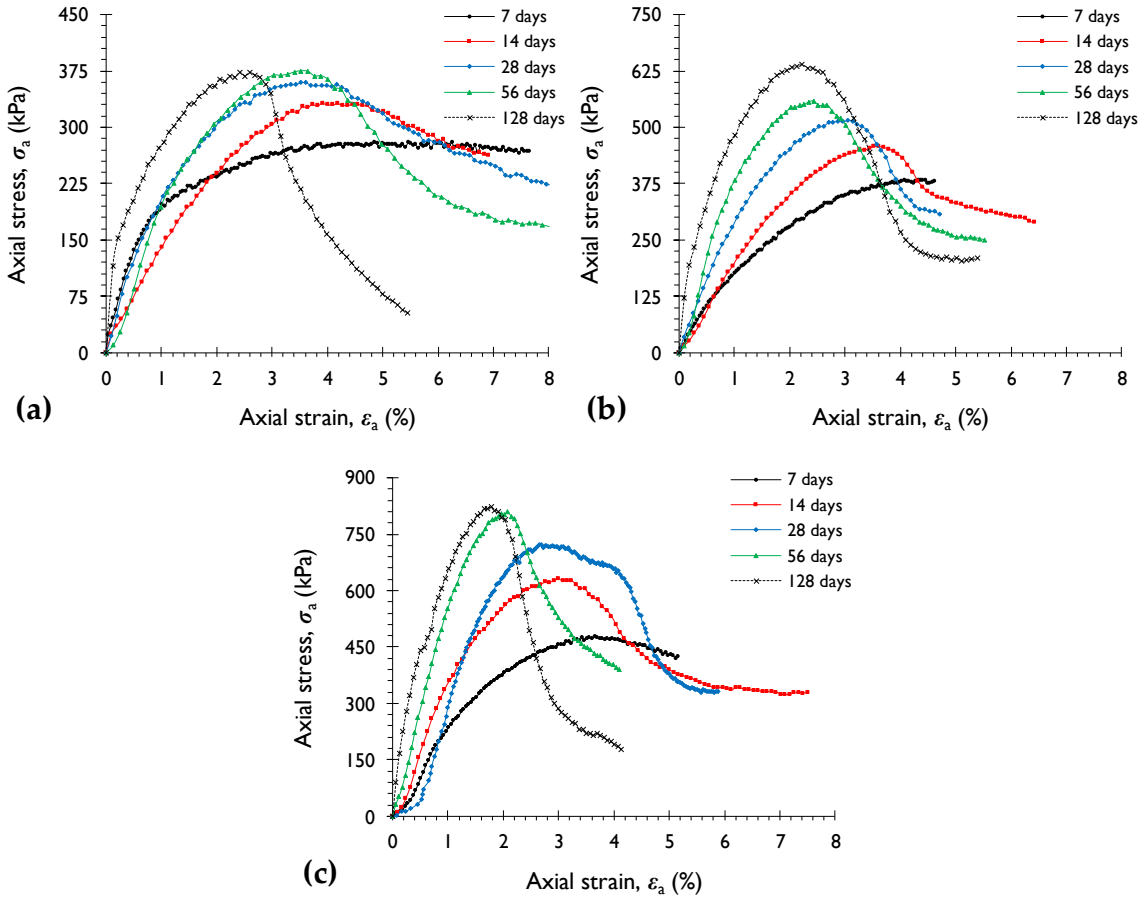

Figure A1. UC stress–strain curves for various MC-treated mixtures: (a) $M_{1.5}F_0T_z$; (b) $M_{2.5}F_0T_z$; (c) $M_{3.0}F_0T_z$ (z = {7, 14, 28, 56, 128}).

Stress–strain curves, obtained from the UC tests, for various MC + FA-treated mixtures—$M_xF_yT_z$ where x = {1.5, 2.5}, y = {0.5, 1.0, 1.5, 2.0, 2.5}, and z = {7, 14, 28, 56, 128}—are provided in Figure A2.

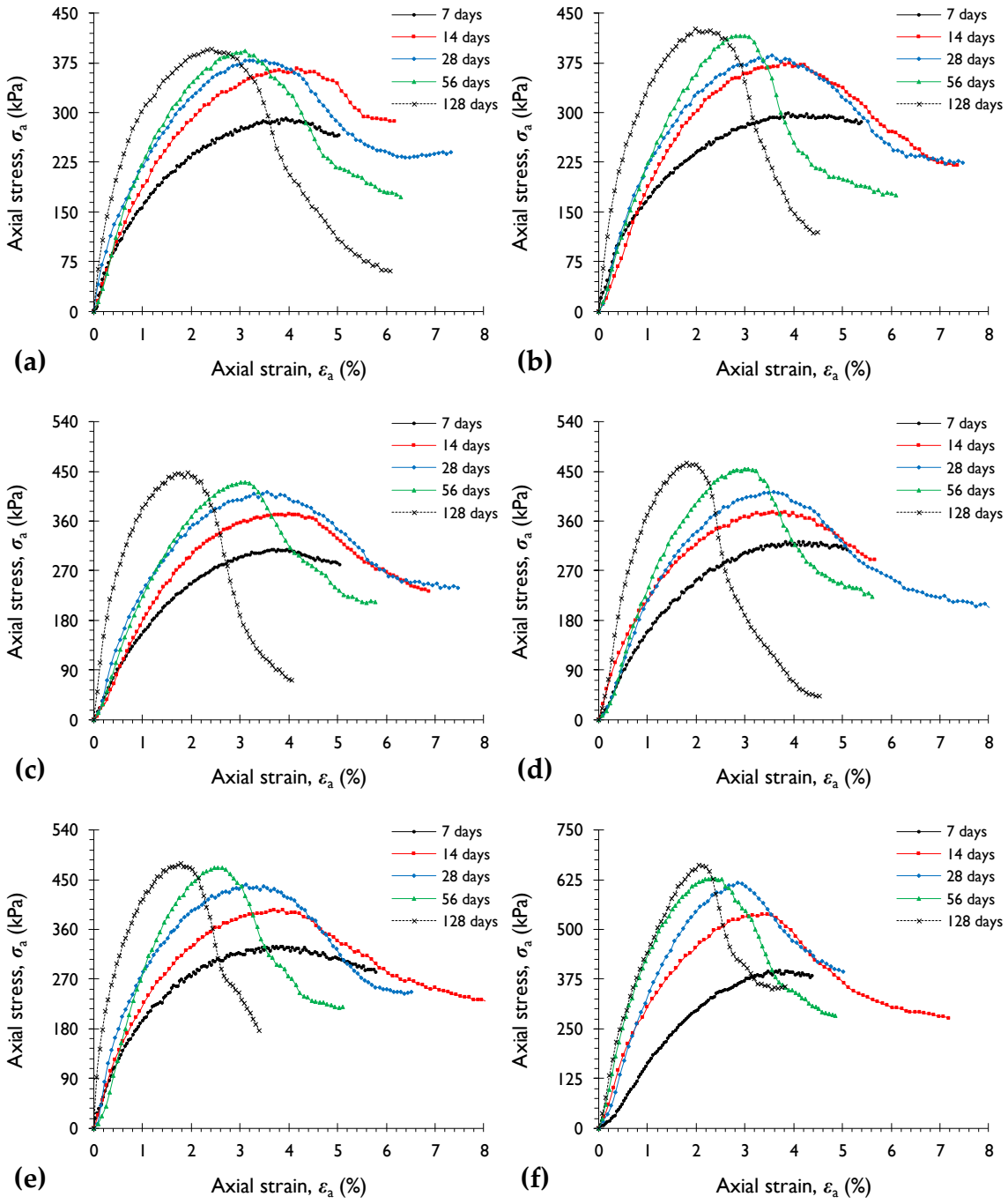

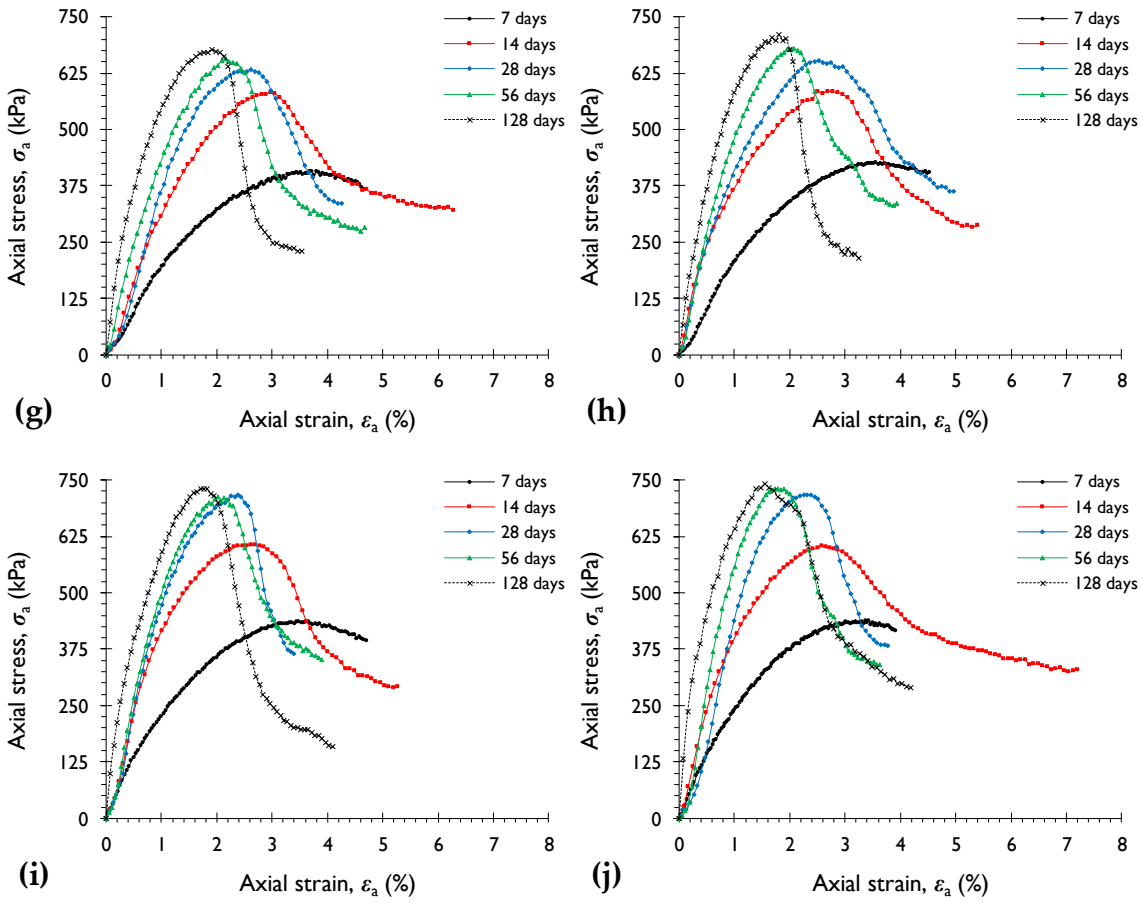

Figure A2. UC stress-strain curves for various MC + FA-treated mixtures: (a) $M_{1.5}F_{0.5}T_z$; (b) $M_{1.5}F_{1.0}T_z$; (c) $M_{1.5}F_{1.5}T_z$; (d) $M_{1.5}F_{2.0}T_z$; (e) $M_{1.5}F_{2.5}T_z$; (f) $M_{2.5}F_{0.5}T_z$; (g) $M_{2.5}F_{1.0}T_z$; (h) $M_{2.5}F_{1.5}T_z$; (i) $M_{2.5}F_{2.0}T_z$; (j) $M_{2.5}F_{2.5}T_z$ (z = {7, 14, 28, 56, 128}).

Chapter 3— Strength Development and Strain Localization Behaviour of Cemented Paste Backfills Using Portland Cement and Fly Ash

Statement of Authorship

Yue Zhao[a] , Abbas Taheri[b]*, Amin Soltani[c]*, Murat Karakus[d] and An Deng[e]

[a] **PhD Student** - School of Civil, Environmental and Mining Engineering, The University of Adelaide, Adelaide 5005, Australia (Email: Yue.Zhao@adelaide.edu.au)

[b] **Senior Lecturer** - School of Civil, Environmental and Mining Engineering, The University of Adelaide, Adelaide 5005, Australia (Email: Abbas.Taheri@adelaide.edu.au)

[c] **Research Fellow** - Geotechnical Engineering, Infrastructure Engineering, The University of Melbourne, Melbourne 3010, Australia (Email: amin.soltani@outlook.com.au)

[d] **Associate Professor** - School of Civil, Environmental and Mining Engineering, The University of Adelaide, Adelaide 5005, Australia (Email: Murat.Karakus@adelaide.edu.au)

[e] **Senior Lecturer** - School of Civil, Environmental and Mining Engineering, The University of Adelaide, Adelaide 5005, Australia (Email: An.Deng@adelaide.edu.au)

***Correspondence:** Abbas Taheri, Amin Soltani

Publication Details:

Zhao, Y., Taheri, A., Soltani, A., Karakus, M., & Deng, A. (2019). Strength Development and Strain Localization Behaviour of Cemented Paste Backfills Using Portland Cement and Fly Ash. *Materials (Basel), 12*(20). doi:10.3390/ma12203282

Statement of Authorship

Title of Paper	Strength Development and Strain Localization Behavior of Cemented Paste Backfills Using Portland Cement and Fly Ash
Publication Status	☑ Published ☐ Accepted for Publication ☐ Submitted for Publication ☐ Unpublished and Unsubmitted w ork w ritten in manuscript style
Publication Details	Zhao, Y., Taheri, A., Soltani, A., Karakus, M., & Deng, A. (2019). Strength Development and Strain Localization Behavior of Cemented Paste Backfills Using Portland Cement and Fly Ash. *Materials (Basel), 12*(20). doi:10.3390/ma12203282

Principal Author

Name of Principal Author (Candidate)	Yue Zhao		
Contribution to the Paper	Overall paper preparation		
Overall percentage (%)	60%		
Certification:	This paper reports on original research I conducted during the period of my Higher Degree by Research candidature and is not subject to any obligations or contractual agreements with a third party that would constrain its inclusion in this thesis. I am the primary author of this paper.		
Signature		Date	10/01/2020

Co-Author Contributions

By signing the Statement of Authorship, each author certifies that:

i. the candidate's stated contribution to the publication is accurate (as detailed above);

ii. permission is granted for the candidate in include the publication in the thesis; and

iii. the sum of all co-author contributions is equal to 100% less the candidate's stated contribution.

Name of Co-Author	Abbas Taheri Senior Lecturer, School of Civil, Environmental and Mining Engineering, The University of Adelaide		
Contribution to the Paper	Development of research idea, Supervised research, review and revision for the paper		
Signature		Date	06/01/2020

Name of Co-Author	Amin Soltani Research Fellow In Geotechnical Engineering, Infrastructure Engineering, The University of Melbourne		
Contribution to the Paper	Involved with analysis of results and writing up the original draft		
Signature		Date	07/01/2020

Name of Co-Author	Murat Karakus Associate Professor, School of Civil, Environmental and Mining Engineering, The University of Adelaide		
Contribution to the Paper	Development of research idea, Paper review and revision		
Signature		Date	06/01/2020

Name of Co-Author	An Deng Senior Lecturer, School of Civil, Environmental and Mining Engineering, The University of Adelaide		
Contribution to the Paper	Development of research idea, Paper review and revision		
Signature		Date	10/01/2020

Please cut and paste additional co-author panels here as required.

Abstract

This study examines the combined performance of Portland cement (PC), the binder, and fly ash (FA), the additive, towards improving the mechanical performance of the South Australian copper-gold underground mine cemented paste backfill (CPB) system. A series of unconfined compressive strength (UCS) tests were carried out on various mix designs to evaluate the effects of binder and/or additive contents, as well as curing time, on the CPB's strength, stiffness and toughness. Moreover, the failure patterns of the tested samples were investigated by means of the three-dimensional digital image correlation (DIC) technique. Making use of several virtual extensometers, the state of axial and lateral strain localization was also investigated in the pre- and post-peak regimes. The greater the PC content and/or the longer the curing period, the higher the developed strength, stiffness and toughness. The use of FA alongside PC led to further strength and stiffness improvements by way of inducing secondary *pozzolanic* reactions. Common strength criteria for CPBs were considered to assess the applicability of the tested mix designs; with regards to *stope stability*, 4% PC + 3% FA was found to satisfy the minimum 700 kPa threshold, and thus was deemed as the optimum choice. As opposed to external measurement devices, the DIC technique was found to provide strain measurements free from bedding errors. The developed field of axial and lateral strains indicated that strain localization initiates in the pre-peak regime at around 80% of the UCS. The greater the PC (or PC + FA) content, and more importantly the longer the curing period, the closer the axial stress level required to initiate localization to the UCS, thus emulating the failure mechanism of *quasi-brittle* materials such as rock and concrete. Finally, with an increase in curing time, the difference between strain values at the localized and non-localized zones became less significant in the pre-peak regime and more pronounced in the post-peak regime.

Keywords: cemented paste backfill; Portland cement; fly ash; curing time; unconfined compressive strength; digital image correlation; strain localization

1. Introduction

Mine tailings are among the largest and most problematic sources of solid waste, owing to their extensive production, durability over time, and potential health hazards — approximately 14 billion tons of tailings were produced globally by the mining industry in 2010 (Jones and Boger 2012). As of late, the concept "sustainable mining" has gained increased attention; it can be defined as a set of engineering practices which effectively maintain a perfect balance between infrastructure performance and the social, economic and ecological processes required to maintain human equity, diversity, and the functionality of natural systems (Zhang et al. 2019). Consequently, the transition towards *sustainable mining* warrants incorporating/reusing mine wastes, particularly tailings, as a "controlled low-strength material (CLSM)" in conventional infrastructure systems.

In its simplest terms, a CLSM can be defined as a high-density slurry composed of soil (mainly sands and/or silts), a cementitious binder (mainly Portland cement), and water — depending on the intended application, the slurry may be thickened to obtain a desired rheological behaviour to accommodate facile pumping and effective field implementation. In this context, recent studies have reported innovative solutions to utilize mine tailings as an "additive" in the production of cement clinker, concrete and ceramic products; such approaches, which are becoming routine in practice, have promoted the sustainability of the mining industry (Cai et al. 2009; Huang et al. 2013; Chen et al. 2015). Mine tailings prepared as CLSMs are self-compacting and flowable in character, and thus can be employed as a sustainable replacement for conventional structural fillings, e.g., backfilling of mined voids, bridge abutments, pipeline beddings, and subbases in pavements (Qian et al. 2011; Naganathan et al. 2012).

Cemented paste backfill (CPB) is a simple CLSM system composed of dewatered tailings, a cementitious binder, and processed mine water; it is often thickened to obtain a non-settling character for facile pumping into mined cavities resulted from underground mine operations (Fall et al. 2010; Yilmaz and Fall 2017; Zhang et al. 2018; Zhao et al. 2018). The desired rheological behaviour, the non-settling character, often emerges at a solids content (by total mass) of 70–85% (Rankine and Sivakugan 2007; Orejarena and Fall 2010; Sivakugan et al. 2015). In essence, CPB technology recycles tailings into underground mine excavations, and thus reduces the volume of surface-disposed tailings, mitigates the burden on the environment, and assists waste management (Zhang et al. 2018; Yilmaz et al. 2003;

Sivakugan et al. 2006; Belem and Benzaazoua 2007; Huang et al. 2011). Over the past two decades, several systematic studies have been carried out to identify the governing variables which influence the mechanical performance (mainly strength and stiffness) of CPB systems (Benzaazoua et al. 2004; Kesimal et al. 2004 &2005; Fall and Samb 2009; Taheri and Tatsuoka 2012 & 2015; Wu et al. 2018). This includes the physical, chemical and mineralogical properties of the tailings, the chemical composition of the mixing water, binder type (and its content), the adopted tailings–binder–water mix design (or solids content), and the in-situ stress and curing conditions. Although the effects of these variables have been well understood and documented in the research literature, the reported results are still not consistent, as the physical properties, chemical composition and mineralogical background of the tailings often varies from mine to mine. Accordingly, CPB projects are mainly characterized as site-specific, requiring the application of standard test methods, along with fundamental analysis and design procedures, to develop an acceptable design scheme.

According to the compressive damage zone (CDZ) crack framework, the failure process in *quasi-brittle* materials, and hence potentially CPBs, under compressive loading takes place within a so-called "local damage zone (LDZ)", where distributed cracking accompanied by a single major crack (i.e., single shear failure) or multiple major cracks (i.e., splitting failure) take place (Markeset and Hillerborg 1995; van Mier 2008; Tung and Tue 2015). In this framework, the stress-strain response in the pre-peak regime describes the compressive behaviour of the material in the entire sample (Munoz et al. 2016[b]). Upon achieving the peak stress, accumulated large deformations take place (during unloading) outside of the damage zone; this is referred to as *strain localization* (Panteleev et al. 2014; Munoz and Taheri 2017 & 2019). Quite clearly, a comprehensive understanding of the strain localization behaviour of CPBs will be beneficial towards evaluating its damage evolution and failure mechanism under real-life loading regimes. To the authors' knowledge, however, there are still no studies addressing the strain localization behaviour of CPBs, and as such, further research is urgently required.

In view of the above, this study investigates the strength development and strain localization behaviour of the South Australian copper-gold underground mine CPB system through a comprehensive experimental program. For this purpose, ordinary Portland cement (PC), the main cementitious binder, and fly ash (FA), the sustainable *pozzolan* additive, were

employed. A series of unconfined compressive strength (UCS) tests were carried out on various PC + FA mix designs to evaluate the effects of binder and/or additive contents, as well as curing time, on the strength, stiffness and toughness of the CPB system. Common strength criteria for CPBs were also considered to assess the suitability of the tested mix designs for real-life applications. Moreover, an accurate non-contact strain measurement scheme — by means of the three-dimensional digital image correlation (DIC) technique — was implemented to (**i**) measure the full-field of strain development on the surface of CPB samples; and (**ii**) characterize the deformations and strains of CPB samples with and without strain localization. Making use of several virtual extensometers, the state of strain localization was also investigated in both the axial and lateral directions.

2. Materials and Methods

2.1.Mine Tailings

A large quantity of processed mine tailings, sourced from a copper-gold underground mine in South Australia, was used in the present study (Zhao et al. 2018). The geotechnical properties of the tailings were determined in accordance with relevant ASTM (American Society for Testing and Materials) and Australian standards, and the results are tabulated in Table 1. In terms of grain-size distribution, the tailings consisted of 39% fines (< 75 μm) and 61% sand (0.075–2 mm). The liquid limit (LL) — as determined for 20-mm cone penetration depth using the 80 g–30 ° fall-cone device — and standard thread-rolling plastic limit (PL) were measured as LL = 19.2% and PL = 13.1%, respectively; thus, producing a plasticity index (PI = LL − PL) of 6.1%, such that the fines fraction of the tailings was classified as *clay–silt with low plasticity* (CL–ML) in accordance with the Unified Soil Classification System (USCS). The standard Proctor compaction test indicated an optimum water content of 8.7%, along with a maximum dry density of 2.06 g/cm^3. The specific gravity of the tailings was found to be G_s = 2.61, which is slightly lower compared with that reported for natural CL–ML soils (Blotz et al. 1998). The chemical composition of the tailings, as supplied by the distributor, was mainly dominated by silicon dioxide (SiO_2) and ferric oxide (Fe_2O_3), with mass fractions of 38.27% and 37.70%, respectively (see Table 1).

2.2.Binder, Additive and Mine Water

Ordinary PC often serves as a benchmark binding agent with respect to underground mine backfilling applications (Zhao et al. 2018). To effectively simulate the actual conditions of

the South Australian copper-gold underground mine, a large quantity of PC was sourced from a local manufacturer and was used as the main cementitious binder for CPB preparations. Its physical and chemical properties, as supplied by the manufacturer, are presented in Table 2. Moreover, standard Class C FA was used as the siliceous–aluminous *pozzolan* additive to explore the possibility of partially replacing the main cementitious binder (or PC), thereby obtaining a more sustainable CPB design. The chemical composition of FA, as supplied by the manufacturer, was mainly dominated by silicon dioxide (SiO_2), calcium oxide (CaO) and aluminium trioxide (Al_2O_3), with mass fractions of 40.2%, 24.3% and 18.7%, respectively.

A large amount of processed mine water, collected from the same copper-gold underground mine, was used for CPB preparations. The chemical composition of the mine water, as supplied by the distributor, is presented in Table 3. The chemical composition was mainly dominated by chloride (Cl^-), sodium (Na^+) and sulphate (SO_4^{2-}) ions, with concentrations of 5800 mg/L, 3800 mg/L and 2400 mg/L, respectively. Other chemical properties included a pH of 7.5, such that the mine water was characterized as a *neutral* substance.

2.3.Mix Designs and Sample Preparations

A total of twenty PC + FA mix designs, as outlined in Table 4, were examined in this study. For ease of presentation, the following coding system is used to designate the various mix designs:

$$P_aF_bT_c \tag{1}$$

where P_a = a% PC; F_b = b% FA; and T_c = c days of curing.

The binder (PC or PC + FA), solids and water contents were all mass-based; they were, respectively, defined as:

$$(\%)\ \mathrm{BC} = \frac{M_\mathrm{B}}{M_\mathrm{T} + M_\mathrm{B}} \times 100 \tag{2}$$

$$(\%)\ \mathrm{SC} = \frac{M_\mathrm{T} + M_\mathrm{B}}{M_\mathrm{T} + M_\mathrm{B} + M_\mathrm{W}} \times 100 \tag{3}$$

$$(\%)\ \mathrm{WC} = \frac{M_{\mathrm{W}}}{M_{\mathrm{T}} + M_{\mathrm{B}}} \times 100 \tag{4}$$

where BC = binder content (PC or PC + FA); SC = solids content; WC = water content; M_{T} = mass of tailings; M_{B} = mass of binder (PC or PC + FA); and M_{W} = mass of processed mine water.

Some reports indicate that the cost of CPB implementation tends to vary from 10% to 20% of the mine's total operating cost, and the main cementitious binder, or PC, represents up to 75% of the total CPB cost (Zhao et al. 2018). In this regard, South Australian mining standards recommend a maximum PC content of 5% (by total dry mass). Accordingly, in this study, the tested PC contents ranged from 1% to 5% (see Table 4).

The tailings and binder, i.e., PC or PC + FA, were blended in dry form in accordance with the selected mix designs outlined in Table 4. Mixing was carried out for approximately 5 minutes to gain visible homogeneity of the ingredients. The required amount of mine water corresponding to a water content of WC = 30% — equivalent to a solids content of SC = 77% — was added to each blend and thoroughly mixed by a mechanical mixer to obtain slurries of uniform consistency. It should be noted that the choice of WC = 30% (or SC = 77%) was selected in accordance with South Australian mining standards; this water content produces the desired rheological behaviour to accommodate facile pumping of the paste into mined cavities (Zhao et al. 2018). The resultant slurries were poured into cylindrical molds in one-third height increments; each layer was tamped 25 times using a small metal rod to remove entrapped air. The molds were then transferred to a humidity chamber, maintained at 70% relative humidity and a temperature of 25 ℃, where curing was allowed for 14 days prior to testing. For those mix designs containing 4% PC, additional curing periods of 28 and 56 days were also considered to examine the effects of curing time on the CPB's stress-strain attributes. It should be noted that the cylindrical molds measured 100 mm in height and 42 mm in diameter, thus producing a height-to-diameter ratio of 2.38 for the prepared samples, which is on par with that commonly adopted in the research literature (Fall et al. 2010; Zhao et al. 2018; Benzaazoua et al. 2004; Kesimal et al. 2004; Wu et al. 2018).

2.4.UCS Test

The prepared 42-mm diameter by 100-mm long samples were subjected to the UCS test, as per ASTM C39–18, by means of a closed-loop servo-controlled hydraulic compressive

machine with a maximum load capacity of 250 kN — Instron-1342 model (Instron®, Norwood, MA, USA). Upon demolding, the two ends of the prepared samples were covered with a thin layer of dental paste to minimise interface friction, and to ensure surface homogeneity and hence uniform load distribution during compressive loading (Lee and William 1977). The prepared samples were axially compressed at a constant displacement rate of 0.1 mm/min. Axial deformations and the corresponding axial forces were digitally recorded by a real-time data acquisition system; the former was recorded using two external linear variable differential transducers (LVDTs), while the latter, the axial force, was measured by means of an external load cell (see Figure 1c). Moreover, a direct-contact lateral extensometer — 632.12F20-series (MTS Systems Corp., Eden Prairie, MN, USA) — mounted at mid-length of the samples provided a signal for lateral deformations (see Figures 1b and 1c).

2.5.Three-Dimensional DIC Technique

DIC refers to a group of non-contact methods which acquire images of an object, store the images in digital form, and perform image processing to extract full-field shape, deformation and motion measurements (Sutton et al. 2009). The present study specifically focuses on employing the three-dimensional DIC technique to characterize the relationships between strain localization and the macro-scale mechanical deformations of PC + FA CPB samples. In its simplest terms, the three-dimensional DIC technique is based on the calculation of surface deformations using a number of digital images acquired from a reference undeformed and subsequent deformed states (Sutton et al. 2009; Chu et al. 1985). The method involves the use of two high-resolution digital cameras positioned in such a manner that the surface patterns of the sample, undergoing compressive loading, can be captured from two different angles; in this manner, a three-dimensional measurement of the sample's shape and displacements can be created.

As demonstrated in Figures 1a and 1b, the two digital cameras — positioned on the left and right sides of the desired sample — were symmetrically focused on the sample to capture digital grey-scale images during the UCS test. The used DIC set-up consisted of two Fujinon HF75SA-1 (Fujifilm Holdings Corp., Tokyo, Japan) monochrome cameras; camera specifications included an iris range of F1.4 – F22, a focal length of 75 mm, and a resolution of 5 megapixels. Moreover, uniform illumination was provided by two adjustable goose-neck halogen lights to ensure adequate contrast across the sample's surface during imaging

(see Figures 1a and 1b). The images were captured automatically using the VIC-Snap software package (Correlated Solutions Inc., Irmo, SC, USA). Prior to the UCS tests, each of the two cameras was stereo calibrated using a 30-mm standard target having a uniformly-spaced marker grid; calibration of the cameras was carried out by taking a minimum of 30 image-pairs at the calibration target (Munoz et al. 2016[b]). During the UCS tests, the cameras were programmed to capture images automatically at a frame rate of one picture per second. For each of the tested samples, the first image-pair was defined as the undeformed state and served as a reference for the VIC-3D software package (Correlated Solutions Inc., Irmo, SC, USA) to recreate the deformation field on the subsequent image-pairs by means of the software's built-in image processing algorithms.

3. Results and Discussion

3.1.Effect of PC + FA on UCS

Figure 2a illustrates the variations of UCS against FA content for various mix designs tested at 14 days of curing — $P_aF_bT_{14}$ where a = {1, 2, 3, 4, 5}, and b = {0, 1, 2, 3}. For any given FA content, the greater the PC content, the higher the developed UCS, following a monotonically-increasing trend. As typical cases, for FA = 2%, the use of 1%, 2%, 3%, 4% and 5% PC resulted in UCS values of q_u = 75.3 kPa, 231.7 kPa, 268.8 kPa, 363.5 kPa and 446.7 kPa, respectively. Similarly, for any given PC content, an increase in FA content promoted a notable, yet less pronounced increase in the UCS. For instance, the samples $P_4F_0T_{14}$, $P_4F_1T_{14}$, $P_4F_2T_{14}$ and $P_4F_3T_{14}$ resulted in q_u = 265.3 kPa, 335.5 kPa, 363.5 kPa and 379.7 kPa, respectively. Figure 2b illustrates the variations of UCS against curing time for various mix designs containing 4% PC — $P_4F_bT_c$ where b = {0, 1, 2, 3}, and c = {14, 28, 56}. For any given FA content, an increase in curing time promoted a major increase in the UCS, following a monotonically-increasing trend, thus signifying a time-dependent amending mechanism, i.e., *pozzolanic reactions* (Zhang et al. 2012; Zhao et al. 2018; Sharma and Sivapullaiah 2016; Firoozi et al. 2017; Soltani et al. 2017; Behnood 2018). The sample $P_4F_2T_{14}$, for instance, resulted in q_u = 363.5 kPa, while the same mix design cured for 28 and 56 days led to higher values of 468.3 kPa and 648.3 kPa, respectively.

Common strength criteria for CPBs used in mining applications are summarised in Table 5. As is evident from Figure 2, the UCS for various PC + FA mix designs ranges between 59.7 kPa (for $P_1F_0T_{14}$) and 708.5 kPa (for $P_4F_3T_{56}$), thus indicating that none of the tested samples meets the prerequisite for *roof support* applications, i.e., q_u > 4000 kPa. The sample $P_4F_3T_{56}$

resulted in q_u = 708.5 kPa, and thus satisfies the minimum 700 kPa threshold suggested for *stope stability*. For *surface disposal* applications, as well as *general construction practices*, all mix designs, excluding $P_4F_0T_{14}$, $P_4F_1T_{14}$, $P_4F_0T_{28}$ and $P_aF_bT_{14}$, i.e., a = {1, 2, 3}, and b = {0, 1, 2, 3}, well meet the $q_u \geq 345$ kPa criterion. Finally, all samples, excluding $P_1F_bT_{14}$, i.e., b = {0, 1, 2, 3}, satisfy the requirement for *eliminating liquefaction* in underground disposal applications.

The secant modulus at 50% of the UCS, denoted as E_{50}, serves as a measure of the material's stiffness in the elastic compression domain (Zhang et al. 2012; Taheri and Tani 2008; Soltani et al. 2019[a]). The variations of E_{50}, as outlined in Figure 3, exhibited a trend similar to that observed for the UCS; in general, for any given FA content, the greater the PC content, the higher the developed stiffness, following a monotonically-increasing trend. As typical cases, the samples $P_1F_2T_{14}$, $P_2F_2T_{14}$, $P_3F_2T_{14}$, $P_4F_2T_{14}$ and $P_5F_2T_{14}$ resulted in E_{50} = 6.2 MPa, 9.7 MPa, 11.2 MPa, 18.9 MPa and 42.2 MPa, respectively. Moreover, for any given PC content, an increase in FA content led to a notable, yet less pronounced increase in E_{50}. For instance, the sample $P_4F_0T_{14}$ resulted in E_{50} = 11.7 MPa, while the same mix design treated with 1%, 2% and 3% FA promoted higher values of 15.5 MPa, 18.9 MPa and 24.2 MPa, respectively. Much like the UCS, the effect of curing time was found to be positively-proportional to the sample's stiffness. The sample $P_4F_2T_{14}$, for instance, resulted in E_{50} = 18.9 MPa, while the same mix design cured for 28 and 56 days promoted higher values of 41.1 MPa and 52.5 MPa, respectively.

The area under a typical axial stress–axial strain curve (i.e., axial strain refers to that obtained by the external LVDTs, as shown in Figure 1c) up to the peak point (or the UCS) signifies the energy stored by a sample undergoing deformation, and thus serves as a measure of the material's toughness (Zhang et al. 2012; Zhao et al. 2018; Soltani et al. 2019[b]). Much like the UCS and E_{50}, the development of peak strain energy (or toughness) was found to be positively-proportional to the PC and/or FA contents, as well as the curing time (see Figure 4). The samples $P_4F_0T_{14}$ and $P_4F_2T_{14}$, for instance, resulted in peak strain energies of E_U = 4.0 kPa and 6.3 kPa, while the mix designs $P_5F_0T_{14}$, $P_5F_2T_{14}$, $P_4F_0T_{28}$ and $P_4F_2T_{28}$ resulted in E_U = 4.6 kPa, 7.4 kPa, 4.9 kPa and 7.6 kPa, respectively.

The axial strain at failure, denoted as ε_u and obtained by the external LVDTs, is an indication of the material's ductility; lower ε_u values manifest a more brittle (or less ductile) character (Zhang et al. 2012; Soltani et al. 2017). Figure 5a illustrates the variations of UCS against ε_u

for the tested samples. The greater the UCS, the lower the ductility, following a monotonically-decreasing trend — $q_u = 1998\varepsilon_u^{-1.57}$ (with $R^2 = 0.957$). As such, the developed ductility was inversely-proportional to the PC and/or FA contents, as well as the curing time. The greater the PC and/or FA contents, the lower the axial strain at failure and hence the more brittle the sample failures.

Figure 5b illustrates the variations of E_{50} against q_u for the tested mix designs. The variations of E_{50} were situated within the $0.04q_u < E_{50} < 0.125q_u$ domain (E_{50} in MPa, and q_u in kPa). Moreover, E_{50} exhibited a rather strong correlation with the UCS. In this regard, simple correlative models in the forms of $E_{50} = 0.076q_u$ (with $R^2 = 0.812$) and $E_{50} = 3.72 \exp[4.7 \times 10^{-3} q_u]$ (with $R^2 = 0.909$) can be derived, and thus implemented for indirect estimations of E_{50}.

In the presence of water, PC initiates a series of chemical reactions in the tailings–water medium, which alter the composite's fabric into a coherent matrix of enhanced strength attributes. The primary reactions include hydration of calcium silicates and calcium aluminates, both major components of PC, with water, thereby leading to the formation and propagation of strong cementation products/gels — calcium–silicate–hydrates (C-S-H) and calcium–aluminate–hydrates (C-A-H) — which encourage the development of a uniform, dense matrix coupled with enhanced strength and stiffness performance (Benzaazoua et al. 2004; Firoozi et al. 2017). In this case, the greater the PC content, the greater the number of developed cementation products and hence the higher the mobilized strength and stiffness (e.g., see 0% FA in Figures 2a and 3a). It should be noted that the primary reactions occur almost independently of the nature of the host material (or in this case tailings).

A by-product of PC hydration is calcium hydroxide or hydrated lime ($Ca(OH_2)$), which promotes secondary reactions with any *pozzolan* agents present in the host material; the amount of released $Ca(OH)_2$ is approximately 30% by mass of the added PC (Firoozi et al. 2017). Pozzolanic reactions are strongly time- and often temperature-dependent. During pozzolanic reactions, calcium cations (Ca^{2+}) and hydroxide anions (OH^-), both by-products of the hydration stage, gradually react with silicate (SiO_2) and aluminate (Al_2O_3) units from the tailings, thus producing additional C-S-H, C-A-H and C-A-S-H products in the matrix; these cementation products encourage flocculation and/or aggregation of the tailings particles and hence a further increase in the composite's UCS and stiffness over time (e.g., see Figures 2b and 3b) (Zhang et al. 2012; Zhao et al. 2018; Firoozi et al. 2017). Quite clearly,

the commencement and evolution of pozzolanic reactions is strongly dependent on the amount of released $Ca(OH)_2$ (or the PC content), as well as the amount of available silicate and aluminate units (or pozzolan materials) in the matrix.

The addition of FA alongside PC induces the development of pozzolanic reactions, and hence cementation products, in the matrix through two potential pathways. As mentioned in Section 2.2, the Class C FA used in this study contains a notable fraction of calcium oxide (CaO). In the presence of water, these CaO units can be ionized to Ca^{2+} and OH^{-}, thereby reacting with the remaining silicate and aluminate units in the tailings, as well as those present in FA itself, which in turn result in the development of additional cementation products and hence an increased strength and stiffness. Moreover, the Ca^{2+} and OH^{-} ions, formed through the ionization of $Ca(OH)_2$ after the hydration stage, may also react with FA's silicate and aluminate units, and thus encourage additional pozzolanic reactions over time. Accordingly, these additional cementation products lead to improved mobilized strength and stiffness compared with similar PC inclusions containing no FA. As is evident from Figures 2a and 2b, for any given PC content, the developed strength, stiffness and toughness were consistently in favour of the FA content.

3.2.Field Strain Patterns

Figures 6a and 6b illustrate the field of axial strains developed for the sample $P_4F_0T_{14}$ at various axial stress levels in the pre- and post-peak regimes, respectively. As outlined in Figure 6a, a total of four axial stress levels, i.e., $0.25q_u$, $0.5q_u$, $0.75q_u$ and q_u (or the UCS), were considered to investigate the field of axial strain development during the pre-peak regime. The field of axial strains developed at $0.25q_u$, $0.5q_u$ and the most part of $0.75q_u$ each exhibited a rather uniform colour pattern, thus implying that, up to $0.75q_u$, the sample undergoes uniform deformation during compressive loading. According to the CDZ crack framework, the failure process in *quasi-brittle* materials, and rocks in particular, under compressive loading takes place within a LDZ, where distributed cracking accompanied by a single major crack (i.e., single shear failure) or multiple major cracks (i.e., splitting failure) take place (Markeset and Hillerborg 1995; van Mier 2008; Tung and Tue 2015). In this framework, the stress-strain response in the pre-peak regime describes the compressive behaviour of the material in the entire sample (Munoz and Taheri 2019). Upon achieving the peak stress (or q_u), accumulated large deformations take place (during unloading) outside of the damage zone; this is referred to as *strain localization* (Panteleev et al. 2014; Munoz and

Taheri 2017 & 2019). Theoretically, the behaviour of CPB samples, particularly those containing high binder contents, should be consistent with the CDZ framework. However, as the CPB samples tested in this study contain low PC (or PC + FA) contents, their stress-strain evolution may be different from that of conventional *quasi-brittle* materials such as rock and concrete. As is evident from Figure 6a, the CPB sample $P_4F_0T_{14}$ well complies with the CDZ framework up to $0.75q_u$, beyond of which strain localization gradually takes place within the LDZ — at $0.75q_u$, the slight yellow-to-green colour pattern, which represents an increase in strain density, signifies a linear plane of LDZ and hence a potential shear failure zone. As the axial stress approaches the UCS (or q_u), the colour gradient transitions to a non-uniform, blue-to-purple pattern at some locations, thereby indicating a further increase in strain density and hence the presence of multiple potential failure planes. Upon achieving the UCS, the axial stress begins to drop and the sample's character progressively transitions towards a strain-softening behaviour. As outlined in Figure 6b, a total of four axial stress levels — $0.9q_u$, $0.7q_u$, $0.5q_u$ and $0.3q_u$ — were considered to investigate the field of axial strain development during the post-peak regime. The field of axial strains developed at these four stress levels all exhibited a non-uniform, blue-to-purple colour pattern, thereby implying that the sample undergoes non-uniform, permanent deformation within the entire unloading domain. Moreover, normal shear faulting, which occurs in rock-like samples, was not observed in the CPB sample; instead, multiple large cracks — various vertical and horizontal shear bands — were found to evolve at different locations.

Figures 6c and 6d illustrate the field of lateral strains developed for the sample $P_4F_0T_{14}$ at various axial stress levels in the pre- and post-peak regimes, respectively. Much like the field of axial strains shown in Figure 6a, the field of lateral strains developed during the pre-peak regime manifested a rather uniform colour pattern up to $0.75q_u$, thereby indicating that the sample undergoes uniform deformation with no major signs of strain localization (see Figure 6c). A visual comparison between Figures 6b and 6d indicates that the locations of the LDZs identified by means of the post-peak lateral strain patterns (i.e., Figure 6d) are generally identical to those identified using their post-peak axial strain pattern counterparts (i.e., Figure 6b). It should be noted that these similarities between the developed field of axial and lateral strains were consistently observed for all of the tested samples during the pre- and post-peak regimes; therefore, additional contour graphs demonstrating the field of lateral strain development will not be presented. Moreover, the FA inclusions, under the current experimental design (see Table 4), did not alter the CPB's failure pattern, as well as its field

strain development in the pre- and post-peak regimes; for various mix designs tested at 14 days of curing, e.g., $P_4F_bT_{14}$ where $b = \{0, 1, 2, 3\}$, the same unevenly-distributed splitting failure pattern was noted. On the contrary, the variables "PC content" and "curing time" were found to have some notable impacts on the field strain development. As such, to accommodate a more concise presentation of the experimental data, only the effects of PC content and curing time on strain localization will be discussed in the following.

Figure 7 illustrates the effects of PC content — $P_aF_0T_{14}$ where $a = \{1, 2, 3, 5\}$ — on the field of axial strains developed at various axial stress levels in the post-peak regime, i.e., q_u, $0.9q_u$, $0.7q_u$, $0.5q_u$ and $0.3q_u$. Much like the results obtained for the sample $P_4F_0T_{14}$ in the pre-peak regime (see Figure 6a), strain localization in the samples containing 1%, 2%, 3% and 5% PC was found to initiate prior to, or immediately after, achieving the UCS (or q_u). As is evident from Figure 7, the samples $P_1F_0T_{14}$, $P_2F_0T_{14}$, $P_3F_0T_{14}$ and $P_5F_0T_{14}$ did not exhibit normal shear faulting in the post-peak regime; instead, the failure process involved the evolution of multiple vertical and horizontal shear bands at different locations, which is consistent with that observed for the sample $P_4F_0T_{14}$ (see Figure 6b). For the sample $P_1F_0T_{14}$, the concentrated blue-to-purple colour pattern, first encountered at the UCS, increased progressively (as accumulated large deformations transpire at the LDZ), and thus signifies future failure planes (see Figure 7a). As a result of 2% PC inclusion, however, strain localization was found to transpire with a rather irregular shape, and as such, potential failure planes could not be identified with confidence (see Figure 7b). In Figures 7c and 7d, i.e., $P_3F_0T_{14}$ and $P_5F_0T_{14}$, the blue and purple colour patterns at the UCS indicate multiple potential failure zones, which eventually led to multiple fracturing. As discussed in Section 3.1, for any given curing time, the greater the PC content, the higher the developed UCS, following a monotonically-increasing trend. With an increase in PC content, and hence the CPB's strength, the failure pattern gradually transitions from "multiple extension" — where multiple parallel fractures occurred along the axial direction (see $P_1F_0T_{14}$ in Figure 7a) — to "multiple fracturing" — where sample disintegration occurred in the form of several planes at various angles (e.g., see $P_4F_0T_{14}$ in Figure 6b, and $P_5F_0T_{14}$ in Figure 7d).

Figure 8 illustrates the effects of curing time — $P_4F_0T_c$ where $c = \{14, 28, 56\}$ — on the field of axial strains developed at various axial stress levels in the post-peak regime, i.e., q_u, $0.9q_u$, $0.7q_u$, $0.5q_u$ and $0.3q_u$. As a result of curing, the failure pattern was found to gradually transition towards a shear faulting (or single shear) character; for any given PC (or PC + FA)

content, the longer the curing period, the more pronounced the shear faulting effect. Much like the sample cured for 14 days (or $P_4F_0T_{14}$), the sample cured for 28 days (or $P_4F_0T_{28}$) exhibited some blue colour patterns at the UCS, which signify potential failure zones (compare Figures 8a and 8b at q_u). In the post-peak regime, irregular strain localization was noted on the surface of both samples; this was perceived from the purple-to-pink colour gradients observed in the areas of interest corresponding to the axial strains (e.g., see Figures 8a and 8b at $0.9q_u$). A visual comparison between the samples $P_4F_0T_{14}$ and $P_4F_0T_{28}$ also indicated that the LDZ reduced in size due to extended curing. Moreover, the failure pattern transitioned from "multiple fracturing" at 14 days of curing to "multiple/double shear" at 28 days of curing, where two large X-shaped shear bands, along with some irregular micro-cracks, transpired on the surface of $P_4F_0T_{28}$. Unlike the samples cured for 14 and 28 days, the sample cured for 56 days (or $P_4F_0T_{56}$) manifested a thin purple region in the post-peak regime, which represents an inclined plane of LDZ (see Figure 8c). At 56 days of curing, which is often sufficient for binder hydration, the failure pattern transitions to a clearly-visible single shear (or shear faulting) character, accompanied by some minor cracks; this failure pattern is rather similar to that reported for rock-like materials (Munoz et al. 2016[a]). As such, the greater the PC content, and more importantly the longer the curing period, the more consistent the stress-strain evolution with that of conventional *quasi-brittle* materials such as rock and concrete.

3.3.Localization of the Stress-Strain Curves

Typical stress-strain curves, obtained by means of various measurement techniques, for the samples $P_4F_0T_{14}$, $P_4F_0T_{28}$ and $P_4F_0T_{56}$ are provided in Figures 9a, 9b and 9c, respectively. The axial and lateral strains, as outlined in the figures, were obtained by two different measurement techniques: (**i**) external measurement devices — the average of the two LVDTs for axial strain (see Figure 1c), and the direct-contact chain extensometer for lateral strain (see Figure 1c); and (**ii**) three-dimensional DIC. Using the VIC-3D software, four virtual axial extensometers, i.e., E_0, E_1, E_2 and E_3, as well as two virtual lateral extensometers, i.e., E_4 and E_5, were appointed to measure the local stress-strain characteristics; the locations of these virtual extensometers are shown in Figure 9. The extensometer E_0 captures the axial strains along with the entire sample, thus representing the overall average axial deformation (comparable to the external LVDTs) during compressive loading. The extensometer E_1 measures the axial strains outside of the LDZ, while E_2 and E_3 capture the axial strains in regions where strain localization takes place. Similarly, the irreversible lateral strains were

measured by means of two local virtual extensometers — E_4 and E_5, which, respectively, measure the lateral strains outside and inside of the LDZ. As is evident from Figure 9, the axial strains measured by E_0 displayed a trend similar to that captured by the LVDTs. Much like E_0, the LVDTs represent the overall average axial deformation along with the entire sample, however, with a certain level of contained bedding error. In contrast, strain measurements by means of the DIC technique are free from bedding errors (Munoz et al. 2016[b]; Nguyen et al. 2011; Zhang et al. 2012; Song et al. 2013). Given that the bedding error varies from sample to sample, the overall average axial strain recorded by the DIC technique, i.e., E_0, can be employed to describe the stress-strain attributes of CPB samples with an increased degree of accuracy. For any given CPB sample, e.g., $P_4F_0T_{14}$, the stress-strain curves in the pre-peak regime - LVDT, E_0, E_1, E_2 and E_3, as shown in Figure 9a - were found to perfectly overlap with each other (up to approximately $0.8q_u$), thus indicating that the sample undergoes uniform axial deformation with no major signs of strain localization. Similarly, the lateral strains generated by the external chain extensometer, E_4 and E_5 were rather identical up to approximately 80% of the UCS (e.g., see Figure 9a).

As is evident from Figure 9, for any given PC (or PC + FA) content, an increase in curing time led to a decrease in the axial strain localization behaviour during the pre-peak regime. The sample $P_4F_0T_{14}$ achieved its UCS at 2.49%, 3.11% and 3.46% based on E_1, E_0 and E_2, respectively (see Figure 9a). After the UCS, however, strain localization takes place, and the three virtual extensometers generate different values with notable differences. For further reference, the axial strain at the UCS, based on E_1, E_0 and E_2, was measured as 2.05%, 2.45% and 2.63% for $P_4F_0T_{28}$, and 1.31%, 1.46% and 1.67% for $P_4F_0T_{56}$, respectively (see Figures 9b and 9c). In the pre-peak regime, the effect of curing time was found to be positively-proportional to the axial stress level required to initiate localization. As demonstrated in Figure 9, the axial stress at which localization initiates can be taken as q_1 = 202.5 kPa, 259.5 kPa and 372.8 kPa for the samples $P_4F_0T_{14}$, $P_4F_0T_{28}$ and $P_4F_0T_{56}$, respectively. Taking into account the samples' UCS values, i.e., q_u = 265.3 kPa, 325.2 kPa and 432.7 kPa, the axial stress level required to initiate localization can be calculated as $0.76q_u$, $0.8q_u$ and $0.86q_u$, respectively. In essence, as the curing time increases, the axial stress level required to initiate localization approaches the UCS, thus emulating the failure mechanism of *quasi-brittle* materials such as rock and concrete (Munoz and Taheri 2017 & 2019). Unlike the pre-peak strains, for any given PC (or PC + FA) content, the post-peak axial and lateral strains exhibited a more pronounced strain localization effect with an increase in curing time; in

this regard, the effect of curing was found to be more dominant on the lateral strain localization (e.g., compare the post-peak axial and lateral strains in Figures 9a and 9c). For the sample $P_4F_0T_{56}$, as shown in Figure 9c, the virtual extensometers E_1, E_2 and E_4 (located outside of the LDZ where shear failure takes place) experienced inelastic unloading, and the strain rarely increased after the UCS. Finally, with an increase in curing time, the difference between strain values at the localised and non-localized zones becomes less significant in the pre-peak regime and more pronounced in the post-peak regime.

Typical stress-strain curves, obtained by means of various measurement techniques, for the samples $P_2F_0T_{14}$, $P_3F_0T_{14}$ and $P_5F_0T_{14}$ are provided in Figures 10a, 10b and 10c, respectively. At any given curing time, an increase in PC content resulted in a decrease in the axial strain localization behaviour during the pre-peak regime. This effect, however, was slightly less pronounced compared with that imposed by an increase in curing time. Much like the effect of curing time, the effect of PC content was found to be positively-proportional to the axial stress level required to initiate localization. At any given curing time, the greater the PC content, the closer the axial stress level required to initiate localization (or q_1) to the UCS (q_u), and as such, the more similar the failure mechanism of the CPB sample to that of rock and concrete. For instance, the axial stress level required to initiate localization was obtained as $q_1 = 0.71q_u$, $0.74q_u$ and $0.80q_u$ for the samples $P_2F_0T_{14}$, $P_3F_0T_{14}$ and $P_5F_0T_{14}$, respectively (see Figure 10).

Typical stress-strain curves, obtained by means of various measurement techniques, for the samples $P_4F_1T_{14}$, $P_4F_2T_{14}$ and $P_4F_3T_{14}$ are provided in Figures 11a, 11b and 11c, respectively. Unlike curing time and PC content, FA content did not significantly alter the localization behaviour. At any given curing time, and for any given PC content, the axial stress level required to initiate localization (or q_1) was found to be rather independent of the FA content. For instance, as demonstrated in Figure 11, the axial stress level required to initiate localization for the samples $P_4F_1T_{14}$, $P_4F_2T_{14}$ and $P_4F_3T_{14}$ can be, respectively, calculated as $q_1 = 0.78q_u$, $0.77q_u$ and $0.78q_u$; these values are nearly equal to that obtained for the same 4% PC cured for 14 days containing no FA (i.e., $P_4F_0T_{14}$ with $q_1 = 0.76q_u$, as outlined in Figure 9a).

4. Conclusions

The present study has arrived at the following conclusions:

- The greater the PC content and/or the longer the curing period, the higher the developed strength, stiffness and toughness, with the former, the PC content, portraying a more significant role. The axial strain at failure — an indication of the material's ductility — demonstrated a trend similar to that observed for the strength and stiffness; however, in an adverse manner. The use of FA alongside PC led to further strength and stiffness improvements by way of inducing secondary *pozzolanic* reactions. Common strength criteria for CPBs were considered to assess the applicability of the tested PC + FA mix designs; with regards to stope stability, for instance, the sample $P_4F_3T_{56}$ was found to satisfy the minimum 700 kPa threshold, and thus was deemed as the optimum choice.
- As opposed to external measurement devices, the DIC technique was found to provide strain measurements free from bedding errors. The developed field of axial and lateral strains indicated that strain localization initiates in the pre-peak regime at around 80% of the UCS. The greater the PC (or PC + FA) content, and more importantly the longer the curing period, the closer the axial stress level required to initiate localization to the UCS, thus emulating the failure mechanism of *quasi-brittle* materials such as rock and concrete — the failure process changed from "multiple fractures parallel and perpendicular to the axial loading direction" to "sample disintegration" where a single major failure plane became noticeable. For instance, the axial stress level required to initiate localization increased from $0.76q_u$ for $P_4F_0T_{14}$ to $0.86q_u$ for $P_4F_0T_{56}$. Finally, with an increase in curing time, the difference between strain values at the localised and non-localized zones became less significant in the pre-peak regime and more pronounced in the post-peak regime.

References

ASTM D4609–08. (2008). *Standard Guide for Evaluating Effectiveness of Admixtures for Soil Stabilization*, ASTM International: West Conshohocken, PA, USA. doi:10.1520/d4609-08.

Behnood, A. (2018). Soil and clay stabilization with calcium- and non-calcium-based additives: A state-of-the-art review of challenges, approaches and techniques. *Transportation Geotechnics, 17*, 14-32. doi:10.1016/j.trgeo.2018.08.002

Belem, T., & Benzaazoua, M. (2007). Design and Application of Underground Mine Paste Backfill Technology. *Geotechnical and Geological Engineering, 26*(2), 147-174. doi:10.1007/s10706-007-9154-3

Benzaazoua, M., Fall, M., & Belem, T. (2004). A contribution to understanding the hardening process of cemented pastefill. *Minerals Engineering, 17*(2), 141-152. doi:10.1016/j.mineng.2003.10.022

Blotz, L. R., Benson, C. H., & Boutwell, G. P. (1998). Estimating optimum water content and maximum dry unit weight for compacted clays. *Journal of Geotechnical & Geoenvironmental Engineering, 124*(9), 907. doi:10.1061/(ASCE)1090-0241(1998)124:9(907).

Brackebusch, F.W. (1994). Basics of paste backfill systems. *Mining Engineering*, 46(1), 1175–1178. doi: 10.1016/0148-9062(95)90153-V

Cai, J. W., Zhang, S. B., Hou, G. X., Wang, C. M., & Feng, X. X. (2009). Effects of ferrous mill tailings as aggregates on workability and strength of concrete. *J. Wuhan Univ. Technol*, 31(*7)*, 104–107. doi:10.3963/j.issn.1671-4431.2009.07.027

Chen, S., Wang, H., Zhang, J., Xing, H., & Wang, H. (2015). Low-Strength Similar Materials for Backfill Mining: Insight from Experiments on Components and Influence Mechanism. *Geotechnical Testing Journal, 38*(6), 20140103. doi:10.1520/gtj20140103

Chu, T.C., Ranson, W.F., & Sutton, M.A. (1985). Applications of digital-image-correlation techniques to experimental mechanics. *Experimental Mechanics* 25**,** 232–244. doi:10.1007/BF02325092

Fall, M., & Samb, S. S. (2009). Effect of high temperature on strength and microstructural properties of cemented paste backfill. *Fire Safety Journal, 44*(4), 642-651. doi:10.1016/j.firesaf.2008.12.004

Fall, M., Cúestin, J. C., Pokharel, M., & Touré, M. (2010). A contribution to understanding the effects of curing temperature on the mechanical properties of mine cemented tailings backfill. *Engineering Geology, 114*(3-4), 397-413. doi:10.1016/j.enggeo.2010.05.016

Firoozi, A. A., Guney Olgun, C., Firoozi, A. A., & Baghini, M. S. (2017). Fundamentals of soil stabilization. *International Journal of Geo-Engineering, 8*(1). doi:10.1186/s40703-017-0064-9

Grice, T. (1998). Underground Mining with Backfill. *In Proceedings of 2nd Annual Summit — Mine Tailings Disposal Systems*, Australasian Institute of Mining and Metallurgy: Carlton, Victoria, Australia, 234–239.

Huang, S., Xia, K., & Qiao, L. (2011). Dynamic tests of cemented paste backfill: effects of strain rate, curing time, and cement content on compressive strength. *Journal of Materials Science, 46*(15), 5165-5170. doi:10.1007/s10853-011-5449-0

Huang, X., Ranade, R., & Li, V. C. (2013). Feasibility Study of Developing Green ECC Using Iron Ore Tailings Powder as Cement Replacement. *Journal of Materials in Civil Engineering, 25*(7), 923-931. doi:10.1061/(asce)mt.1943-5533.0000674

Jewell, R. J., & Fourie, A. B. (2002). *Paste and Thickened Tailings — A Guide*, 1st ed., Australian Centre for Geomechanics: Perth, Western Australia, Australia, 103–126.

Jones, H., & Boger, D. V. (2012). Sustainability and Waste Management in the Resource Industries. *Industrial & Engineering Chemistry Research, 51*(30), 10057-10065. doi:10.1021/ie202963z

Kesimal, A., Yilmaz, E., & Ercikdi, B. (2004). Evaluation of paste backfill mixtures consisting of sulphide-rich mill tailings and varying cement contents. *Cement and Concrete Research, 34*(10), 1817-1822. doi:10.1016/j.cemconres.2004.01.018

Kesimal, A., Yilmaz, E., Ercikdi, B., Alp, I., & Deveci, H. (2005). Effect of properties of tailings and binder on the short-and long-term strength and stability of cemented paste backfill. *Materials Letters, 59*(28), 3703-3709. doi:10.1016/j.matlet.2005.06.042

Lee, Y. H., & William, K. (1977). Mechanical Properties of Concrete in Uniaxial Compression. *ACI Materials Journal, 94*(6). doi:10.14359/329

Markeset, G., & Hillerborg, A. (1995). Softening of concrete in compression — Localization and size effects. *Cement and Concrete Research, 25(4),* 702–708, doi:10.1016/0008-8846(95)00059-L.

Munoz, H., & Taheri, A. (2017). Local Damage and Progressive Localization in Porous Sandstone During Cyclic Loading. *Rock Mechanics and Rock Engineering, 50*(12), 3253-3259. doi:10.1007/s00603-017-1298-8

Munoz, H., & Taheri, A. (2019). Postpeak Deformability Parameters of Localized and Nonlocalized Damage Zones of Rocks under Cyclic Loading. *Geotechnical Testing Journal, 42*(6), 20170266. doi:10.1520/gtj20170266

Munoz, H., Taheri, A., & Chanda, E. (2016[a]). Rock cutting characteristics on soft-to-hard rocks under different cutter inclinations. *International Journal of Rock Mechanics and Mining Sciences, 87,* 85-89. doi:10.1016/j.ijrmms.2016.05.014

Munoz, H., Taheri, A., & Chanda, E. K. (2016[b]). Pre-Peak and Post-Peak Rock Strain Characteristics During Uniaxial Compression by 3D Digital Image Correlation. *Rock Mechanics and Rock Engineering, 49*(7), 2541-2554. doi:10.1007/s00603-016-0935-y

Naganathan, S., Razak, H. A., & Hamid, S. N. A. (2012). Properties of controlled low-strength material made using industrial waste incineration bottom ash and quarry dust. *Materials & Design, 33,* 56-63. doi:10.1016/j.matdes.2011.07.014

Nguyen, T. L., Hall, S. A., Vacher, P., & Viggiani, G. (2011). Fracture mechanisms in soft rock: Identification and quantification of evolving displacement discontinuities by extended digital image correlation. *Tectonophysics, 503*(1-2), 117-128. doi:10.1016/j.tecto.2010.09.024

Orejarena, L., & Fall, M. (2010). The use of artificial neural networks to predict the effect of sulphate attack on the strength of cemented paste backfill. *Bulletin of Engineering Geology and the Environment, 69*(4), 659-670. doi:10.1007/s10064-010-0326-7

Panteleev, I., Plekhov, O., Pankov, I., Evseev, A., Naimark, O., & Asanov, V. (2014). Experimental investigation of the spatio-temporal localization of deformation and damage in sylvinite specimens under uniaxial tension. *Engineering Fracture Mechanics, 129*, 38-44. doi:10.1016/j.engfracmech.2014.08.004

Qian, G., Huang, T., & Bai, S. (2011). Use of Cement-Stabilized Granite Mill Tailings as Pavement Subbase. *Journal of Materials in Civil Engineering*, *23*(11), 1575-1578. doi:10.1061/(asce)mt.1943-5533.0000276

Rankine, R. M., & Sivakugan, N. (2007). Geotechnical properties of cemented paste backfill from Cannington Mine, Australia. *Geotechnical and Geological Engineering*, *25*(4), 383-393. doi:10.1007/s10706-006-9104-5

Sharma, A. K., & Sivapullaiah, P. V. (2016). Ground granulated blast furnace slag amended fly ash as an expansive soil stabilizer. *Soils and Foundations, 56*(2), 205-212. doi:10.1016/j.sandf.2016.02.004

Sivakugan, N., Rankine, R. M., Rankine, K. J., & Rankine, K. S. (2006). Geotechnical considerations in mine backfilling in Australia. *Journal of Cleaner Production, 14*(12-13), 1168-1175. doi:10.1016/j.jclepro.2004.06.007

Sivakugan, N., Veenstra, R., & Naguleswaran, N. (2015). Underground Mine Backfilling in Australia Using Paste Fills and Hydraulic Fills. *International Journal of Geosynthetics and Ground Engineering, 1*(2). doi:10.1007/s40891-015-0020-8

Soltani, A., Deng, A., Taheri, A., & Sridharan, A. (2019[a]). Swell–Shrink–Consolidation Behaviour of Rubber–Reinforced Expansive Soils. *Geotechnical Testing Journal, 42*(3). doi:10.1520/gtj20170313

Soltani, A., Taheri, A., Deng, A., & Nikraz, H. (2019[b]). Tyre rubber and expansive soils: two hazards, one solution. *Proceedings of the Institution of Civil Engineers - Construction Materials*, 1. doi: 10.1680/jcoma.18.00075

Soltani, A., Taheri, A., Khatibi, M., & Estabragh, A. R. (2017). Swelling Potential of a Stabilized Expansive Soil: A Comparative Experimental Study. *Geotechnical and Geological Engineering, 35*(4), 1717-1744. doi:10.1007/s10706-017-0204-1

Song, H., Zhang, H., Kang, Y., Huang, G., Fu, D., & Qu, C. (2013). Damage evolution study of sandstone by cyclic uniaxial test and digital image correlation. *Tectonophysics, 608*, 1343-1348. doi:10.1016/j.tecto.2013.06.007

Sutton, M. A., Orteu, J. J., & Schreier, H. (2009). *Image Correlation for Shape, Motion and Deformation Measurements*, 1st ed., Springer US: New York, USA. ISBN: 9780387787473, doi: 10.1007/978-0-387-78747-3.

Taheri, A., & Tani, K. (2008). Use of down-hole triaxial apparatus to estimate the mechanical properties of heterogeneous mudstone. *International Journal of Rock Mechanics and Mining Sciences, 45*(8), 1390-1402. doi:10.1016/j.ijrmms.2008.01.017

Taheri, A., & Tatsuoka, F. (2012). Stress-strain relations of cement–mixed gravelly soil from multiple–step triaxial compression test results. *Soils Found*, 52, 748–766, doi:10.1016/j.sandf.2012.07.014

Taheri, A., Tatsuoka, F. (2015). Small- and large-strain behaviour of a cement-treated soil during various loading histories and testing conditions. *Acta Geotech*, 10, 131–155, doi:10.1007/s11440-014-0339-7

Tariq, A. (2012). Synergistic and Environmental Benefits of Using Cement Kiln Dust with Slag and Fly Ash in Cemented Paste Tailings. PhD, The University of Western Ontario, London, Ontario, Canada, Available online: http://ir.lib.uwo.ca/etd/560 (accessed on 22 October 2018).

Tung, N. D., & Tue, N. V. (2015). Post-peak behaviour of concrete specimens undergoing deformation localization in uniaxial compression. *Construction and Building Materials, 99*, 109-117. doi:10.1016/j.conbuildmat.2015.09.013

United States Environmental Protection Agency (USEPA). (1986). *Handbook for Stabilization/Solidification of Hazardous Waste*, Report EPA/540/2-86/001, Hazardous Waste Engineering Research Laboratory: Cincinnati, Ohio, USA.

van Mier, J. G. M. (2008). Framework for a generalized four-stage fracture model of cement-based materials. *Engineering Fracture Mechanics, 75*(18), 5072-5086. doi:10.1016/j.engfracmech.2008.07.011

Wu, J., Feng, M., Chen, Z., Mao, X., Han, G., & Wang, Y. (2018). Particle Size Distribution Effects on the Strength Characteristic of Cemented Paste Backfill. *Minerals, 8*(8). doi:10.3390/min8080322

Yilmaz, E., & Fall, M. (2017). Introduction to Paste Tailings Management. In E. Yilmaz & M. Fall (Eds.), *Paste Tailings Management* (pp. 1-5). Cham: Springer International Publishing.

Yilmaz, E., Kesimal, A., Deveci, H., & Ercikdi, B. (2003). The Factors Affecting the Performance of Paste Backfill: Physical, Chemical and Mineralogical Characterization. *First Engineering Sciences Congress for Young Researchers (MBGAK'03)*, Istanbul, Turkey, 683–690.

Zhang, H., Huang, G., Song, H., & Kang, Y. (2012). Experimental investigation of deformation and failure mechanisms in rock under indentation by digital image correlation. *Engineering Fracture Mechanics, 96*, 667-675. doi:10.1016/j.engfracmech.2012.09.012

Zhang, J., Deng, H., Taheri, A., Deng, J., & Ke, B. (2018). Effects of Superplasticizer on the Hydration, Consistency, and Strength Development of Cemented Paste Backfill. *Minerals, 8*(9), 381. doi:10.3390/min8090381

Zhang, J., Soltani, A., Deng, A., & Jaksa, M. B. (2019). Mechanical Performance of Jute Fiber-Reinforced Micaceous Clay Composites Treated with Ground-Granulated Blast-Furnace Slag. *Materials (Basel), 12*(4). doi:10.3390/ma12040576

Zhao, Y., Soltani, A., Taheri, A., Karakus, M., & Deng, A. (2018). Application of Slag–Cement and Fly Ash for Strength Development in Cemented Paste Backfills. *Minerals, 9*(1), 22. doi:10.3390/min9010022

List of Tables

Table 1. Geotechnical properties and chemical composition of the mine tailings.

Geotechnical Properties	Standard	Value	Chemical Components	MF (%) [1]
Specific gravity, G_s	ASTM D854–14	2.61	SiO_2	38.27
Fines content [< 75 μm] (%)	ASTM D422–07	39	Fe_2O_3	37.70
Sand content [0.075–2 mm] (%)	ASTM D422–07	61	Al_2O_3	7.19
Liquid limit, LL (%)	AS 1289.3.9.1–15	19.2	K_2O	2.33
Plastic limit, PL (%)	AS 1289.3.2.1–09	13.1	CaO	0.81
Plasticity index, PI (%) [2]	AS 1289.3.3.1–09	6.1	MgO	0.75
USCS classification	ASTM D2487–11	CL–ML [3]	TiO_2	0.56
Optimum water content (%)	ASTM D698–12	8.7	Na_2O	0.07
Maximum dry density (g/cm^3)	ASTM D698–12	2.06	Other	12.32

[1] Mass fraction; [2] PI = LL − PL; and [3] *Clay–Silt with low plasticity*.

Table 2. Physical and chemical properties of PC.

Properties	Value	Standard
Fineness index (m^2/g)	370–430	AS 2350.8–06
Initial setting time (min)	105	AS 2350.4–06
Final setting time (min)	180	AS 2350.4–06
3-Day compressive strength (MPa)	31	AS 2350.11–06
7-Day compressive strength (MPa)	42	AS 2350.11–06
28-Day compressive strength (MPa)	60	AS 2350.11–06
Portland clinker (% by mass)	85–93	—
Natural gypsum (% by mass)	5–7	—
Mineral additives (% by mass)	< 8	—
Sulphur trioxide, SO_3 (% by mass)	2.8	—
Equivalent alkalis (% by mass)	0.5	—
Chloride, Cl^- (% by mass)	0.05	—
Loss on ignition, LOI [at 1000 ℃] (%)	3–4	—

Table 3. Chemical composition of the processed mine water.

Chemical Components	Concentration (mg/L)
Chloride, Cl^-	5800
Sodium, Na^+	3800
Sulphate, SO_4^{2-}	2400
Calcium, Ca^{2+}	480
Potassium, K^+	380
Magnesium, Mg^{2+}	280
Nitrate, NO_3^-	6

Table 4. Mix designs and their properties.

Designation	PC (%) [1]	FA (%) [1]	SC (%) [2]	WC (%) [3]	Tests
$P_1F_0T_{14}$	1	0	77	30	UCS [4] + DIC [5]
$P_1F_1T_{14}$	1	1	77	30	
$P_1F_2T_{14}$	1	2	77	30	
$P_1F_3T_{14}$	1	3	77	30	
$P_2F_0T_{14}$	2	0	77	30	UCS + DIC
$P_2F_1T_{14}$	2	1	77	30	
$P_2F_2T_{14}$	2	2	77	30	
$P_2F_3T_{14}$	2	3	77	30	
$P_3F_0T_{14}$	3	0	77	30	UCS + DIC
$P_3F_1T_{14}$	3	1	77	30	
$P_3F_2T_{14}$	3	2	77	30	
$P_3F_3T_{14}$	3	3	77	30	
$P_4F_0T_{14,28,56}$	4	0	77	30	UCS + DIC
$P_4F_1T_{14,28,56}$	4	1	77	30	
$P_4F_2T_{14,28,56}$	4	2	77	30	
$P_4F_3T_{14,28,56}$	4	3	77	30	
$P_5F_0T_{14}$	5	0	77	30	UCS + DIC
$P_5F_1T_{14}$	5	1	77	30	
$P_5F_2T_{14}$	5	2	77	30	
$P_5F_3T_{14}$	5	3	77	30	

[1] Equation (2); [2] Equation (3); [3] Equation (4); [4] Unconfined compressive strength; and [5] Digital image correlation.

Table 5. Strength criteria for CPBs adopted in mining applications (modified from Zhao et al. 2018).

Applications	UCS, q_u (kPa)	Reference
Roof support	> 4000	[Grice 1998; Tariq 2012]
Stope stability	700–2000	[Brackebusch 1994]
Surface disposal	≥ 345	[USEPA 1986]
General construction practices	≥ 345	[Zhao et al. 2018; ASTM D4609–08]
Eliminating liquefaction	150–300	[Tariq 2012; Jewell and Fourie 2002]

List of Figures

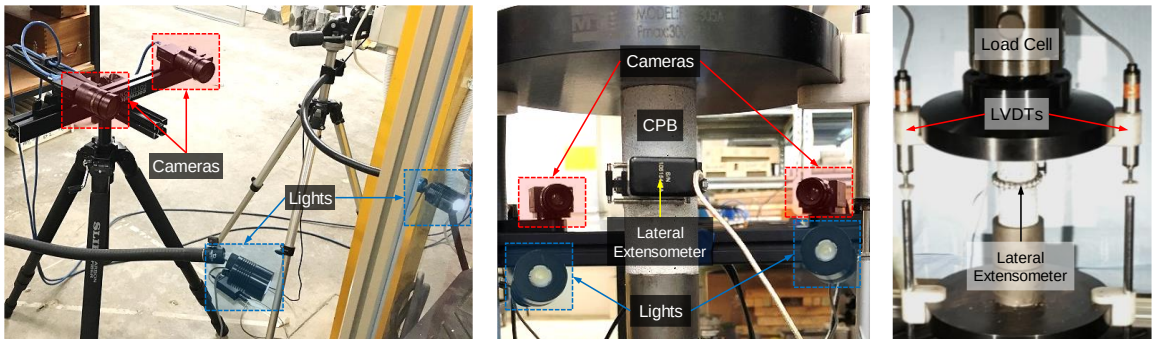

Figure 1. UCS + DIC testing system: (a) Two-camera stereo set-up; (b) Rear view of the experimental set-up during compressive loading; and (c) Front view of the experimental set-up during compressive loading.

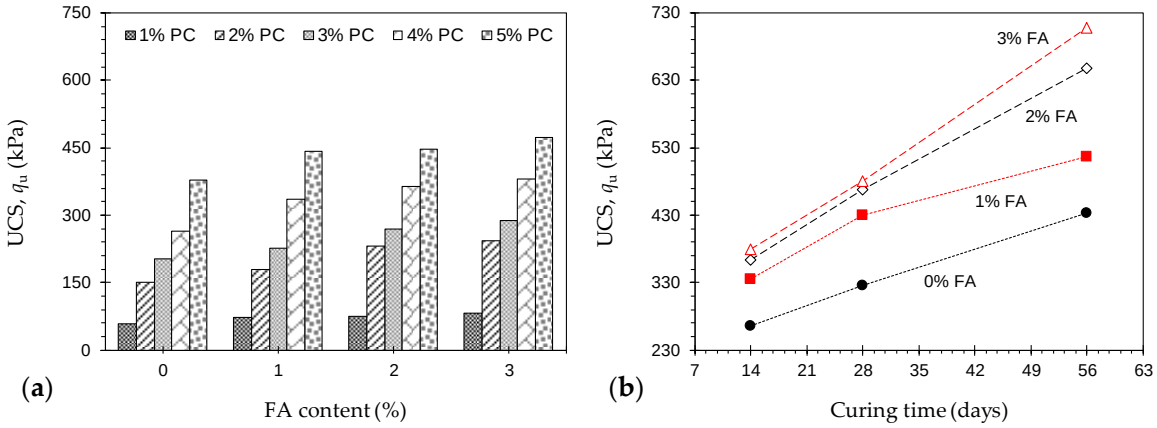

Figure 2. (a) Variations of UCS against FA content for various mix designs tested at 14 days of curing - $P_aF_bT_{14}$ where a = {1, 2, 3, 4, 5}, and b = {0, 1, 2, 3}; and (b) Variations of UCS against curing time for various mix designs containing 4% PC - $P_4F_bT_c$ where b = {0, 1, 2, 3}, and c = {14, 28, 56}.

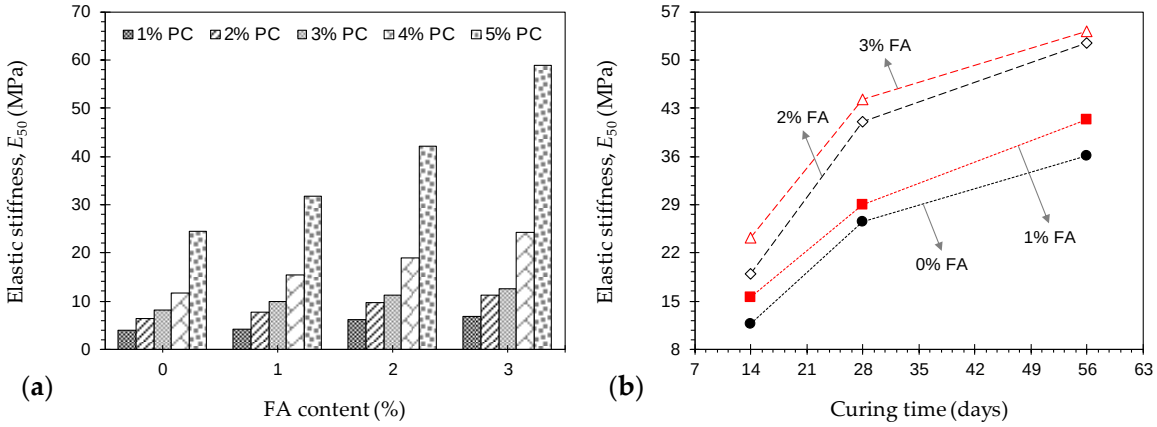

Figure 3. (a) Variations of E_{50} against FA content for various mix designs tested at 14 days of curing - $P_aF_bT_{14}$ where a = {1, 2, 3, 4, 5}, and b = {0, 1, 2, 3}; and (b) Variations of E_{50} against curing time for various mix designs containing 4% PC - $P_4F_bT_c$ where b = {0, 1, 2, 3}, and c = {14, 28, 56}.

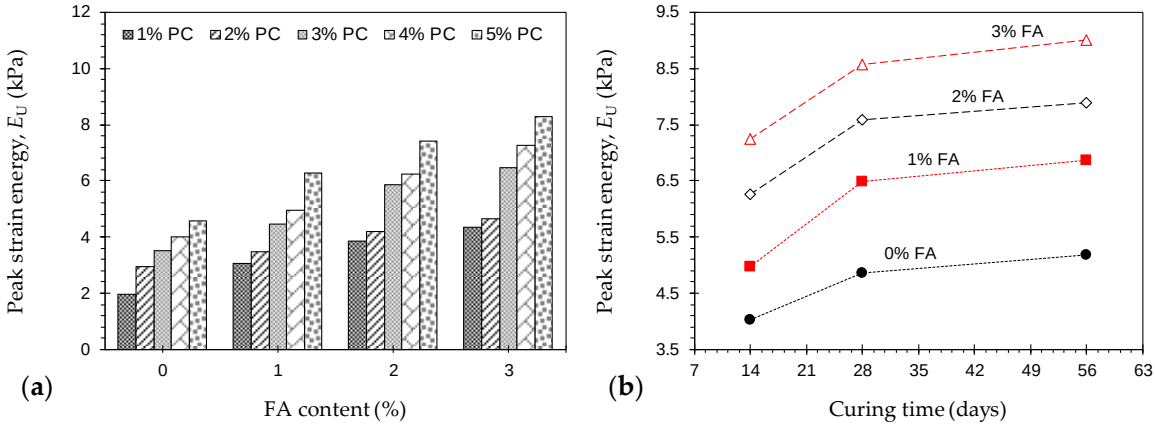

Figure 4. (a) Variations of E_U against FA content for various mix designs tested at 14 days of curing - $P_aF_bT_{14}$ where a = {1, 2, 3, 4, 5}, and b = {0, 1, 2, 3}; and (b) Variations of E_U against curing time for various mix designs containing 4% PC - $P_4F_bT_c$ where b = {0, 1, 2, 3}, and c = {14, 28, 56}.

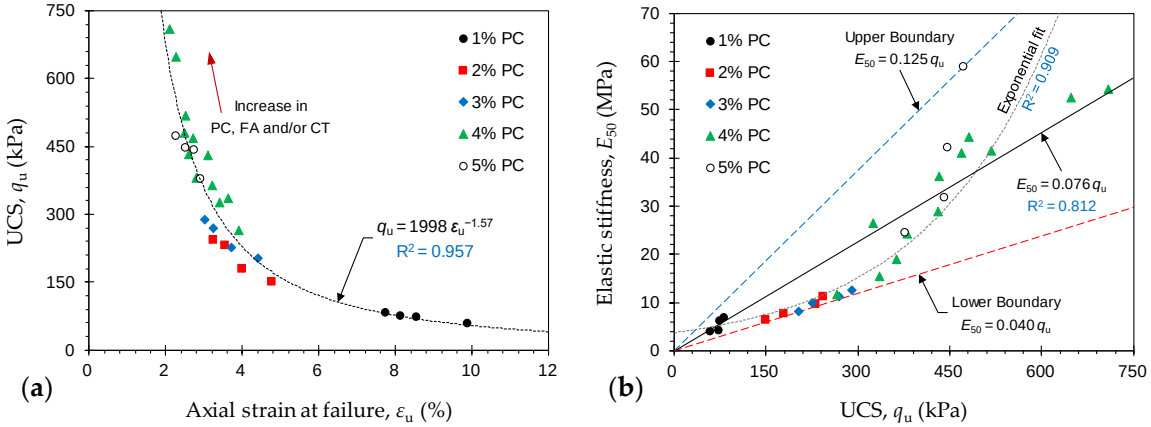

Figure 5. (a) Variations of UCS against axial strain at failure ε_u - obtained by the external LVDTs - for the tested mix designs (CT = curing time); and (b) Variations of E_{50} against UCS for the tested mix designs.

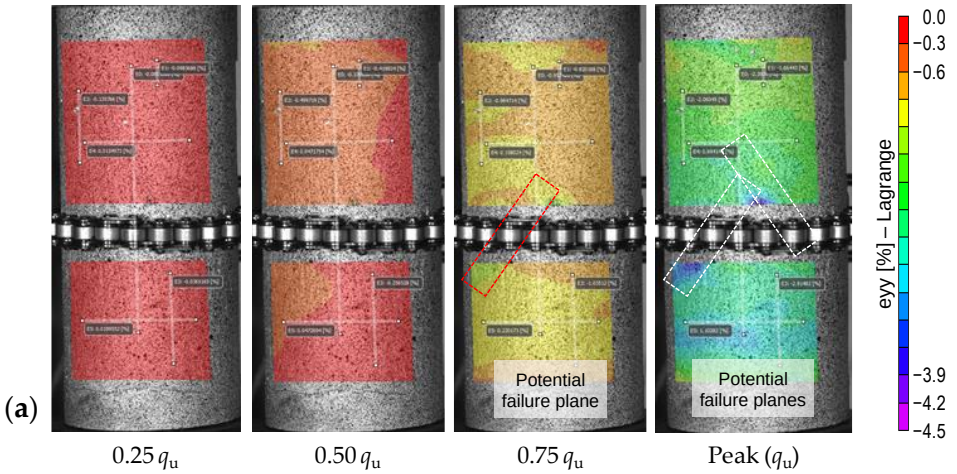

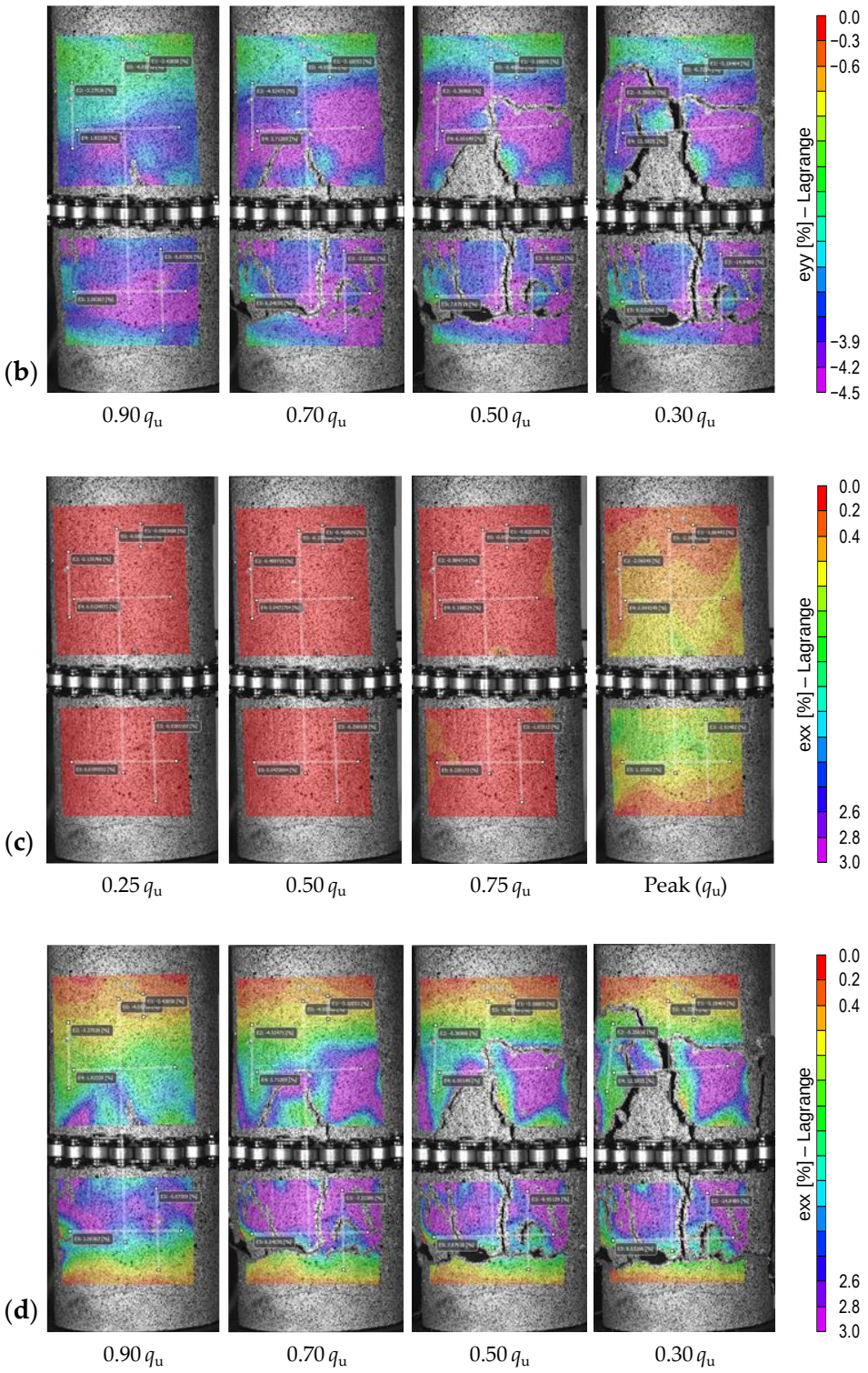

Figure 6. Field of strains developed at various axial stress levels for the sample $P_4F_0T_{14}$: (a) Axial pre-peak; (b) Axial post-peak; (c) Lateral pre-peak; and (d) Lateral post-peak.

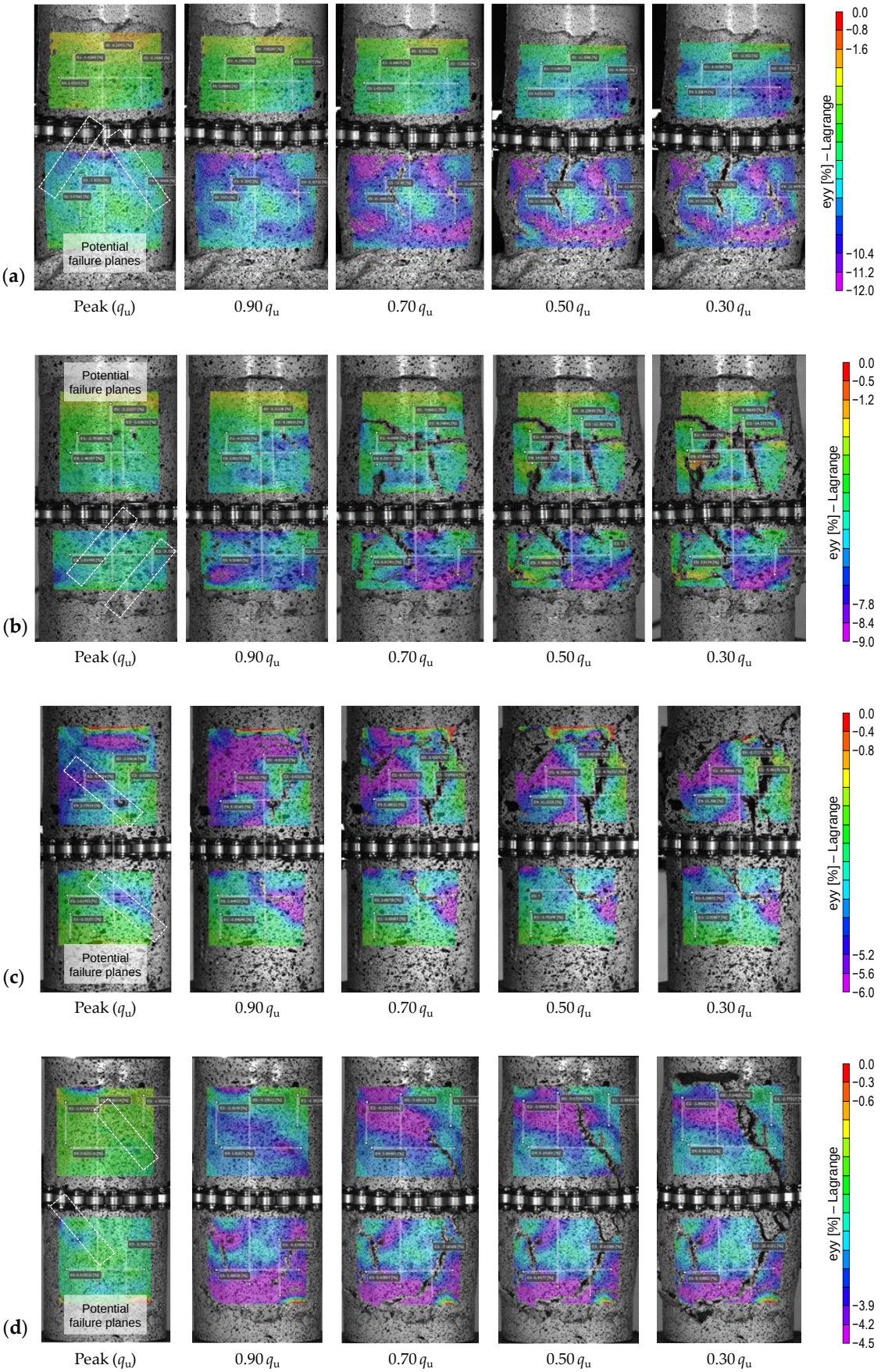

Figure 7. Effect of PC content on strain localization — field of axial strains developed at various post-peak axial stress levels: (a) $P_1F_0T_{14}$; (b) $P_2F_0T_{14}$; (c) $P_3F_0T_{14}$; and (d) $P_5F_0T_{14}$.

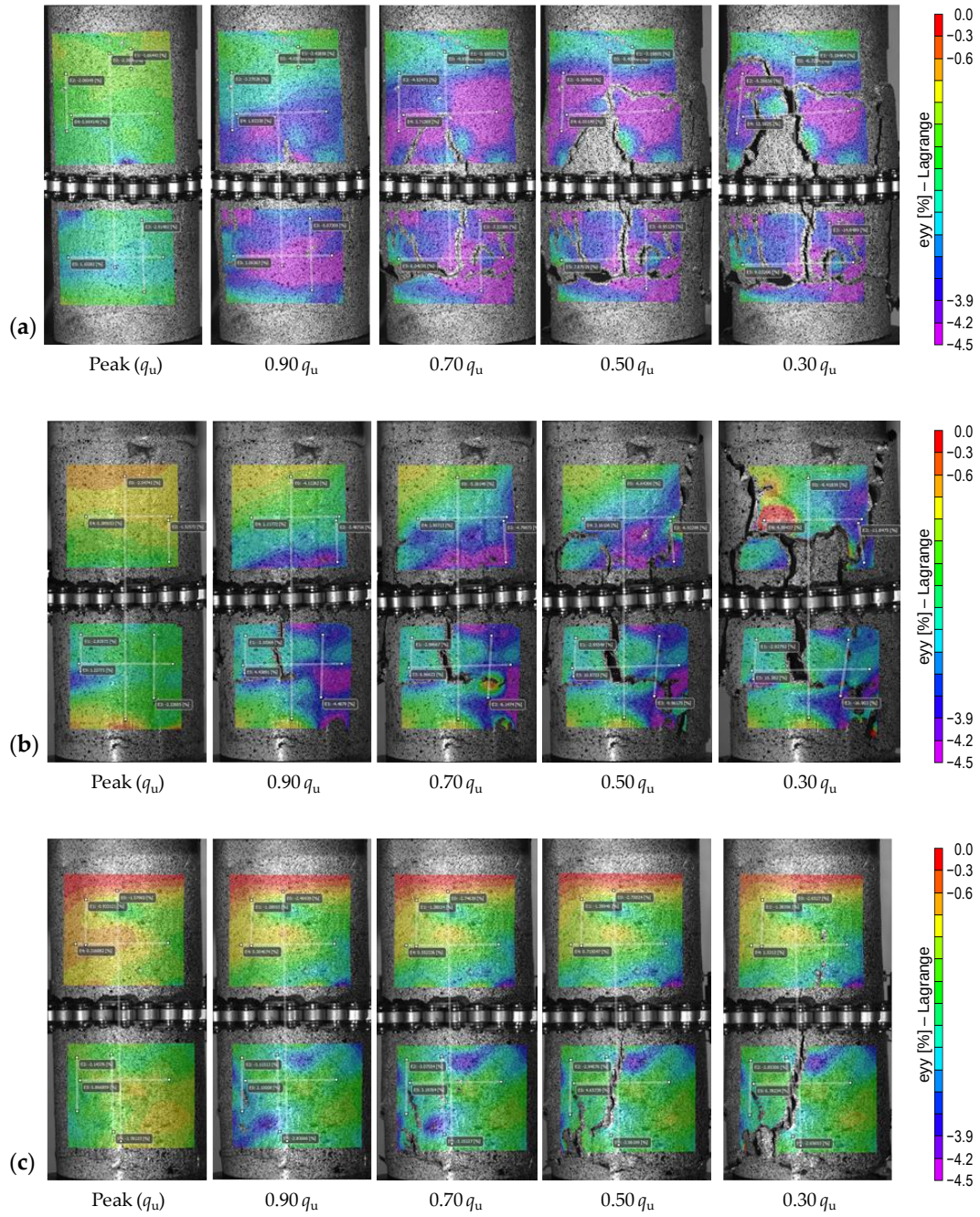

Figure 8. Effect of curing time on strain localization — field of axial strains developed at various post-peak axial stress levels: (a) $P_4F_0T_{14}$; (b) $P_4F_0T_{28}$; and (c) $P_4F_0T_{56}$.

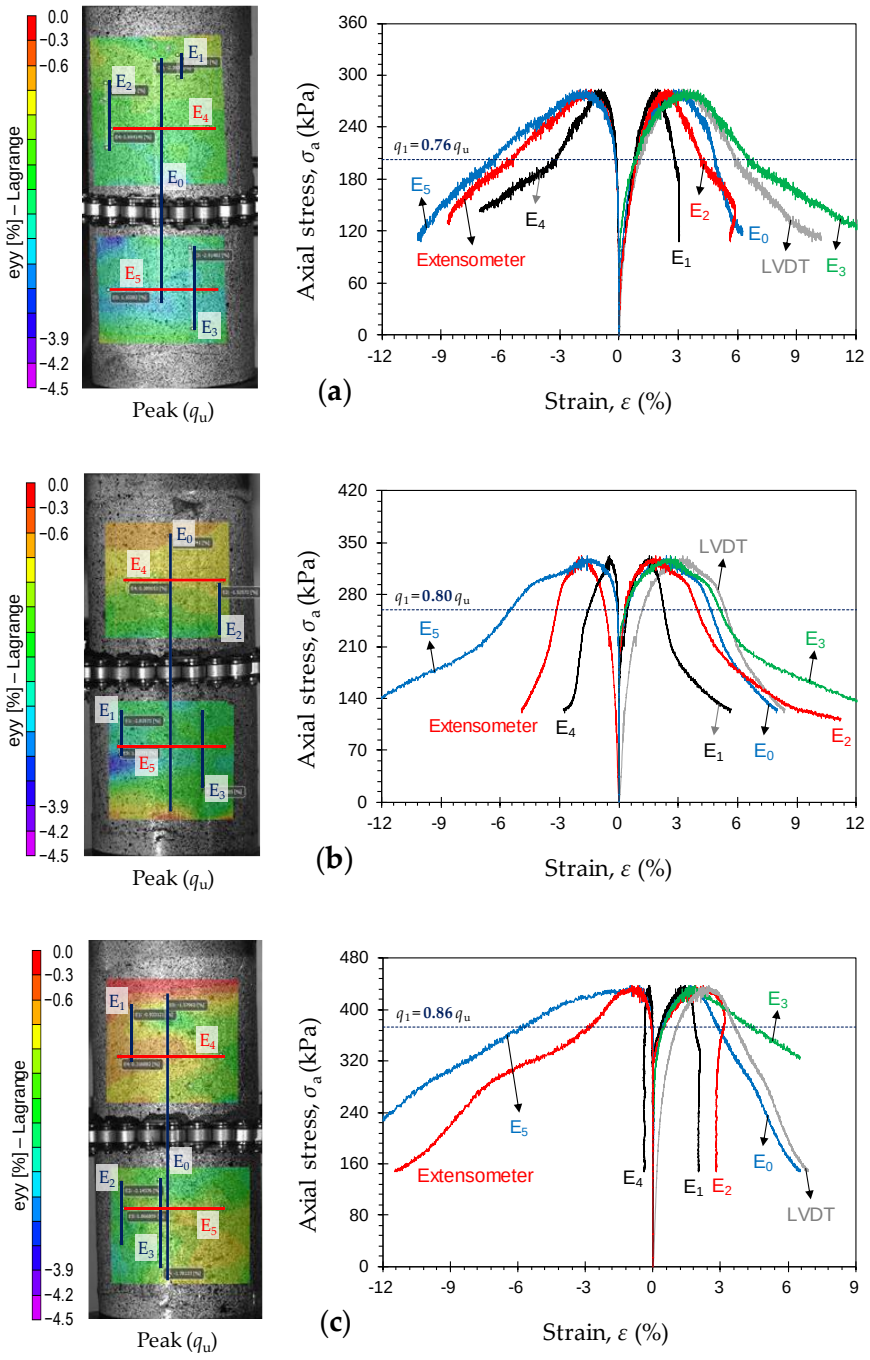

Figure 9. Typical stress-strain curves, obtained by means of various measurement techniques, for the tested samples: (a) $P_4F_0T_{14}$; (b) $P_4F_0T_{28}$; and (c) $P_4F_0T_{56}$.

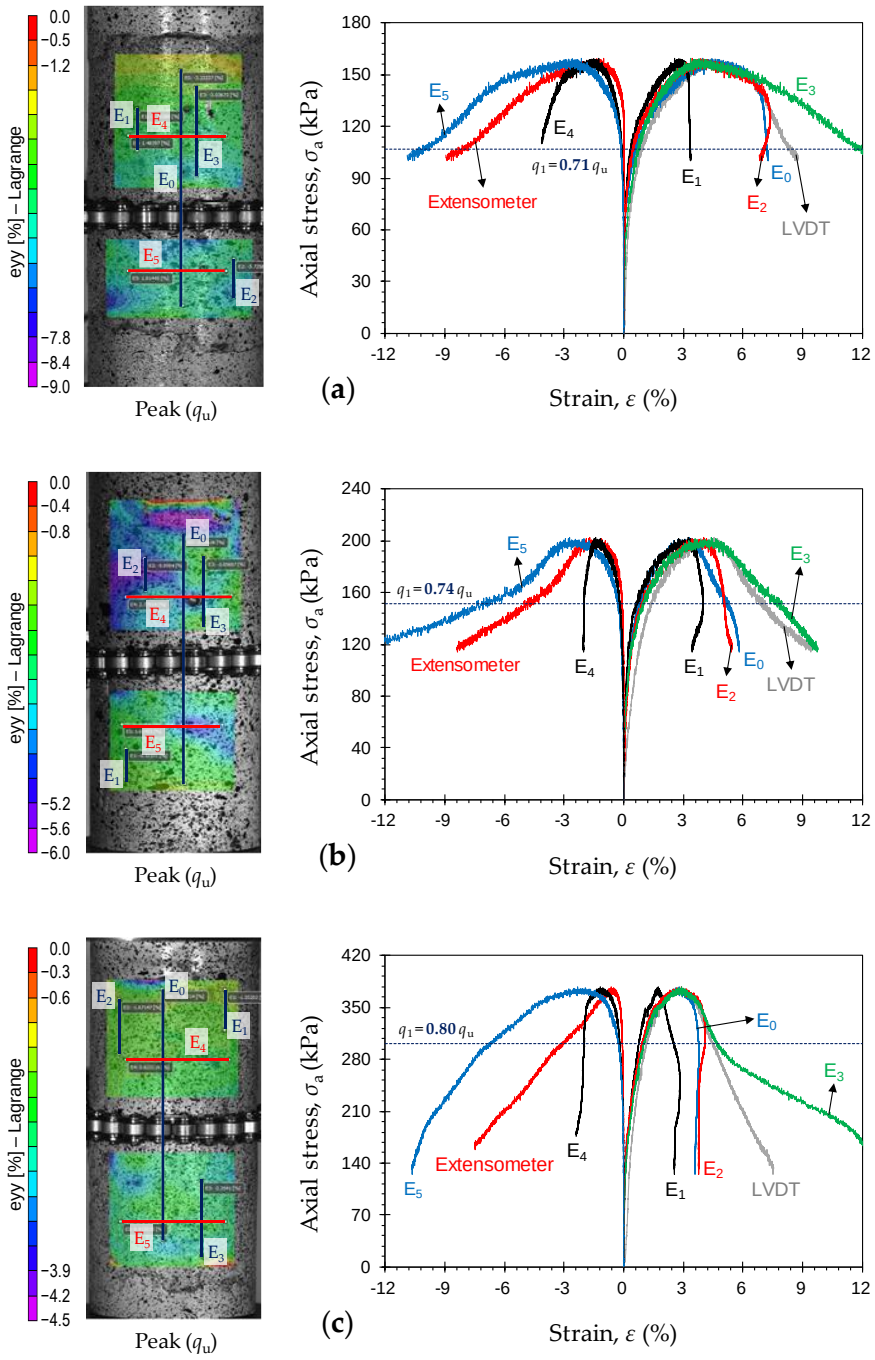

Figure 10. Typical stress-strain curves, obtained by means of various measurement techniques, for the tested samples: (a) $P_2F_0T_{14}$; (b) $P_3F_0T_{14}$; and (c) $P_5F_0T_{14}$.

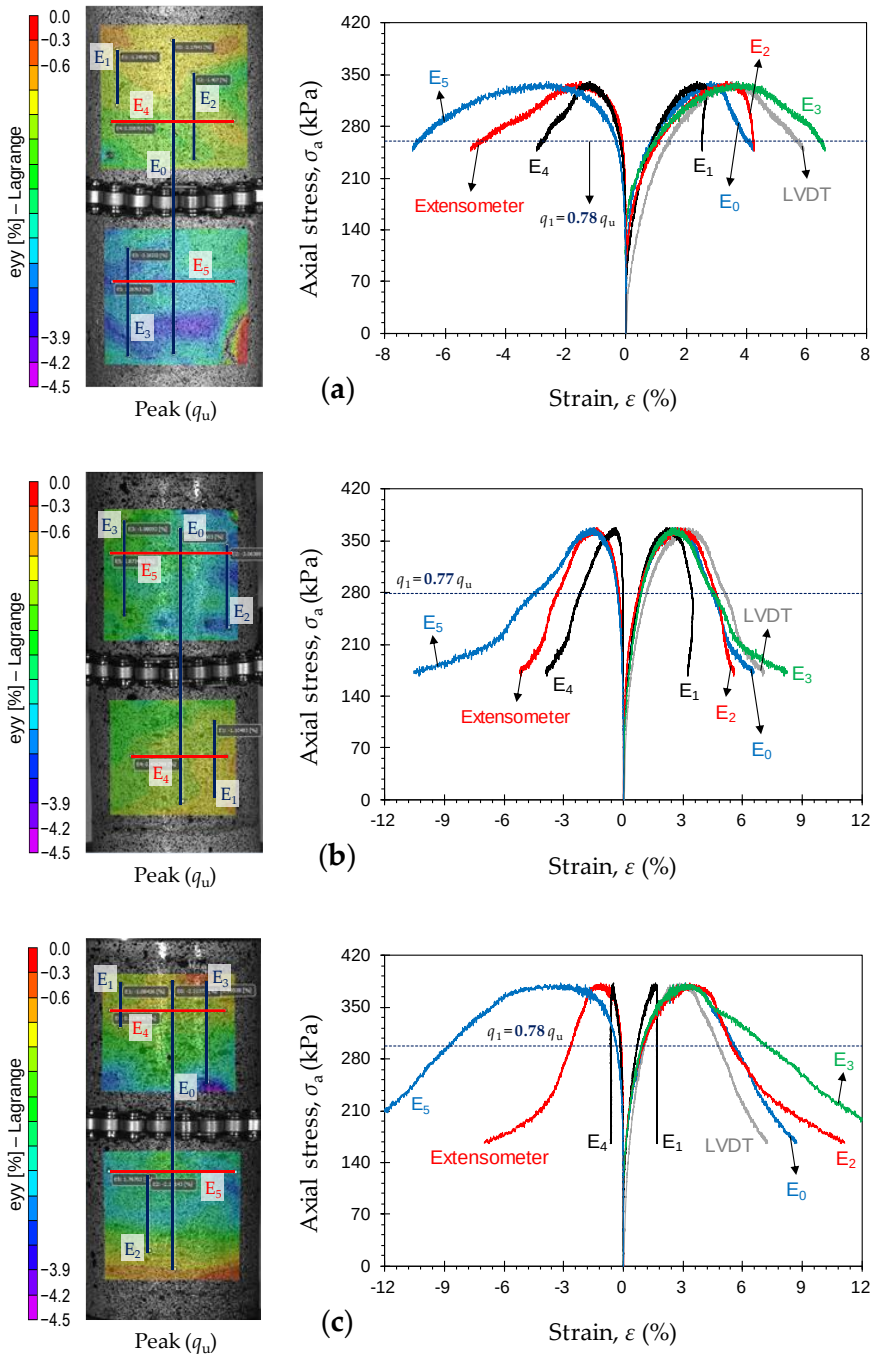

Figure 11. Typical stress-strain curves, obtained by means of various measurement techniques, for the tested samples: (a) $P_4F_1T_{14}$; (b) $P_4F_2T_{14}$; and (c) $P_4F_3T_{14}$.

Chapter 4— Effects of water content, water type and temperature on the rheological behaviour of Slag-cement and fly ash-cement Paste backfill

Statement of Authorship

Yue Zhao[a] , Abbas Taheri[b]*, Murat Karakus[c], Zhongwei Chen[d] and An Deng[e]

[a] **PhD Student** - School of Civil, Environmental and Mining Engineering, The University of Adelaide, Adelaide 5005, Australia (Email: Yue.Zhao@adelaide.edu.au)

[b] **Senior Lecturer** - School of Civil, Environmental and Mining Engineering, The University of Adelaide, Adelaide 5005, Australia (Email: Abbas.Taheri@adelaide.edu.au)

[c] **Associate Professor** - School of Civil, Environmental and Mining Engineering, The University of Adelaide, Adelaide 5005, Australia (Email: Murat.Karakus@adelaide.edu.au)

[d] **Senior Lecturer** - School of Mechanical and Mining Engineering, The University of Queensland, Brisbane 4072, Australia (Email: zhongwei.chen@uq.edu.au)

[e] **Senior Lecturer** - School of Civil, Environmental and Mining Engineering, The University of Adelaide, Adelaide 5005, Australia (Email: An.Deng@adelaide.edu.au)

***Correspondence:** Abbas Taheri

Publication Details:

Zhao, Y., Taheri, A., Karakus, M., Cheng, Z., & Deng, A. (2019). Effects of water content, water type and temperature on the rheological behaviour of Slag-Cement and Fly Ash-cement Paste backfill. *International Journal of Mining Science and Technology*. (Accepted)

Statement of Authorship

Title of Paper	Effects of water content, water type and temperature on the rheological behaviour of Slag-Cement and Fly Ash-cement Paste backfill
Publication Status	☐ Published ☑ Accepted for Publication ☐ Submitted for Publication ☐ Unpublished and Unsubmitted w ork w ritten in manuscript style
Publication Details	Zhao, Y., Taheri, A., Karakus, M., Cheng, Z., & Deng, A. (2019). Effects of water content, water type and temperature on the rheological behaviour of Slag-Cement and Fly Ash-cement Paste backfill. *International Journal of Mining Science and Technology*. Note: [Accepted on 21 Dec 2019]

Principal Author

Name of Principal Author (Candidate)	Yue Zhao		
Contribution to the Paper	Overall paper preparation		
Overall percentage (%)	70%		
Certification:	This paper reports on original research I conducted during the period of my Higher Degree by Research candidature and is not subject to any obligations or contractual agreements with a third party that would constrain its inclusion in this thesis. I am the primary author of this paper.		
Signature		Date	10/01/2020

Co-Author Contributions

By signing the Statement of Authorship, each author certifies that:

i. the candidate's stated contribution to the publication is accurate (as detailed above);

ii. permission is granted for the candidate in include the publication in the thesis; and

iii. the sum of all co-author contributions is equal to 100% less the candidate's stated contribution.

Name of Co-Author	Abbas Taheri Senior Lecturer, School of Civil, Environmental and Mining Engineering, The University of Adelaide		
Contribution to the Paper	Development of research idea, Supervised research, review and revision for the paper		
Signature		Date	06/01/2020

Name of Co-Author	Murat Karakus Associate Professor, School of Civil, Environmental and Mining Engineering, The University of Adelaide		
Contribution to the Paper	Development of research idea, Paper review and revision		
Signature		Date	06/01/2020

Name of Co-Author	Zhongwei Chen Senior Lecturer, School of Mechanical and Mining Engineering, The University of Queensland		
Contribution to the Paper	Involved in the experimental study. Paper review and revision		
Signature		Date	08/01/2020

Name of Co-Author	An Deng Senior Lecturer, School of Civil, Environmental and Mining Engineering, The University of Adelaide		
Contribution to the Paper	Development of research idea, Paper review and revision		
Signature		Date	10/01/2020

Please cut and paste additional co-author panels here as required.

Abstract

The pumping ability and placement performance of fresh cemented paste backfill (CPB) in underground mined cavities depend on its rheological properties. Hence, it is crucial to understand the rheology of fresh CPB slurry, which is related to CPB mixture design and the temperature underground. This paper presents an experimental study investigating the effects of binder type, content, water chemical properties and content, and temperature, on the rheological properties of CPB material prepared using the tailings of a copper mine in South Australia. Portland cement (PC), a newly released commercially manufactured cement called Minecem(MC) and fly ash (FA) were used as the binders added to the mine tailing materials. Various amounts of two different water types were added to the mixtures in the preparation of backfill material slurry. Six different temperatures ranging from 5 to 60 ℃ were, to investigate the effect of temperature on CPB rheology. Overall, the increasing water content and decreasing temperature lead to lower yield stress. Based on the results obtained from the rheological properties of CPB slurry, it was found that at room temperature (25 ℃), with regards to the unconfined compressive strength (UCS) performance, the replacement of 4% PC mixed CPB (28 days UCS 425 kPa) to 3% MC mixed CPB (28 days UCS 519 kPa), reduced the slurry yield stress from 210.7 to 178.5 Pa. The results also show that the chemical composition of water affects the yield stress of CPB slurry and that MC mitigates the negative effect of mine processed water (MW) and thus lead to improve the rheological properties of the slurry. However, the results suggest that the rheological properties of a mixture using MC is very sensitive to the water volume and temperature change. Therefore, using MC in backfill requires better quality control in slump mixing.

Keywords: cemented paste backfill; minecem; rheology; yield stress; fly ash; portland cement

1. Introduction

Mine tailings, deposited after minerals been extracted, are the largest source of waste in mine processing. Approximately 14 billion tons of tailings were produced globally by the mining industry in 2010 (Jones and Boger 2012; Zhao et al. 2018). Tailings have been traditionally deposited into tailings storage facilities which associated with severe environmental, geotechnical and economic concerns (Dold 2014; Franks et al. 2011; Liu et al. 2016). Cement paste backfill (CPB) has increasingly been used to fill the mined cavities in underground mine operations, to re-use tailings in underground mines (Belem and Benzaazoua 2007; Zhang et al. 2012; Fall et al. 2010; Sivakugan et al. 2006). Cemented paste backfill (CPB) recycles processed tailings into underground mined voids, which reduces the volume that needs to be surface-disposed. Using CPB thus mitigates the potential environmental impacts associated with tailings disposal and assists waste management (Fall et al. 2010; Sivakugan et al. 2015; Yilmaz et al. 2014; Rankine and Sivakugan 2007). These refilled CPB can then performs as both the support system and working platform for further ore extraction. CPB is a high-density slurry composed of tailings, a low proportion of cementitious binders (3%-7%) and processed mine water to meet the requirements of designed mechanical properties, where the cementitious binder normally used for CPB operation is Portland cement (PC). In an attempt to minimise costs for binder usage, various alternative binders and additives such as newly developed cement blends, fly ashes, nano-silica particles and superplasticizers have been implemented (Jones and Boger 2012; Zhao et al. 2018 & 2019; Dold 2014; Rankine and Sivakugan 2007; Zhang et al. 2018 & 2019; Xu et al. 2018).

On the other hand, after the mix of CPB slurry, fresh CPB is transported to underground voids by gravity or is pumped through pipelines and boreholes. Thus, CPB slurry should be thickened to obtain a non-settling character for facile pumping into mined cavities resulted from underground mine operations (Sivakugan et al. 2015; Yilmaz et al. 2014; Rankine and Sivakugan 2007). In a general case of pipeline transport, CPB slurry with a yield stress of less than 200 Pa is required (Zhao et al. 2018). Hence the flowability of the paste backfill is an essential parameter in paste design. The rheological properties (i.e. yield stress and viscosity) are associated with the amount of energy consumed to ensure flowability (Kwak et al. 2005; Ouattara et al. 2017; Wu et al. 2013 & 2014). Optimising the CPB flowability in

mines will help to optimise the energy consumed by pumping, and reduce the risk of pipe clogging (Wu et al. 2013 & 2014).

Several studies have been conducted in past years to understand CPB's rheological behaviour better, and it is affecting factors. These studies show that the rheological behaviour is affected by external (e.g. temperature, time) and internal (e.g., cement content, the addition of slag, fly ash or superplasticizers, water type and content) factors. Although the effects of these variables have been widely documented in the literature, the reported results are not consistent as the physical, chemical and mineralogical properties of the tailings varies from mine to mine (Kwak et al. 2005; Ouattara et al. 2017; Wu et al. 2013, 2014 & 2015; Paterson 2013; Heikal et al. 2005; Huynh et al. 2006; Niroshan et al. 2018; Qian and Kawashima 2018).

In this study, the rheological properties of CPB slurry are studied with different concentrations of a newly developed slag-blended cement called Minecem (MC), Portland cement (PC) and fly ash (FA), the pozzolan additive, under various water and temperature condition using the tailings material from a South Australian copper-gold underground mine. MC was chosen for this study as it increases the mechanical properties of CPB compare to PC; however, the effect of MC on the rheological properties of CPB has not been reported previously (Zhao et al. 2018). A series of rheometer tests (for yield stress) were carried out on various MC+FA and PC+FA designs for evaluating the effects of binder and additive contents, as well as water content, water type and temperature on the rheological properties of CPB slurry. The coupled effect of binder type, water content, water type and temperature are discussed as well.

2. Materials

The materials used in this study include tailings, two types of binders (Minecem and Portland cement), fly ash (as an additive to reduce the amount of binder), and both fresh and mine-processed water.

2.1.Mine Tailings

The processed tailings used to study the rheological properties of the paste backfill were sourced from a copper-gold underground mine in South Australia. The tailings sample had an initial water content of about 40%; it was then thoroughly dried in an oven to accurately

control binder and water content. The tailings' particle size distribution was determined with an electric sieve shaker and a sedimentation test. The results of the particle size distribution are shown in Fig. 1. The figure shows that the tailings contained roughly 16% of fine materials, passing 20 micrometres. As a rule of thumb, tailings that contain a minimum of 15% fine material by weight, which passes the 20-micron meter, are suitable for making paste fill (Yilmaz et al. 2014).

Table 1 summarises the chemical element composition of the tailings material provided. The main chemical elements are silicon (26.39%), iron (17.86%) and aluminium (3.81%), with smaller amounts of potassium (1.94%), calcium (0.58%), magnesium (0.45%) and titanium (0.28%); and minor amounts of copper, gold, silver, uranium and cobalt. The quantitative XRD (X-ray diffraction spectrum) analyses carried out on the tailings sample indicated that the sample contained approximately 30% amorphous material. The most abundant minerals detected were quartz, at 27.3%, hematite, at 21.1% and muscovite, at 18.4%.

2.2.Binders and additives

Two binders were used as the major binder. They included a Portland cement (PC), and a newly released commercially manufactured cementitious agent for backfill purposes, referred to as Minecem (MC). MC is a slag-blended cement specifically developed for underground mine backfilling applications. The chemical composition of MC, as supplied by the manufacturer, consists of ground-granulated blast-furnace slag (50%), Portland cement clinker (20%), cement kiln dust (<15%), natural gypsum (5-7%), limestone (<7%), and other mineral additives (Table 2). As stated by the manufacturer, an MC content of 3% (by total dry mass) is anticipated to satisfy standard strength criteria for cemented paste backfills adopted in mining applications. Type C fly ash (FA) was also used as an additive to replace the main binder partially. Fig. 2 displays all the materials used in CPB preparation (dry tailings, binders and fly ash).

2.3.Mine water

The type and quality of water used for making CPB can have an impact on the yield stress of backfill (Wu et al. 2015). Processed water obtained from the mine was used to prepare samples for the laboratory test. The chemical characteristics of the processed water are shown in Table 3. The mine processed water (MW) had a pH value close to neutral and was

used to make CPB in the mine. Tap water (FW) was also used to investigate the influence of dissolved salts that exist in the mine-processed water on CPB viscosity properties.

3. Experimental program

3.1.Mix designs and sample preparations

In this study, the original CPB mixture as recommended by the manufacturer in the mine included 4% Portland cement (PC) and 23% water. The PC then was replaced by 3% MC, as MC demonstrated better strength performance (Zhao et al. 2018). The choice of water content (W_c)=23% was selected as per the mine's requirements; this provides the rheological behaviour required to accommodate easy pumping of the paste into mined cavities.

The binder or binder+additive (MC or PC+FA) and water contents were, respectively, defined as:

$$\mathrm{B_c} = \frac{m_B}{m_B + m_T} \times 100 \tag{1}$$

$$W_c = \frac{m_W}{m_B + m_T + m_W} \times 100 \tag{2}$$

Where $\mathrm{B_c}$ is the binder or binder plus additive content, %; W_c the water content, %; m_B the mass of binder or binder plus additive; m_T the mass of dry tailings; and m_W the mass of processed mine water.

The mine aimed to reduce the amount of binder and replace it with fly ash, which is a waste material. Therefore, this study investigated the rheological properties of CPB containing 3% or less MC and 4% or less PC with different amounts of FA. CPB with 3% MC, 23% water that was prepared at a room temperature of 25 ˚C was considered as the benchmark samples. The intention was to investigate the effects of different binder contents, water contents and temperature values. Each time one of these parameters was changed, where the other parameters remained constant.

The tailings and binder (or binder+additive) were mixed in the dry form under the adopted contents summarised in Table 4. The required amount of processed mine water or tap water corresponding to water content in Table 4 was added to each blend and thoroughly mixed

by a mechanical mixer for approximately 5 min to obtain slurries of uniform consistency at room temperature (around 25 ˚C). After mixing, the CPB slurries were heated or frozen by the MCR 102 Rheometer to a designed temperature (in Table 4) before testing.

3.2.Rheometer testing system

Rheometer vane testing allows for the measurement of the rheological properties of different materials. The MCR 102 Rheometer was used in this study. The MCR rheometers are based on a concept in which the low friction-bearing (Vane) resides at the cutting edge of the sample. Any type of rheological tests in rotational mode is possible with the MCR rheometers. The modularity of MCR rheometer allows for the integration of a wide range of temperature devices and application-specific accessories (Fuyan et al. 2015; Simon and Grabinsky 2013). Fig. 3a displays the MCR 102 Rheometer, which was used to investigate the yield stresses of the CPB samples.

The vane method requires the rotation of a vane, consisting of four perpendicular blades, immersed in the suspension under investigation. The vane's geometry aims to minimise slippage between the sample and the instrument fixture. A schematic diagram of the vane-shear apparatus is shown in Fig. 3b. When measuring the yield stress, the rotation device (3) of the rheometer produces the torque required to rotate the vane. The resistance that the specimen opposes during rotation of the vane (1)(torque, T) is measured by a torsion head (2) and displayed on the instrument console or indicator (4). (Fuyan et al. 2015; Simon and Grabinsky 2013). For the assumption that the fluid yields along with the vane blades, the instant yield stress (i.e. shear stress) induced in the specimen due to the rotating vane is calculated using the following equation:

$$\tau_i = \frac{T_i}{\pi D_v^2 \left(\frac{L_v}{2} + \frac{D_v}{6} \right)} \tag{3}$$

Where τ_i is the calculated instant yield stress, Pa; T_i the corresponding torque experienced by the vane, N m; D_v the vane diameter, mm; and L_v the vane length, mm.

In order to produce consistent and repeatable results, two types of tests were conducted using the rheometer: a constant shear rate (CSR) test and a flow curve (FC) test. Before testing, the freshly mixed paste was well mixed, using a 12 mm vane rotator at a rotation speed of

100 r/min for 20 s, to break the particle agglomerates in the suspension. Following a 5 s pause, two separate tests were carried out following CSR and FC methods.

For the CSR test, the vane-and-cup test was used to measure the yield stress of the material directly, using a constant, low rotation speed, which was 0.1 rotation per minute (r/min). In this constant shear rate mode, the vane suddenly starts rotating at a constant speed. With the vane's slow rotation, shear stress vs. time and viscosity vs. time curves were recorded over 200 s. In the CSR test, as the rotation speed of the vane was low (i.e. 0.1 r/min), the mixed paste was considered to be in a steady-state. The peak value of the shear stress vs. time curve was ultimately presenting the yield stress and the viscosity at a static state (Ouattara et al. 2017; Wu et al. 2013 & 2014; Fuyan et al. 2015; Simon and Grabinsky 2013). Fig. 4a shows the results from 3% MC, with 23% mine-processed water at room temperature (T=25 ˚C), as a typical result. Fig. 4a, the peak value of the shear stress and viscosity vs. time curves ultimately presented the yield stress and the viscosity in the static state equal, respectively, 425.6 Pa and 4267 Pa s.

For the FC tests, the 12 mm vane rotates at different rotation speeds, which was increased in a stepwise manner from 5 rotation per second (rps or strain rate at five s^{-1}) to 135 r/s. At each rotation speed, shear stress and viscosity were recorded after reaching equilibrium. The data collected in the FC tests had to be fitted into rheological models for analysis. The Bingham model, which describes the flow curve of material with yield stress and a constant viscosity (Newtonian behaviour) at stresses above the yield stresses, was used for the data analysis.

The Bingham model is one of the most common models used for cementitious materials (Lang et al. 2015; Haiqiang et al. 2016; Jiang and Fall 2017; Estabragh et al. 2012; Coussot et al. 2002). The model is given below:

$$\tau = \tau_0 + \mu \dot{\gamma} \tag{4}$$

Where τ is the shear stress, Pa; $\dot{\gamma}$ the shear rate; τ_0 the Bingham yield stress, Pa; μ the plastic viscosity, Pa s.

An example of the shear stress and viscosity vs shear rate curve is given in Fig. 4b for the CPB of 3% MC, with 23% mine-processed water at room temperature (T=25 ˚C). Fig. 4b, the intersection of the Y-axis and the shear stress trend line represent the yield stress value

in the dynamic state, which is equal to 178.5 Pa. The slope of the yield stress vs. shear rate curve represent the dynamic viscosity, which is equal to 0.385 Pa s.

4. Results and discussions

Cementitious materials' yield stress forms from both the microstructure of the particle-to-particle network through colloidal interaction, or direct contact, and cement hydration bonding (calcium-silicate-hydrate or C-S-H and portlandite or C-H). The result of the CSR method measured static yield stress corresponds to a state before the structure is broken down, which is the stress necessary to initiate flow. Meanwhile, the FC result represents the dynamic yield stress represents the minimum stress needed to sustain or terminate the flow of the material (Sharma and Sivapullaiah 2016). The existence of separate dynamic and static yield stresses in the same material is known in cement-based systems. As shown in Fig. 4, the static yield stress and viscosity are higher than the dynamic values that consider the corresponding structural states. The reason why the static yield stress is higher than the dynamic yield stress is that the static yield stress corresponds to an undisturbed, well-connected microstructure, while the dynamic yield stress corresponds to a broken-down microstructure (Qian and Kawashima 2018; Lee et al. 2017; Mahlaba et al. 2011). With the help of the MCR 102 rheometer, both static and dynamic yield stress and viscosity values were measured using CSR and FC methods. At 25 ˚C, the difference between two yield stress and viscosity results of FC and CSR, with the same binder content of MC=3%, and using the different volumes of mine-processed water are graphically displayed in Fig. 5.

Overall, the results of the CSR method and the FC method have a similar trend for the two values (yield stress and viscosity). Dynamic yield stress is representing the minimum stress needed to sustain or terminate the flow of the material, which is usually adopted to investigate the pumping energy requirement for CPB slurry (Wu et al. 2013). Therefore, in order to keep this paper more concise, only the results of the flow curve method, which representing dynamic yield stress are presented and discussed.

The effects of various parameters on the rheological properties of fresh CPB, including the binder type and content, water type and content, and initial temperature are discussed below.

4.1.Effect of water content

Fig. 6 shows the relations between the yield stress versus water content for three different binders (MC, PC and FA) when the binder content is 3%. Fig. 6 shows that, regardless of binder type, the yield stress decreases with an increase in water content. It is due to the reduced number of direct particle-particle contacts and the increased thickness of the lubricating film around the solid particles in the higher-water-content specimens, making it easier for the particles to slide past one another during shearing (Wu et al. 2015; Simon and Grabinsky 2013).

The results presented in Fig. 6 also show that the yield stress of CPB that is mixed with MC (MC-CPB) is much more sensitive to water content change than the one mixed with PC (PC-CPB). For CPB with 23% or more water content, the use of MC results in a more workable paste, even with the same binder content. The trend of fly ash contributes less to the slurry's yield stress than both of the primary binders.

In the presence of PC and water in CPB, a series of short/immediate- and long-term chemical reactions initiated in the tailings-binder medium, hence amending the tailings fabric into a unitary mass of enhanced mechanical performance. Long-term chemical reactions consist of pozzolanic reactions, which are strongly time-dependent and less effective on the early age CPB workability. The short-term chemical reactions include cation exchange and flocculation-agglomeration, short-term reactions lead to a notable increase in soil plasticity, workability, and early age strength and swell-consolidation capacity (Estabragh et al. 2012; Lee et al. 2017; Mahlaba et al. 2011). Under the influence of short-term chemical reactions, the cemented paste backfill prepared with Portland cement (PC-CPB) tends to be less influenced by water content change.

FA often contains a low content of cementitious material; and FA is dominated by large fractions of silicate and, particularly, aluminate. As such, the addition of FA, alongside cementitious binder as its activator, induces the development of pozzolanic reactions (or cementation products) in the matrix. A short-term chemical reaction could not be found in FA-tailing mixtures (Lee et al. 2017; Mahlaba et al. 2011). The yield stress of CPB that is mixed with FA (FA-CPB) mainly contribute to the particle-to-particle network through colloidal interaction, and hence the workability of cemented paste backfill prepared with fly ash (FA-CPB) is more sensitive to water content (Wu et al. 2015).

MC is a slag-blended cement that mainly consists of ground-granulated blast-furnace slag (50%), Portland cement clinker (20%). Comparing to PC, it has a larger average particle size and less short-term cementitious material. As a result, the yield stress of cemented paste backfill prepared with Minecem (MC-CPB) mixed with 23% or more water is lower than the stress of PC-CPB and the yield stress of MC-CPB mixed with 18% or less water is higher than the yield stress of PC-CPB.

4.2.Effect of binder type and content

One of the aims of this study was to compare the rheological behaviour of PC-CPB and MC-CPB. Fig. 7 compares the yield stress of PC-CPB and MC-CPB of different percentages and mixed with a different amount of FA as an additive when the water content is equal to 23%. The figure shows that, in general, with the same amount of binder, the MC-CPB has better rheological properties when compared with the PC-CPB.

However, the unconfined compressive strength (UCS) after 28 days' curing, using PC-CPB with 3% and 4% binder usage are 363.5 and 425 kPa respectively. MC-CPB with 3% binder results in 519 kPa UCS after 28-days' curing (Zhao et al. 2018). Therefore, with regards to the stope stability (UCS performance), MC-CPB with 3% binder usage can be regarded as a sustainable alternative for conventional PC-CPB with 4% dosage. The yield stress for 4% PC-CPB and 3% MC-CPB are 210.7 Pa and 178.5 Pa, respectively. 3% of MC-CPB has a significant advantage over 4% PC-CPB in terms of yield stress. Hence, with regards to the stope stability, the use of MC reduced the yield stress compare to PC.

Fig. 7 shows the evolution of the yield stress of the CPB samples with increasing FA content, at various MC and PC dosage levels. The results demonstrated that regardless of the type and amount of the binder, yield stress increases slightly with the addition of a small amount of FA. Right after mixing, the sample with 4% PC and 2% FA showed the highest yield stress, followed by a mixture with 3% MC and 2% FA. The result is likely due to the higher forms of cementitious and pozzolanic gels such as calcium silicate hydrates, calcium aluminate hydrates, and ettringite. The hydrated products surrounding the ash particles will bond adjacent tailings particles and will increase the specific surface area and surface energy, leading to the particle assembly (Haiqiang et al. 2016). Furthermore, as shown in Fig. 7, the addition of FA result in a more significant increment of yield stress for MC-CPB to the yield stress for PC-CPB.

As explained previously, the 3% MC-CPB has a slightly higher 28 days' curing UCS than does 4% PC-CPB. While comparing the yield stress of 3% MC-CPB and 4% PC-CPB, the 3% MC-CPB had much lower yield stress than 4% PC-CPB. Therefore, the results show that for the same stope strength requirement, the use of MC mitigates both the binder dosage and the energy required to ensure adequate pipeline transport of CPB.

4.3.Effect of water type

This study investigated a comparison of the yield stress of the CPB samples, made using two types of water: tap water or fresh water (FW) and mine-processed water (MW). Fig. 8 compares the yield stress of two binders (i.e. MC and PC) in which the samples demonstrated a trend similar to that demonstrated in Fig. 8 concerning the addition of fly ash.

Mahlaba et al. concluded that the use of a more salty brine would result in a less workable paste using a given binder content (Mahlaba et al. 2011). Simon and Grabinsky also suggested that the particle-to-particle interactions in a cement paste slurry with an ionic strength elevated by increasing the saline content lead to higher yield stress (Simon and Grabinsky 2013). Furthermore, the high level of calcium (480 mg/L) and magnesium (280 mg/L) was found in favour of forming cementitious hydration bonding (Wu et al. 2015).

The CPB samples with mine-processed water in this study generated higher yield stress values. It can be seen in Fig. 8 that the magnitude of the CPB slurry's yield stress using mine water is 30-50 Pa higher than TW CPB slurry for the same binder type and content. This significant difference in the yield stress value is mainly due to the difference in the composition of mine-processed water. By using mine-processed water, the thickness of the paste may elevate the energy requirements for paste transportation and may make the paste more susceptible to pipeline blockages. Comparing MC-CPB and PC-CPB, the use of mine-processed water had an overall smaller increase in the yield stress of MC-CPB than PC-CPB; 28.6 and 45.7 Pa on average, respectively. The results show that the use of MC mitigates the negative influences of mine-processed water on CPB yield stresses when compared to PC.

4.4.Effect of temperature

Every underground mine is unique with regards to its temperature conditions. The temperature in the underground varies with the geographical location and other factors, such as the depth of the mine, geological conditions/age of formations and other human-induced temperature variations (Fall et al. 2010). In order to understand the application of the

experimental results to field conditions, the present study investigated the effect of temperature on the yield stress of CPB. The results, which are illustrated in Fig. 9, clearly show the significant influence of the temperature on the yield stress of CPB slurry mixtures. The increase in the temperature results in an overall increase in the yield stress of CPB.

Contrary to these results, Lee et al., reported that the increase of temperature results in FA-CPB slurry mixtures with lower yield stress (Lee et al. 2017). They mentioned that the increase of temperature increases both the ionic and particle activities in addition to the occurrence of aggregation breakdown. Increase of the temperature would improve the paste's fluidity, which is coherent with all liquid. However, the yield stress of CPB also depends on binder coagulation. Lee et al. further explained that the difference in yield stresses at different temperatures becomes less sensitive for higher temperatures, indicating that the acceleration of FA hydration at higher temperatures produces more substantial amounts of cementitious products, which, in turn, increases yield stress (Lee et al. 2017).

In Fig. 9, both yield stresses for MC-CPB and PC-CPB increase with an increase in temperature. Wu et al. also found a similar effect for temperature on the yield stress of CPB using Portland cement. This is due to the reason that raising the temperature accelerates the progress of cement hydration, which in turn increases the yield stress in the mixture (Wu et al. 2013 & 2014). Therefore, increasing the temperature has two opposite effects on the yield stress: (a) decreasing the yield stress due to the accelerated particle-to-particle movement; (b) increasing yield stress due to the accelerating binder hydration. The influence of effect (b) becomes more significant with the increase of binder cementitious and content. The result presented in Fig. 9 shows that the effect (b) is more significant in this study and masks effect (a).

As shown in Fig. 9, the yield stresses for the MC-CPB, at all the temperatures, for CPB with 23% or more water content is lower than those measured for the PC-CPB. For slurries containing more than 23% water, the temperature had much less influence on MC-CPB yield stresses than on PC-CPB yield stresses. Where the yield stress of MC-CPB increased dramatically with the increase of temperature when CPB slurry contains less than 23% of water. The results indicate that the yield stress variations of MC-CPB are more sensitive to both water content and temperature variation.

5. Conclusions

This study investigated the rheological performance of CPB material when mixed with different binder types and contents. Portland cement (i.e. PC-CPB) and a new binder, Minecem, which is prepared mainly as a mixture of cement and slag (MC-CPB), were used as the primary binders, while fly ash was used as a supplementary binder. Moreover, the effects of water type and content, and temperature, on the rheological properties of CPB materials were investigated. Based on the results obtained, the following conclusions appear to be warranted:

- Regardless of binder type, the yield stress decreases with an increase in water content. However, the MC-CPB showed a more significant increase in fluidity after an increase in water content. Hence, the variations of MC-CPB viscosity appears to be more sensitive to water-content change.
- With regards to the UCS performance, the replacement of 4% PC-CPB (28 days UCS 425 kPa) to 3% MC-CPB (28 days UCS 519 kPa), reduced the slurry yield stress from 210.7 Pa to 178.5 Pa.
- The FA additive increased the yield stress of the CPB mixtures. This may be due to the dense particle packing. However, lower increments were shown with MC-CPB when compared to PC-CPB.
- The use of mine-processed water increases the yield stress of fresh CPB, and thus reduces its flowability. An increase in the salinity of the pore fluid causes an increase in the yield stress. This effect is more evident for PC-CPB than MC-CPB. Some elements (Ca and Mg) can enrich the binder coagulation, hence further increasing the yield stress.
- Overall regardless of binder type, the yield stress increase with an increase in temperature; however, the increase in temperature influences the two components of CPB yield stress in different ways. The results indicate that the influence of temperature on yield stress for MC-CPB are much more sensitive than that for PC-CPB, while the water content is equal to or less than 23%. Thus, when using MC as an alternative for conventional PC, a better regulatory system might be required for both in situ water content and temperature condition.

References

Belem, T., & Benzaazoua, M. (2007). Design and Application of Underground Mine Paste Backfill Technology. *Geotechnical and Geological Engineering, 26*(2), 175-175. doi:10.1007/s10706-007-9167-y

Coussot, P., Nguyen, Q. D., Huynh, H. T., & Bonn, D. (2002). Viscosity bifurcation in thixotropic, yielding fluids. *Journal of Rheology, 46*(3), 573-589. doi:10.1122/1.1459447

Dold, B. (2014). Submarine Tailings Disposal (STD)—A Review. *Minerals, 4*(3), 642-666. doi:10.3390/min4030642

Estabragh, A.R., Namdar, P., & Javadi, A.A. (2012). Behaviour of cement–stabilized clay reinforced with nylon fiber. *Geosynthetics International*. 19(85).

Fall, M., Célestin, J. C., Pokharel, M., & Touré, M. (2010). A contribution to understanding the effects of curing temperature on the mechanical properties of mine cemented tailings backfill. *Engineering Geology, 114*(3-4), 397-413. doi:10.1016/j.enggeo.2010.05.016

Franks, D. M., Boger, D. V., Côte, C. M., & Mulligan, D. R. (2011). Sustainable development principles for the disposal of mining and mineral processing wastes. *Resources Policy, 36*(2), 114-122. doi:10.1016/j.resourpol.2010.12.001

Fuyan, L., Yuanyuan, Q., Ningxiao, Z., Jie, G., Xuedi, H., & Miao, W. (2015). Yield Stress Measurement of Dense Pastes with Pipe Transport and Vane. *Journal of Dispersion Science and Technology, 37*(11), 1563-1569. doi:10.1080/01932691.2015.1118701

Haiqiang, J., Fall, M., & Cui, L. (2016). Yield stress of cemented paste backfill in sub-zero environments: Experimental results. *Minerals Engineering, 92*, 141-150. doi:10.1016/j.mineng.2016.03.014

Heikal, M., Morsy, M. S., & Aiad, I. (2005). Effect of treatment temperature on the early hydration characteristics of superplasticized silica fume blended cement pastes. *Cement and Concrete Research, 35*(4), 680-687. doi:10.1016/j.cemconres.2004.06.012

Huynh, L., Beattie, D. A., Fornasiero, D., & Ralston, J. (2006). Effect of polyphosphate and naphthalene sulfonate formaldehyde condensate on the rheological properties of dewatered

tailings and cemented paste backfill. *Minerals Engineering, 19*(1), 28-36. doi:10.1016/j.mineng.2005.05.001

Jiang, H., & Fall, M. (2017). Yield stress and strength of saline cemented tailings materials in sub-zero environments: slag-paste backfill. *Journal of Sustainable Cement-Based Materials, 6*(5), 314-331. doi:10.1080/21650373.2017.1280428

Jones, H., & Boger, D. V. (2012). Sustainability and Waste Management in the Resource Industries. *Industrial & Engineering Chemistry Research, 51*(30), 10057-10065. doi:10.1021/ie202963z

Kwak, M., James, D. F., & Klein, K. A. (2005). Flow behaviour of tailings paste for surface disposal. *International Journal of Mineral Processing, 77*(3), 139-153. doi:10.1016/j.minpro.2005.06.001

Lang, L., Song, K.-I., Lao, D., & Kwon, T.-H. (2015). Rheological Properties of Cemented Tailing Backfill and the Construction of a Prediction Model. *Materials, 8*(5), 2076-2092. doi:10.3390/ma8052076

Lee, J. K., Ko, J., & Kim, Y. S. (2017). Rheology of Fly Ash Mixed Tailings Slurries and Applicability of Prediction Models. *Minerals, 7*(9), 165. doi:10.3390/min7090165

Liu, Q., Liu, D., Liu, X., Gao, F., & Li, S. (2016). Research and application of surface paste disposal for clay-sized tailings in tropical rainy climate. *International Journal of Mineral Processing, 157*, 227-235. doi:10.1016/j.minpro.2016.11.014

Mahlaba, J. S., Kearsley, E. P., Kruger, R. A., & Pretorius, P. C. (2011). Evaluation of workability and strength development of fly ash pastes prepared with industrial brines rich in and Cl− to expand brine utilisation. *Minerals Engineering, 24*(10), 1077-1081. doi:10.1016/j.mineng.2011.05.015

Niroshan, N., Sivakugan, N., & Veenstra, R. L. (2018). Flow Characteristics of Cemented Paste Backfill. *Geotechnical and Geological Engineering*. doi:10.1007/s10706-018-0460-8

Ouattara, D., Yahia, A., Mbonimpa, M., & Belem, T. (2017). Effects of superplasticizer on rheological properties of cemented paste backfills. *International Journal of Mineral Processing, 161*, 28-40. doi:10.1016/j.minpro.2017.02.003

Paterson, A. J. C. (2013). Pipeline transport of high density slurries: a historical review of past mistakes, lessons learned and current technologies. *Mining Technology, 121*(1), 37-45. doi:10.1179/1743286311y.0000000020

Qian, Y., & Kawashima, S. (2018). Distinguishing dynamic and static yield stress of fresh cement mortars through thixotropy. *Cement and Concrete Composites, 86*, 288-296. doi:10.1016/j.cemconcomp.2017.11.019

Rankine, R. M., & Sivakugan, N. (2007). Geotechnical properties of cemented paste backfill from Cannington Mine, Australia. *Geotechnical and Geological Engineering, 25*(4), 383-393. doi:10.1007/s10706-006-9104-5

Sharma, A. K., & Sivapullaiah, P. V. (2016). Ground granulated blast furnace slag amended fly ash as an expansive soil stabilizer. *Soils and Foundations, 56*(2), 205-212. doi:10.1016/j.sandf.2016.02.004

Simon, D., & Grabinsky, M. (2013). Apparent yield stress measurement in cemented paste backfill. *International Journal of Mining, Reclamation and Environment, 27*(4), 231-256. doi:10.1080/17480930.2012.680754

Sivakugan, N., Rankine, R. M., Rankine, K. J., & Rankine, K. S. (2006). Geotechnical considerations in mine backfilling in Australia. *Journal of Cleaner Production, 14*(12-13), 1168-1175. doi:10.1016/j.jclepro.2004.06.007

Sivakugan, N., Veenstra, R., & Naguleswaran, N. (2015). Underground Mine Backfilling in Australia Using Paste Fills and Hydraulic Fills. *International Journal of Geosynthetics and Ground Engineering, 1*(2). doi:10.1007/s40891-015-0020-8

Wu, A., Wang, Y., Wang, H., Yin, S., & Miao, X. (2015). Coupled effects of cement type and water quality on the properties of cemented paste backfill. *International Journal of Mineral Processing, 143*, 65-71. doi:10.1016/j.minpro.2015.09.004

Wu, D., Cai, S.-j., & Huang, G. (2014). Coupled effect of cement hydration and temperature on rheological properties of fresh cemented tailings backfill slurry. *Transactions of Nonferrous Metals Society of China, 24*(9), 2954-2963. doi:10.1016/s1003-6326(14)63431-2

Wu, D., Fall, M., & Cai, S. J. (2013). Coupling temperature, cement hydration and rheological behaviour of fresh cemented paste backfill. *Minerals Engineering, 42*, 76-87. doi:10.1016/j.mineng.2012.11.011

Xu, W., Cao, P., & Tian, M. (2018). Strength Development and Microstructure Evolution of Cemented Tailings Backfill Containing Different Binder Types and Contents. Minerals, 8(4). doi:10.3390/min8040167

Yilmaz, T., Ercikdi, B., Karaman, K., & Kulekci, G. (2014). Assessment of strength properties of cemented paste backfill by ultrasonic pulse velocity test. *Ultrasonics*, *54*(5), 1386-1394. doi:10.1016/j.ultras.2014.02.012

Zhang, J., Deng, H., Taheri, A., Deng, J., & Ke, B. (2018). Effects of Superplasticizer on the Hydration, Consistency, and Strength Development of Cemented Paste Backfill. *Minerals, 8*(9), 381. doi:10.3390/min8090381

Zhang, J., Li, M., Taheri, A., Zhang, W., Wu, Z., & Song, W. (2019). Properties and Application of Backfill Materials in Coal Mines in China. *Minerals, 9*(1). doi:10.3390/min9010053

Zhang, Q., Zhang, J., Huang, Y., & Ju, F. (2012). Backfilling technology and strata behaviours in fully mechanized coal mining working face. *International Journal of Mining Science and Technology, 22*(2), 151-157. doi:10.1016/j.ijmst.2011.08.003

Zhao, Y., Soltani, A., Taheri, A., Karakus, M., & Deng, A. (2018). Application of Slag–Cement and Fly Ash for Strength Development in Cemented Paste Backfills. *Minerals, 9*(1), 22. doi:10.3390/min9010022

Zhao, Y., Taheri, A., Soltani, A., Karakus, M., & Deng, A. (2019). Strength Development and Strain Localization Behaviour of Cemented Paste Backfills Using Portland Cement and Fly Ash. *Materials (Basel), 12*(20). doi:10.3390/ma12203282

List of Tables

Table 1. Chemical composition of the used tailings (as supplied by the distributor)

Component	SiO_2	Fe_2O_3	Al_2O_3	K_2O	CaO	MgO	TiO_2	Na_2O	Other
Mass percentage (%)	38.27	37.70	7.19	2.33	0.81	0.75	0.56	0.07	12.32

Table 2. Chemical composition of MC (as supplied by the manufacturer)

Component	Mass percentage (%)
Ground–granulated blast–furnace slag	50
Portland cement clinker	20
Cement kiln dust	<15
Natural gypsum	5–7
Chloride, Cl-	<8
Limestone	<7
Sulphur trioxide, SO_3	<4
Crystalline silica	<1

Table 3. Chemical composition of the processed mine water (as supplied by the distributor)

Component	CL−	SO42−	NO3−	Na+	Ca_2+	K+	Mg_2+
Value (mg/L)	5800	2400	6	3800	480	380	280

Table 4. Mix designs and their properties

(a) Effect of water content

MC content (%)	PC content (%)	FA content (%)	Mixing water type	Water content (%)	Temperature (˚C)
3	0	0	Processed water	13, 18, 23, 28, 33	25
0	3	0	Processed water	13, 18, 23, 28, 33	25
0	0	3	Processed water	13, 18, 23, 28, 33	25

(b) Effect of binder type and content using processed water

MC content (%)	PC content (%)	FA content (%)	Mixing water type	Water content (%)	Temperature (˚C)
2	0	0, 0.5, 1, 1.5, 2	Processed water	23	25
2.5	0	0, 0.5, 1, 1.5, 2	Processed water	23	25
3	0	0, 0.5, 1, 1.5, 2	Processed water	23	25
0	2	0, 0.5, 1, 1.5, 2	Processed water	23	25
0	3	0, 0.5, 1, 1.5, 2	Processed water	23	25
0	4	0, 0.5, 1, 1.5, 2	Processed water	23	25

(c) Effect of binder type and content using tap water

MC content (%)	PC content (%)	FA content (%)	Mixing water type	Water content (%)	Temperature (˚C)
2	0	0, 0.5, 1, 1.5, 2	Tap water	23	25
2.5	0	0, 0.5, 1, 1.5, 2	Tap water	23	25
3	0	0, 0.5, 1, 1.5, 2	Tap water	23	25
0	2	0, 0.5, 1, 1.5, 2	Tap water	23	25
0	3	0, 0.5, 1, 1.5, 2	Tap water	23	25
0	4	0, 0.5, 1, 1.5, 2	Tap water	23	25

(d) Effect of temperature

MC content (%)	PC content (%)	FA content (%)	Mixing water type	Water content (%)	Temperature (˚C)
3	0	0	Processed water	13, 18, 23, 28, 33	5, 15, 25, 35, 45, 60
0	3	0	Processed water	13, 18, 23, 28, 33	5, 15, 25, 35, 45, 60

List of Figures

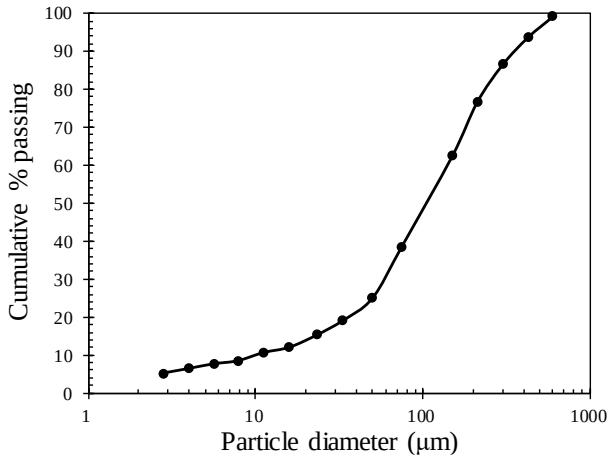

Figure 1. The particle size distribution of used tailings

(a) Dry tailings (b) Minecem (c) Fly ash (d) Portland cement

Figure 2. Materials used for CPB sample preparation

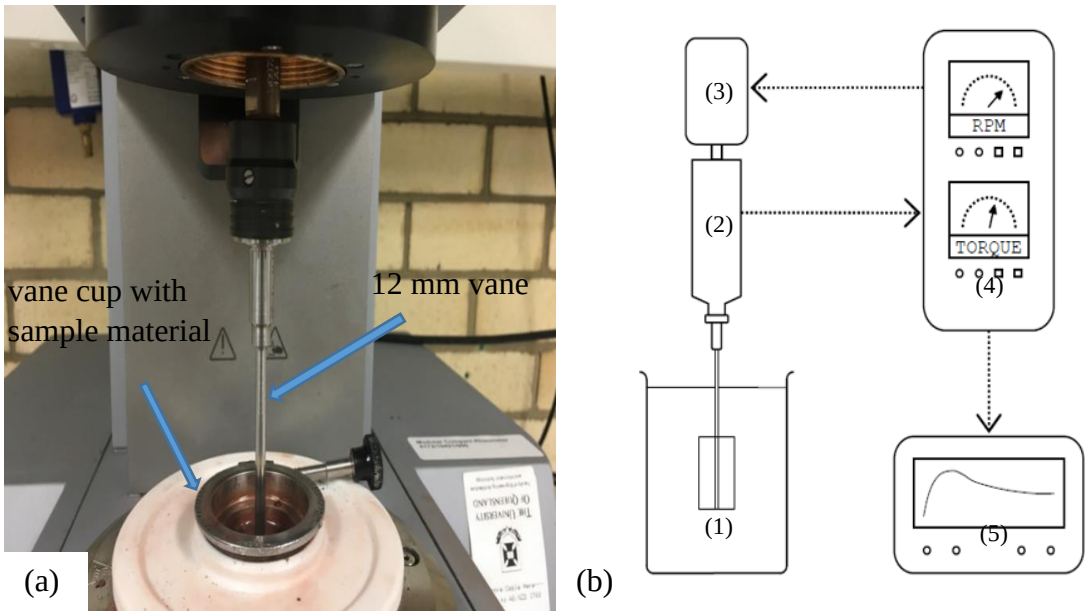

Figure 3. MCR 102 rheometer (a) Photo of the rheometer in use, (b) Schematic diagram ((1) Vane (2) Torsion head (3) Rotation device (4) Instrument console (5) Recorder)

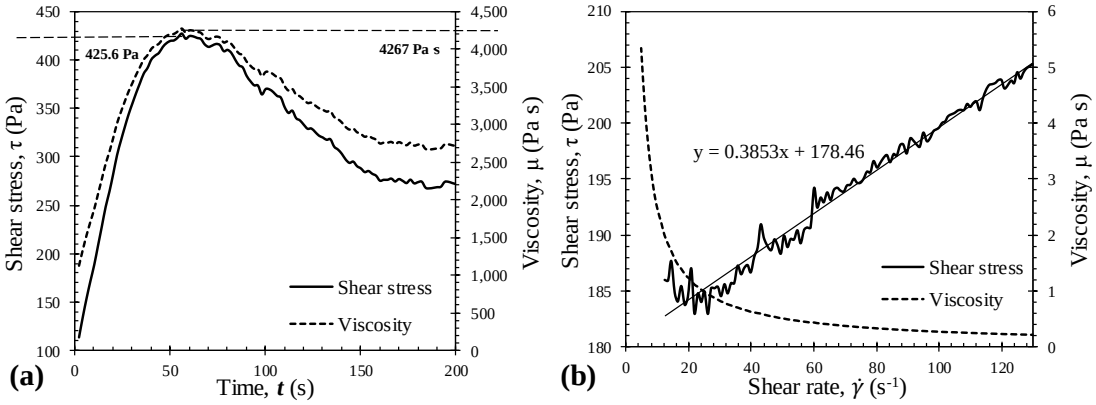

Figure 4. For CPB mixture contains 3% Minecem and 23% processed water at 25 ˚C (a) Shear stress and viscosity vs. time plots for CSR test, (b) Shear stress and viscosity vs. shear rate plots for the FC test

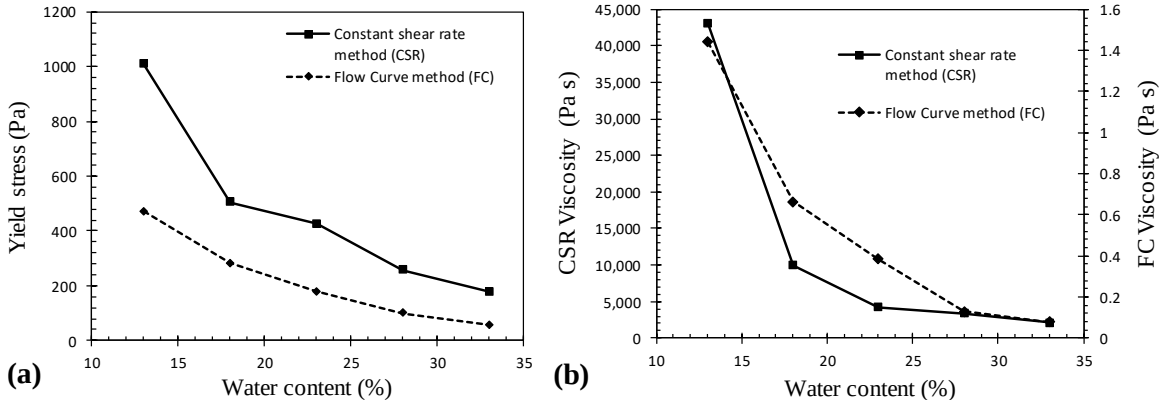

Figure 5. Compare of CSR and FC method while using 3% MC and 23% mine water at 25 ˚C (a) Yield stress, (b) Viscosity

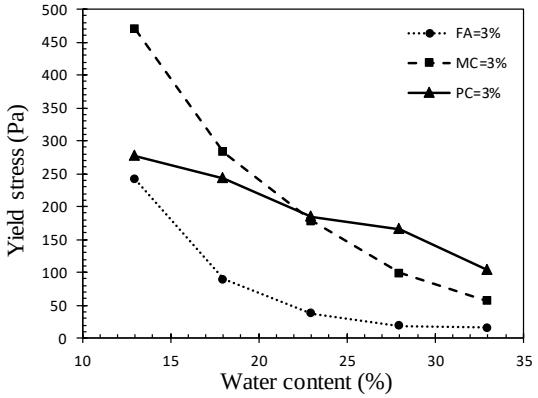

Figure 6. Effect of water content on the different binder used

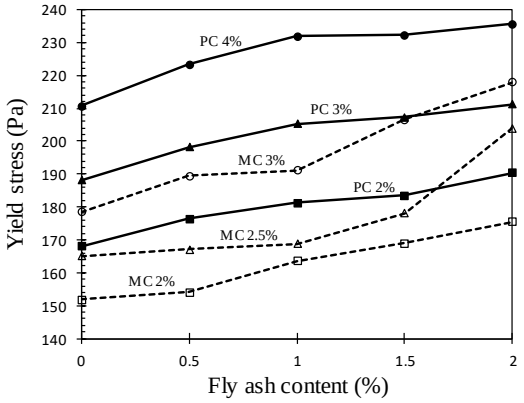

Figure 7. Effect of binder type (MC, PC and fly ash) content on yield stress development using 23% mine processed water at 25 ˚C

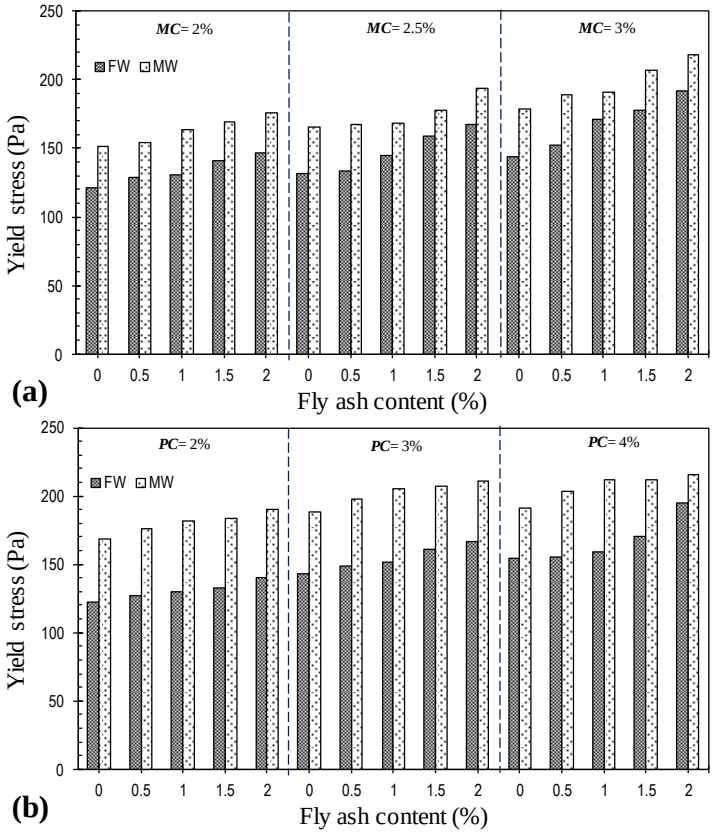

Figure 8. Effect of water type on yield stress development (a) MC-CPB (b) PC-CPB

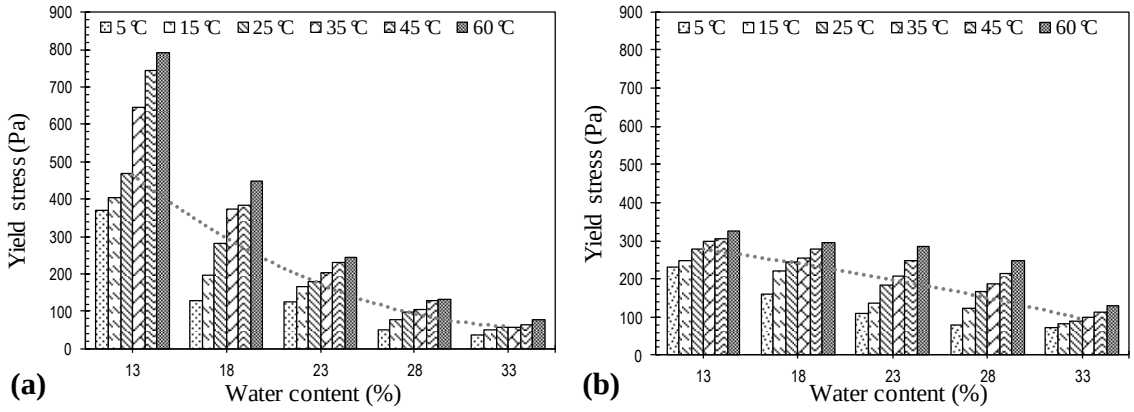

Figure 9. Effect of temperature on yield stress development using mine water (a) MC=3% (b) PC=3%

Chapter 5— The effect of curing under applied stress on the strength of Cement Paste Backfill

Statement of Authorship

Yue Zhao[a]*, Abbas Taheri[b], Murat Karakus[c], and An Deng[d]

[a] **PhD Student** - School of Civil, Environmental and Mining Engineering, The University of Adelaide, Adelaide 5005, Australia (Email: Yue.Zhao@adelaide.edu.au)

[b] **Senior Lecturer** - School of Civil, Environmental and Mining Engineering, The University of Adelaide, Adelaide 5005, Australia (Email: Abbas.Taheri@adelaide.edu.au)

[c] **Associate Professor** - School of Civil, Environmental and Mining Engineering, The University of Adelaide, Adelaide 5005, Australia (Email: Murat.Karakus@adelaide.edu.au)

[d] **Senior Lecturer** - School of Civil, Environmental and Mining Engineering, The University of Adelaide, Adelaide 5005, Australia (Email: An.Deng@adelaide.edu.au)

***Correspondence:** Yue Zhao

Publication Details:

Zhao, Y., Taheri, A., Karakus, M., & Deng, A. (2020). The effect of curing under applied stress on the strength of Cement Paste Backfill. *Journal of Rock Mechanics and Geotechnical Engineering*. (Submitted)

Statement of Authorship

Title of Paper	The effect of curing under applied stress on the strength of Cement Paste Backfill
Publication Status	☐ Published ☐ Accepted for Publication ☑ Submitted for Publication ☐ Unpublished and Unsubmitted w ork w ritten in manuscript style
Publication Details	Zhao, Y., Taheri, A., Karakus, M., & Deng, A. (2020). The effect of curing under applied stress on the strength of Cement Paste Backfill. *Journal of Rock Mechanics and Geotechnical Engineering.*

Principal Author

Name of Principal Author (Candidate)	Yue Zhao		
Contribution to the Paper	Overall paper preparation		
Overall percentage (%)	70%		
Certification:	This paper reports on original research I conducted during the period of my Higher Degree by Research candidature and is not subject to any obligations or contractual agreements with a third party that would constrain its inclusion in this thesis. I am the primary author of this paper.		
Signature		Date	10/01/2020

Co-Author Contributions

By signing the Statement of Authorship, each author certifies that:

i. the candidate's stated contribution to the publication is accurate (as detailed above);
ii. permission is granted for the candidate in include the publication in the thesis; and
iii. the sum of all co-author contributions is equal to 100% less the candidate's stated contribution.

Name of Co-Author	Abbas Taheri Senior Lecturer, School of Civil, Environmental and Mining Engineering, The University of Adelaide		
Contribution to the Paper	Development of research idea, Supervised research, review and revision for the paper		
Signature		Date	06/01/2020

Name of Co-Author	Murat Karakus Associate Professor, School of Civil, Environmental and Mining Engineering, The University of Adelaide		
Contribution to the Paper	Development of research idea, Paper review and revision		
Signature		Date	06/01/2020

Name of Co-Author	An Deng Senior Lecturer, School of Civil, Environmental and Mining Engineering, The University of Adelaide		
Contribution to the Paper	Development of research idea, Paper review and revision		
Signature		Date	10/01/2020

Please cut and paste additional co-author panels here as required.

Abstract

After placing the Cement Paste Backfill (CPB) material in the stope, and during the setting and hardening processes, the weight of CPB stope applies an axial load over the CPB paste, from the upper layer to the bottom layer of the stope, may result in a consolidation of early-aged backfill material in the lower layers which is called self-consolidation. Because of this phenomenon, the mechanical properties of CPB in-situ could be considerably different from laboratory results. Hence, it is crucial to understand the effect of self-consolidation on the behaviour of backfill material. This paper presents an experimental study of investigating the effects of axial applied stress (A_s) during curing, which represents the various self-consolidation condition and curing time on the mechanical properties of CPB material prepared using the tailings of a copper mine in South Australia and a newly released commercially manufactured cement called Minecem (MC). New curing under pressure equipment is designed and manufactured to cure CPB samples under pressure. The equipment is capable of applying and measuring axial load during curing and then measure the passive pressure that is applied laterally to the sample. Using this equipment, the samples were cured under different weights in environmentally-controlled curing room. The samples were tested under uniaxial and triaxial compressive loading condition. Scanning electron microscopy (SEM) studies were also carried out to observe the evolution of fabric in response to A_s. The axial applied stress (A_s) during curing improved the bonding/connection interface generated between the tailing aggregates and thus led to improved mechanical performance compared with CPB samples containing the same binder under the sample curing period with less or none axial applied stress. The greater the A_s, the higher the developed strength, toughness and stiffness. For instance, a sample that is cured under 3.6 MPa axial load for 28 days demonstrates an unconfined compressive strength value of five times more than a sample that is cured under atmospheric curing condition. Under the triaxial compression test, all CPB samples showed strain-hardening under triaxial compression. However, the greater A_s during curing and/or the longer the curing period, the higher the deviator stress at 5% axial strain (q_5), toughness and stiffness, with the former, the applied axial pressure, portraying a more significant role. Passive lateral stress was measured during the curing period and was found to be representative of underground barricade stress.

Keywords: cemented paste backfill; minecem; self-consolidation; axial applied stress; passive lateral stress; barricade stress

1. Introduction

Cement Paste Backfill (CPB) is a relatively new backfilling method, originating in the 1980s. CPB consists of mine tailings mixed with a low proportion of binders, and a relatively high proportion of water (Rankine and Sivakugan, 2007). This technology has been widely used to fill underground, mined voids. It provides an alternative disposal method for the tailings from mineral processing (Kesimal et al. 2005; Orejarena and Fall 2010; Sivakugan et al. 2015; Belem et al. 2002; Fall et al. 2010; Ouattara et al. 2017; Zhao et al. 2019). Over the past few decades, CPB technology has increasingly been used to revive mined cavities in underground mine operations, owing to its low operating cost. It minimises the adversities associated with tailings disposal, and it has higher mechanical performance compared with other backfilling methods, i.e. rock fills and hydraulic fills (Fall et al. 2010; Ouattara et al. 2017).

CPB is a cement mixed geomaterial. Properties of cement mixed materials are subjected to curing and loading conditions (Taheri and Tatsuoka 2012 & 2015; Taheri et al. 2012). Factors that affect the properties of CPB, such as chemical composition, particle size, tailings' distribution, binder types, water to cement ratios, and temperature, have been presented in the previous studies (Fall et al. 2005; Kesimal et al. 2005; Klein and Simon 2006; Ouellet et al. 2004; Zhang et al. 2018 & 2019; Zhao et al. 2018 & 2019). Numerous researchers have indicated that laboratory studies using conventional molds, which are typically used to determine mine backfill design values, tend to underestimate the mechanical strength of a given CPB mixture when assessed over the same curing period as field-acquired data (le Roux et al. 2013; Grabinsky et al. 2008). Some studies show the laboratory-made CPB samples are underestimating 50% to 200% of the strength of CPB specimens obtained by coring from in situ backfill stope (Belem and Benzaazoua 2007; Revell 2004).

Self-weight consolidation of the backfill material after placement is one major factor which may contribute to the in situ strength of CPB. In an in situ condition, mine fills are on an enormous scale with at least 20 m height. After placing the CPB material in the stope, and during the setting and hardening processes, the weight of CPB stope applies an axial load over the CPB paste, from the upper layer to the bottom layer of the stope, may facilitate the consolidation of early-aged bottom layers. In this study, this consolidation is called self-consolidation. With the increase of backfill depth, because of the weight of CPB in the stope, the bottom layers of CPB are cured under pressure.

In order to determine the effect of self-consolidation on the behaviour of backfill material, Yilmaz et al. (2009) developed a system called CUAPS (Curing under Applied Pressure System). Using this system, the CPB samples in the lab were cured under specific applied pressures to imitate in situ curing conditions and a strength increase of 20% to 50% was found (Yilmaz et al. 2015). However, the maximum applied pressure during curing was limited to 300 kPa (equivalent axial stress to 10 m CPB underground). In addition, the passive lateral pressure that is applied to the CPB sample during curing has not been investigated in the literature. Moreover, previous studies on the under-pressure cured sample were only limited to uniaxial compressive testing. To the best of our knowledge, the behaviour of this material under confined loading never has been investigated.

The present study investigates the influence of various axially applied pressures using a newly developed slag-blended cement for three different curing times in confined and unconfined loading condition. A novel curing under pressure equipment is designed and developed, which can apply axial stress to the sample during curing and measure the passive lateral stress. Using this equipment, axial stress was applied to the CPB sample during curing up to 150 m self-weight height. A series of uniaxial and triaxial compression tests were carried out to evaluate the effect of self-weight curing on the strength, brittleness and stiffness of the CPB samples that are cured for a different period of time under different confining pressures. Scanning electron microscopy (SEM) studies were carried out to observe the evolution of fabric in response to the applied stress during curing. Lateral passive stress resulted from applied axial pressure during curing was measured to investigate the passive pressure that may apply to barricade during backfill placement.

2. Materials

2.1.Mine Tailings

Processed tailing was sourced from a copper-gold underground mine located in South Australia and used in the present study. Table 1 illustrates the physical and mechanical properties of the tailings, determined as per relevant ASTM and Australian standards (AS).

Characterisation results indicate that the tailings sample has a specific gravity G_s of 2.4. The conventional grain-size analysis carried out by ASTM D422–07, indicated a fines fraction (<75 μm) of 38.6%, along with 55.2% fine sand (0.075–0.425 mm) and 6.2% medium sand (0.425–2 mm). Atterberg limits were determined using an experimental procedure adapted

from standard ASTM D4318. Mine tailings showed only slight plasticity, with a liquid limit of 19.2% and a plastic limit of 13.1. These tailings can be categorised as non-plastic silt (ML) according to the Unified Soil Classification System. The standard Proctor compaction test carried out by ASTM D698–12, indicated an optimum water content of 8.7% and a maximum dry unit weight of γ_{dmax} = 20.2 kN/m^3.

The chemical composition of the tailings is provided in Table 1. The chemical composition mainly consists of silicon dioxide (SiO_2) and iron oxide (Fe_2O_3), with mass fractions of 38.27% and 37.70%, respectively.

2.2.Binders and Mixing water

A commercially manufactured cementitious agent, commonly traded as Minecem in Australia (hereafter referred to as MC), was used as the binder. Minecem is a slag–blended cement specifically developed for underground, mine-backfilling applications. The chemical composition of MC, as supplied by the manufacturer, consists of granulated blast furnace slag (50%), Portland cement clinker (20%), cement kiln dust (< 15%), natural gypsum (5–7%), limestone (< 7%), and other mineral additives (see Table 2). Minecem content of 3% by total dry weight, according to the manufacturer, ought to satisfy standard strength criteria for cemented paste backfills that are used in mining applications.

The mixing water used was mine-processed water, which was sourced from the mine. The chemical composition of the processed mine water is presented in Table 2. The pH was found to be 7.5, from which the water was characterised as a neutral substance.

3. Experimental Program

3.1.Curing Apparatus

3.1.1. General Set-up

A Curing under Pressure Apparatus (CPA), was developed to mimic in situ placement and curing in the mine stop. The apparatus is developed slightly different from the system previously manufactured by Yilmaz et al. (2009). The top of CPA was connected to a single convoluted air spring with a maximum allowable pressure of 600 kPa. The applied pressure was provided by an ENERPAC hydraulic pump, as shown in Figure 1. The applied axial load can then be translated through the centre plate and a 20 kN capacity load cell to a PVC piston on top of the CPB sample during curing. The axially applied load was recorded by

the load cell and can be translated to axial pressure using the area of the sample top surface. Once the load level reaches the prescribed value, six screw nuts above and below the centre plate should then be tightened to keep the continuous axial pressure during CPB curing. This curing apparatus can simulate different placement and curing conditions at maximum allowable pressure up to 6 MPa.

On the bottom of this CPA, a special designed double-layer mold was placed on the base plate with a 5 mm $\times$ 5 mm hole with a porous stone (at the bottom plate) which allow the water to drain. The inner part of the mold was contributed by three 120 degrees arch to form a circle for 5 mm thickness with an inner radius of 63mm. After curing progress, the inner part could be extracted from the outer layer together with the CPB sample to prevent any damage during demolding. The outer layer of the mold is a rigid transparent metal round tube with 1mm thickness. The outer mold is designed as thin as possible to make the deformation easier to be measured for the passive lateral strain, which will be discussed in Section 3.1.2.

3.1.2. Passive lateral stress measurement

As shown in Figure 2b, two strain gauges were attached on the surface of the steel mold outer layer. The outer layer of the mold was designed thin enough to maximise the measured lateral deformation. Three calibration tests have been done, to define the relationship between the lateral deformation of steel mold and the passive lateral stress resulted from axial pressure and the results are shown in Figure 2a. Using those results, the measured steel mold deformation for various tests can be calculated to passive stress in the lateral direction.

The CPA was used to estimate the CPB under the specific height of backfill stope. Figure 3 displays the layout and position of an ideal specimen without considering the filling sequence. During the test, when applying stress in the axial direction, passive lateral stress occurred, where the axial stress is the total overburden pressure that would have occurred. If no arching effect happens where there is no stress redistribution to the surrounding rock mass, the passive lateral stress may represent the barricade stress when the CPB specimen is at the same level as the barricade.

3.2.Sample Preparation

In this study, the tailings and binder (3% MC content) were mixed in dry form. The required amount of processed mine water corresponding to a water content of 30% was added to each

blend and thoroughly mixed by a mechanical mixer for approximately 5 minutes to obtain slurries of uniform consistency. The choice of binder content and water content were selected as per the mine's requirements. The resultant slurries were poured into the cylindrical double-layer molds (see Section 3.1.1.) (measuring 63 mm in diameter and 130 mm in height) in one-third length increments, each layer being tamped approximately 25 times with a small metal rod to remove entrapped air. The PVC loading piston was then placed into the mold to prevent any leakage of slurries during curing after applying axial pressure.

A total of twelve curing condition designs, as outlined in Table 3, were prepared in this study. For ease of presentation, the following coding system is used to designate the various curing condition designs:

$$A_a T_b \tag{1}$$

where A_a = a MPa axial stress; T_b = b days of curing

In this study, four different axial stress level were selected (0 MPa,1.2 MPa, 2.4 MPa and 3.6 MPa) which almost represent four different overburden dead load for various depth (CPB under 0 m, 50 m, 100 m and 150 m stope) of CPB in a large backfill stope. For each curing design, six samples were prepared at the same batch for two uniaxial compressive loadings (to repeat the test) and four triaxial compressive loadings.

3.3.Uniaxial and Triaxial Compression Tests

Uniaxial compression tests described in the ASTM C39 standard were carried out on CPB samples at a displacement rate of 0.1 mm/min. CPB samples prepared under different curing condition were also subjected to triaxial compression tests described in the ASTM D2850 under four different confining pressure values (i.e. 0.5 MPa, 1 MPa, 2 MPa, 4 MPa) using the same displacement rate of 0.1 mm/min. For ease of presentation, the following coding system is used to designate the various curing condition designs:

$$A_a T_b C_c \tag{2}$$

where A_a = a MPa axial stress; T_b = b days of curing; C_c = c MPa of confining pressure

To ensure sufficient accuracy, six samples were tested under uniaxial compression test for 14 days curing with1.2 MPa axial stress during curing. A mean UCS value of 796 kPa was observed, and the UCS data were found to range within a standard deviation (SD) = 30.9 kPa. The calculated coefficient of variation (CV) is 4.1%, thus validating the sufficient accuracy and, hence, the repeatability of the adopted sample preparation technique and the implemented testing procedure.

3.4.Scanning electron microscopy analysis

The Philips XL20 scanning electron microscope (PHILIPS, Amsterdam, The Netherlands), with a resolution of 4 μm and a maximum magnification ratio of 50,000 ×, was employed for SEM imaging. Scanning electron microscopy (SEM) studies were carried out to investigate the evolution of fabric in response to applied axial stress during curing. A total of 8 mix designs consisting of 4 different applied stress during curing at three different curing periods (i.e. 7, 14 and 28 days) were examined ($A_{0,\ 1.2,\ 2.4,\ 3.6}T_{7,\ 14,\ 28}$).

4. Results and Discussions

4.1.Uniaxial compressive strength

Figure 4 a, b, c illustrates the stress-strain curves, obtained from the UC tests, for various applied axial pressure during curing for different days. As expected, at any given curing time, the greater the applied axial pressure, the higher the peak UC strength, following a monotonically–increasing trend.

With the same 7-day curing time – A_aT_7 where a = {0, 1.2, 2.4, 3.6}, while the applied stress increases, the UCS resulted in 476.5 KPa, 659.1 kPa, 751.3 kPa, 1097.5 kPa, respectively. CPB samples provided a UCS increase of 38.3%, 57.6% and 130.2% for 1.2 MPa, 2.4 MPa, 3.6 MPa applied stress in 7 days curing (Figure 4 a), 29.6%, 105.4%, 206.1% for 1.2 MPa, 2.4 MPa, 3.6 MPa applied stress in 14 days curing (Figure 4b) and 60.3%, 234.5%, 390.7% for 1.2 MPa, 2.4 MPa, 3.6 MPa applied stress in 28 days curing (Figure. 4c) respectively. Overall with the increase of curing time, the influence of axial applied stress becomes more pronounced.

The axial strain at failure, denoted as ε_f, is an indication of the material's ductility. Figure 5a illustrates the variations of axial strain at failure against axial applied stress for the samples tested at various curing times. In general, the higher the axial applied stress and the longer

the curing period, the lower the ductility. As shown in Figure 5a, with an increase in curing pressure, as well as curing time, the samples become more brittle. When samples are cured at 2.4 MPa and 3.6 MPa pressure, their strain failure values at different curing times are close to each other.

The elastic stiffness modulus, defined as the secant modulus at 50% of the peak UC strength and denoted as E_{50}, was also measured for various MC mixtures, and the results are provided in Figure 5b. Similar to the peak UC strength, the development of stiffness was in favour of a greater applied axial stress and a longer curing time. The samples cured for 7 days, for instance, resulted in E_{50} = 12.5 MPa, 23.6 MPa, 64.2 MPa and 106.5 MPa, respectively for applied axial stress equal to 0 MPa, 1.2 MPa, 2.4 MPa and 3.6 MPa. Curing under high axial stress (=3.6 MPa) results in a significant increase in stiffness value of CPB samples.

4.2.Triaxial compression strength

Stress-strain curves, obtained from the triaxial compression tests, for CPB curing under various applied axial pressure under four different confining pressure (0.5 MPa, 1 MPa, 2 MPa, 4 MPa) are provided in Figure A1, A2 and A3 in the Appendix section. The stress-strain locus for all CPB samples did not exhibit a rise-fall behaviour with visually detectable peak point. Thus the CPB is a soft material and signifying a strain-hardening under triaxial compression. Hence the deviator stress and strain energy at 5% axial strain (ε_a= 5%), (i.e. q_5 and E_5) respectively, were selected to represent the material's strength and toughness under triaxial compression.

Figure 6 illustrates the variations of q_5 against confining pressure for the samples A_aT_b where a = {0, 1.2, 2.4, 3.6} and b = {7, 14, 28}. At any given axially applied pressure, the greater the confining pressure, the higher the q_5. As typical cases, for a = {0}, and b = {7}. The use of 0.5 MPa, 1 MPa, 2 MPa, 4 MPa confining pressure result in q_5 values of 1081.3 kPa, 1169.7 kPa, 1212.8 kPa and 1588.5 kPa, respectively. For that fixed a and b values, a q_5 increase of 8.1%, 12.1% and 46.9% for c = {0.5, 1, 2, 4}. For any given curing time, and an increase in axial applied stress promoted a more pronounced increase in the q_5 value. For instance, the samples $A_{2.4}T_7C_{0.5,\ 1,\ 2,\ 4}$ resulted in q_5 = 1727.9 kPa, 2348.3 Pa, 3246.9 kPa and 5439.2 kPa, respectively. Where the q_5 increase for c = {0.5, 1, 2, 4} is 35.9 %, 98.3 % and 209.7 %. Similarly, for any give axial applied stress, an increase in curing time promoted a notable, yet less pronounced increase in q_5. The sample $A_{2.4}T_7$ resulted in 209.7 % increase

between 4 MPa and 0.5 MPa confining pressure, while the 14 and 28 days curing lead to a lower increment of 152.6% and 143.8% between 4 MPa and 0.5 MPa confining pressure.

The area under a typical stress-strain curve up to the failure point (in this case 5% axial strain), defined as strain energy (or energy adsorption capacity) and denoted as E_5, serves as a measure of the material's toughness. Figure 7a illustrates the variations of strain energy at 5% axial strain against axial applied stress for the samples tested under various confining pressures, and cured under different curing time and curing pressure. The variations of strain energy followed a trend similar to that observed for the deviator strength, thus indicating that the greater the applied axial stress during curing and the longer the curing period, the higher the degree of toughness. Also, strain at failure increases with an increase in confining pressure.

The elastic stiffness modulus, defined as the peak tangent modulus the stress-strain and denoted as E_{tan}, was also measured for various CPB samples, and the results are provided in Figure 7b. Similar to the strain energy, the development of stiffness was in favour of a higher axial applied stress, longer curing time and higher confining pressure.

4.3.Fabric Evolution During Consolidation

In the presence of water, calcium-rich binders such as MC act as a precursor agent, initiating a series of short/immediate- and long-term chemical reactions in the tailings-binder medium, thereby amending the tailings fabric into a unitary mass of enhanced mechanical performance. Short-term chemical reactions include cation exchange and flocculation-agglomeration, the amending roles of which are often limited concerning neutrally charged particles such as sands, silts and tailings. For fine-grained soils containing notable fractions of negatively charged clay particles; however, short-term reactions lead to notable improvements in soil plasticity, workability, and early age strength and swell-consolidation capacity (Soltani et al. 2019). Long-term chemical reactions consist of pozzolanic reactions, which are strongly time-dependent; their commencement and evolution require a specific and often prolonged period of curing. During pozzolanic reactions, calcium cations ($Ca2+$) and hydroxide anions (OH^-), both released from the cementitious binder, or in this case MC, gradually react with silicate (SiO_2) and aluminate (Al_2O_3) units from the tailings, thereby resulting in the formation of cementation products/gels, i.e., Calcium–Silicate–Hydrates (C–S–H), Calcium–Aluminate–Hydrates (C–A–H) and Calcium–Aluminate–Silicate–Hydrates (C–A–S–H), which encourage solidification and flocculation of the tailings particles and

hence the development of a uniform, dense matrix coupled with enhanced strength performance. Quite clearly, the commencement and evolution of pozzolanic reactions are strongly dependent on applied axial stress during curing. In general, the higher the applied axial stress during curing, the greater the number of developed cementation products and hence, the higher the developed peak UCS.

Figure 8 illustrates SEM micrographs for the CPB samples at 28 day-curing under a various axially applied stresses during curing (0 MPa, 1.2 MPa, 2.4 MPa, 3.6 MPa). Figure 8a shows that the micro-fabric of the 0 MPa axial stress sample displays a partly loose matrix, along with a notable number of large inter- and intra-assemblage pore-spaces thereby corroborating the existence of an edge-to-edge dispersed structure. Figure 8b illustrates the sample cured under 1.2 MPa applied stress, the micro-fabric become more uniform with less visible pore-spaces and more cementation products were visiable. For the samples cured under 2.4 MPa and 3.6 MPa, as shown in Figure 8c and d, the micro-fabric became more uniform, indicating aggregation of the tailings particles and hence the development of a dense matrix with an edge-to-face flocculated structure. Prevalent cementation products, i.e., C–S–H, C–A–H and C–A–S–H, were visible between and within the tailings aggregates, which portrayed a major role in reducing the number of inter- and intra-assemblage pore-spaces in the matrix.

4.4.Passive lateral stress

During the preparation of the CPB sample cured under applied pressure, the CPA apparatus was used. Two strain gauges were attached outside the steel mold to estimate the passive lateral stress result by the axial load.

During curing, the passive lateral stress increases with the applied axial stress. The calculated peak passive stress in the lateral direction under the influence of different axial loading is shown in Figure 9. An estimated trend of peak barricade stress vs. axial applied stress (or overburden dead load) could be seen from this figure as well. A case study on the in situ axial and lateral stress measurement of CPB stope carried out by Thompson et al. (2012) has shown the horizontal stress (barricade stress) is to be 20% to 50% of the actual axial stress. In Figure 9, the x-axis is the total overburden load without considering the arching effect. Thompson et al. (2012) and Fahey et al. (2009 and 2011) demonstrated that, due to arching effect, the effective axial stress is about 30% to 45% of the total overburden weight. Considering the finding from the studies mentioned above, the lateral stress should be equal

to 6-23% of the overburden weight. The relation between applied stress, A_s and passive lateral stress, σ_l in Figure 9 shows that the passive lateral stress is about 20% of the overburden pressure which is within the 6-23% range. Hence the passive lateral stress measured by the developed equipment could be an acceptable representing the underground barricade stress.

5. Conclusions

In this study, a new Curing under Pressure Apparatus (CPA) is developed, which can apply a very high axial stress to the CPA samples during curing while measuring the passive lateral stress. The CPA is utilized to investigate the mechanical performance of CPB material under uniaxial and triaxial compressive loading with various applied axial pressure during curing. A new binder, Minecem, which is prepared mainly as a mixture of cement and slag (MC-CPB), was used as the binder at 3% content. Moreover, the effects of curing time under various applied axial pressure during curing on the mechanical properties of CPB materials were investigated. Based on the results obtained, the following conclusions appear to be warranted:

- The greater the applied axial pressure during curing, and the longer the curing period, the higher the developed strength, stiffness and toughness whit the CPB sample under both uniaxial and triaxial compression test.
- The axial strain at failure— an indication of the material's ductility — demonstrated a trend similar to that observed for the strength in an adverse manner.
- Regardless of curing time, the uniaxial compressive stress increase with an increase in applied axial pressure during curing. However, the uniaxial compressive stress of CPB sample cured for longer-term showed a more significant increase. A CPB sample that is cured under 3.6 MPa axial load for 28 days curing, the difference demonstrates a UCS five times more than a sample that is cured under atmospheric curing condition.
- Overall, the greater the applied axial pressure during curing and/or the longer the curing period, the higher the deviator stress at 5% axial strain (q_5), toughness and stiffness, with the former, the applied axial pressure, portraying a more significant role.
- The introduce of applied axial pressure during curing improved the bonding/connection interface generated between the tailings aggregates, and thus led to improved mechanical performance compared with CPB inclusions with less or no applied axial pressure during curing.

- The passive lateral stress measures during curing by CPA apparatus were found at about 20% of the applied axial pressure during curing. The passive lateral stress that is measured with a newly developed equipment may represent the stress that is applied to the barricade in an underground mine.

References

Belem, T., Benzaazoua, M., Bussière, B., & Dagenais, A.-M. (2002). Effects of settlement and drainage on strength development within mine paste backfill. *Tailings and Mine Waste'02,* 27-30 January 2002, Fort Collins, Colorado, Balkema, Rotterdam, 139-148.

Belem, T., & Benzaazoua, M. (2007). Design and Application of Underground Mine Paste Backfill Technology. *Geotechnical and Geological Engineering, 26*(2), 175-175. doi:10.1007/s10706-007-9167-y

Fahey, M., Helinski, M., & Fourie, A. (2009). Some aspects of the mechanics of arching in backfilled stopes. *Canadian Geotechnical Journal, 46*(11), 1322-1336. doi:10.1139/t09-063

Fahey, M., Helinski, M., & Fourie, A. (2011). Development of Specimen Curing Procedures that Account for the Influence of Effective Stress During Curing on the Strength of Cemented Mine Backfill. *Geotechnical and Geological Engineering, 29*(5), 709-723. doi:10.1007/s10706-011-9412-2

Fall, M., Benzaazoua, M., & Ouellet, S. (2005). Experimental characterization of the influence of tailings fineness and density on the quality of cemented paste backfill. *Minerals Engineering, 18*(1), 41-44. doi:10.1016/j.mineng.2004.05.012

Fall, M., Célestin, J. C., Pokharel, M., & Touré, M. (2010). A contribution to understanding the effects of curing temperature on the mechanical properties of mine cemented tailings backfill. *Engineering Geology, 114*(3-4), 397-413. doi:10.1016/j.enggeo.2010.05.016

Grabinsky, M., Bawden, W.F., Simon, D., & Thompson, B., (2008). In Situ Properties of Cemented Paste Backfill in an Alimak Stope, *Canadian Geotechnical Conference*, Edmonton, 21-24 September, 790-796.

Kesimal, A., Yilmaz, E., Ercikdi, B., Alp, I., & Deveci, H. (2005). Effect of properties of tailings and binder on the short-and long-term strength and stability of cemented paste backfill. *Materials Letters, 59*(28), 3703-3709. doi:10.1016/j.matlet.2005.06.042

Klein, K., & Simon, D. (2006). Effect of specimen composition on the strength development in cemented paste backfill. *Canadian Geotechnical Journal, 43*(3), 310-324. doi:10.1139/t06-005

le Roux, K., Bawden, W. F., & Grabinsky, M. F. (2013). Field properties of cemented paste backfill at the Golden Giant mine. *Mining Technology, 114*(2), 65-80. doi:10.1179/037178405x44557

Orejarena, L., & Fall, M. (2010). The use of artificial neural networks to predict the effect of sulphate attack on the strength of cemented paste backfill. *Bulletin of Engineering Geology and the Environment, 69*(4), 659-670. doi:10.1007/s10064-010-0326-7

Ouattara, D., Yahia, A., Mbonimpa, M., & Belem, T. (2017). Effects of superplasticizer on rheological properties of cemented paste backfills. International Journal of Mineral Processing, 161, 28-40. doi:10.1016/j.minpro.2017.02.003

Ouellet, S., Bussière, B., Benzaazoua, M., Aubertin, M., & Belem, T. (2004). Effect of binder type and mixing water chemistry on microstructural evolution of cemented paste backfill. *In Proceedings of the 57th annual Canadian geotechnical conference and 5th joint IAH-CNC/CGS conference*, Quebec City, QC, Canada, 25–27.

Rankine, R. M., & Sivakugan, N. (2007). Geotechnical properties of cemented paste backfill from Cannington Mine, Australia. Geotechnical and Geological Engineering, 25(4), 383-393. doi:10.1007/s10706-006-9104-5

Revell M.B. (2004). Paste – how strong is it? *In: Proceedings of the 8th International Symposium on Mining with Backfill*, Nonferrous Metals Society of China, Beijing, China, September 19–21: 286–294.

Sivakugan, N., Veenstra, R., & Naguleswaran, N. (2015). Underground Mine Backfilling in Australia Using Paste Fills and Hydraulic Fills. *International Journal of Geosynthetics and Ground Engineering, 1*(2). doi:10.1007/s40891-015-0020-8

Soltani, A., Deng, A., Taheri, A., & O'Kelly, B. C. (2019). Engineering Reactive Clay Systems by Ground Rubber Replacement and Polyacrylamide Treatment. *Polymers (Basel), 11*(10). doi:10.3390/polym11101675

Taheri, A., & Tatsuoka, F. (2012). Stress-strain relations of cement–mixed gravelly soil from multiple–step triaxial compression test results. *Soils Found*, 52, 748–766, doi:10.1016/j.sandf.2012.07.014

Taheri, A., & Tatsuoka, F. (2015). Small- and large-strain behaviour of a cement-treated soil during various loading histories and testing conditions. *Acta Geotech*, 10, 131–155, doi:10.1007/s11440-014-0339-7

Taheri, A., Sasaki, Y., Tatsuoka, F., & Watanabe, K. (2012). Strength and deformation characteristics of cemented-mixed gravelly soil in multiple-step triaxial compression. *Soils and Foundations*, 52(1): 126-145

Thompson, B. D., Bawden, W. F., & Grabinsky, M. W. (2012). In situ measurements of cemented paste backfill at the Cayeli Mine. *Canadian Geotechnical Journal, 49*(7), 755-772. doi:10.1139/t2012-040

Yilmaz, E., Belem, T., & Benzaazoua, M. (2015). Specimen size effect on strength behaviour of cemented paste backfills subjected to different placement conditions. *Engineering Geology, 185*, 52-62. doi:10.1016/j.enggeo.2014.11.015

Yilmaz, E., Benzaazoua, M., Belem, T., & Bussière, B. (2009). Effect of curing under pressure on compressive strength development of cemented paste backfill. *Minerals Engineering, 22*(9-10), 772-785. doi:10.1016/j.mineng.2009.02.002

Zhang, J., Deng, H., Taheri, A., Deng, J., & Ke, B. (2018). Effects of Superplasticizer on the Hydration, Consistency, and Strength Development of Cemented Paste Backfill. *Minerals, 8*(9), 381. doi:10.3390/min8090381

Zhang, J., Li, M., Taheri, A., Zhang, W., Wu, Z., & Song, W. (2019). Properties and Application of Backfill Materials in Coal Mines in China. *Minerals, 9*(1). doi:10.3390/min9010053

Zhao, Y., Soltani, A., Taheri, A., Karakus, M., & Deng, A. (2018). Application of Slag–Cement and Fly Ash for Strength Development in Cemented Paste Backfills. *Minerals, 9*(1), 22. doi:10.3390/min9010022

Zhao, Y., Taheri, A., Soltani, A., Karakus, M., & Deng, A. (2019). Strength Development and Strain Localization Behaviour of Cemented Paste Backfills Using Portland Cement and Fly Ash. *Materials (Basel), 12*(20). doi:10.3390/ma12203282

List of Tables

Table 1. Physical and Chemical composition of the used tailings.

Physical Properties	Value	Chemical component	Mass percentage (%)
Specific gravity, G_s	2.4	SiO_2	38.27
Fines [< 75 μm] (%)	38.6	Fe_2O_3	37.70
Fine sand [0.075–0.425 mm] (%)	55.2	Al_2O_3	7.19
Medium sand [0.425–2 mm] (%)	6.2	K_2O	2.33
Liquid limit, w_L (%)	19.2	Ca	0.81
Plastic limit, w_P (%)	13.1	Mg	0.75
Plasticity index, I_P (%)	6.1	Ti	0.56
Optimum water content, w_{opt} (%)	8.7	Na_2O	0.07
Maximum dry unit weight, γ_{dmax} (kN/m^3)	20.2	Other	12.32

Table 2. Chemical composition of MC and mine-processed water.

Minecem Chemical Component	Mass percentage (%)	Processed water Component	Value (mg/L)
Granulated blast furnace slag	50	CL^-	5800
Portland cement clinker	20	SO_4^{2-}	2400
Cement kiln dust	< 15	NO_3^-	6
Natural gypsum	5–7	Na^+	3800
Chloride, Cl^-	< 8	Ca^{2+}	480
Limestone	< 7	K^+	380
Sulfur trioxide, SO_3	< 4	Mg^{2+}	280
Crystalline silica	< 1		

Table 3. Design of various curing scenarios with different curing times and applied pressures

Designation	Applied stress, A_s (MPa)	MC Content, M_c (%)	Water Content, W_c (%)
$A_0T_{7,14,28}$	0	3	30
$A_{1.2}T_{7,14,28}$	1.2	3	30
$A_{2.4}T_{7,14,28}$	2.4	3	30
$A_{3.6}T_{7,14,28}$	3.6	3	30

List of Figures

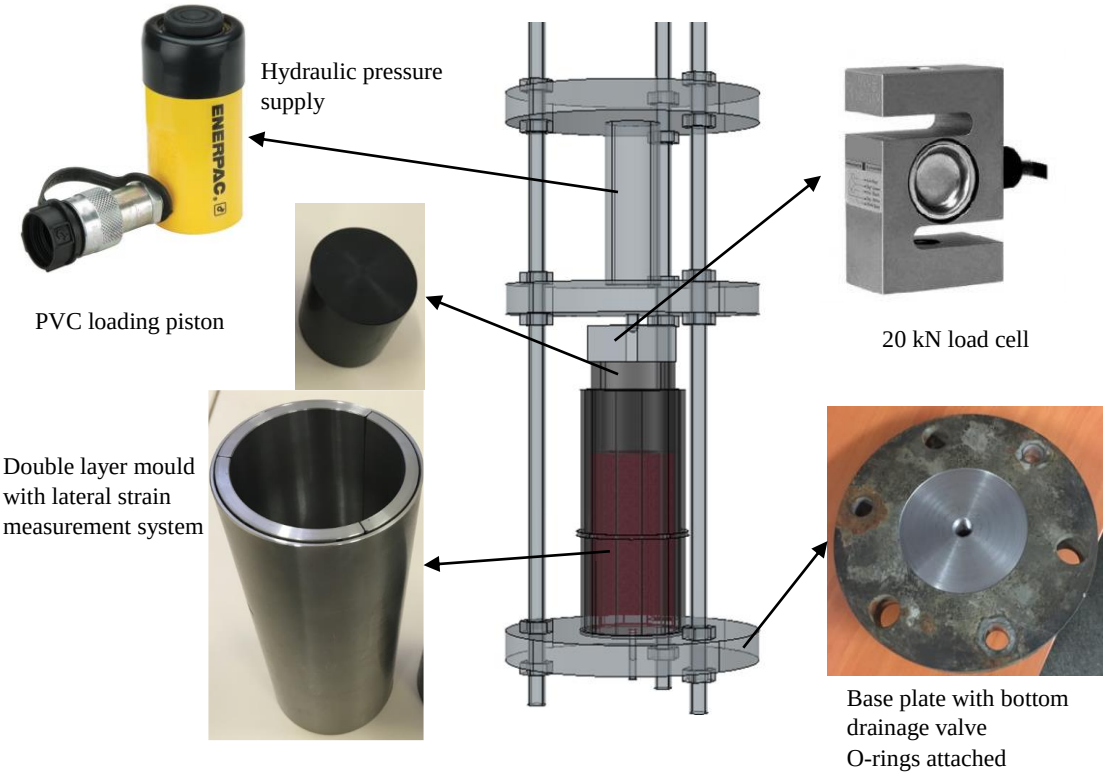

Figure 1. Curing under pressure apparatus (CPA)

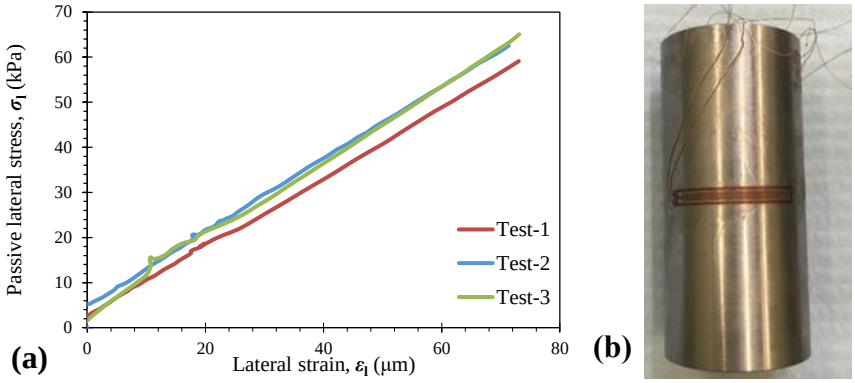

Figure 2. Passive lateral stress measurement: a) calibration of the steel mold, b) Strain gauge on the steel mold

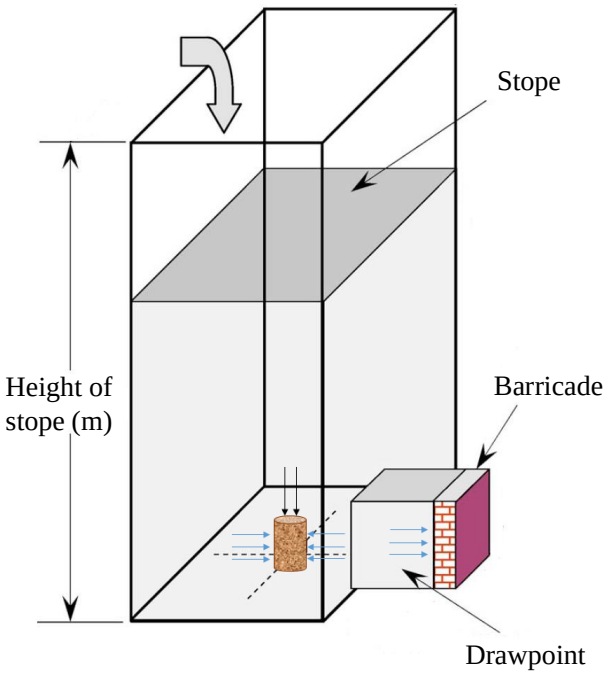

Figure 3. Layout and position of an ideal specimen

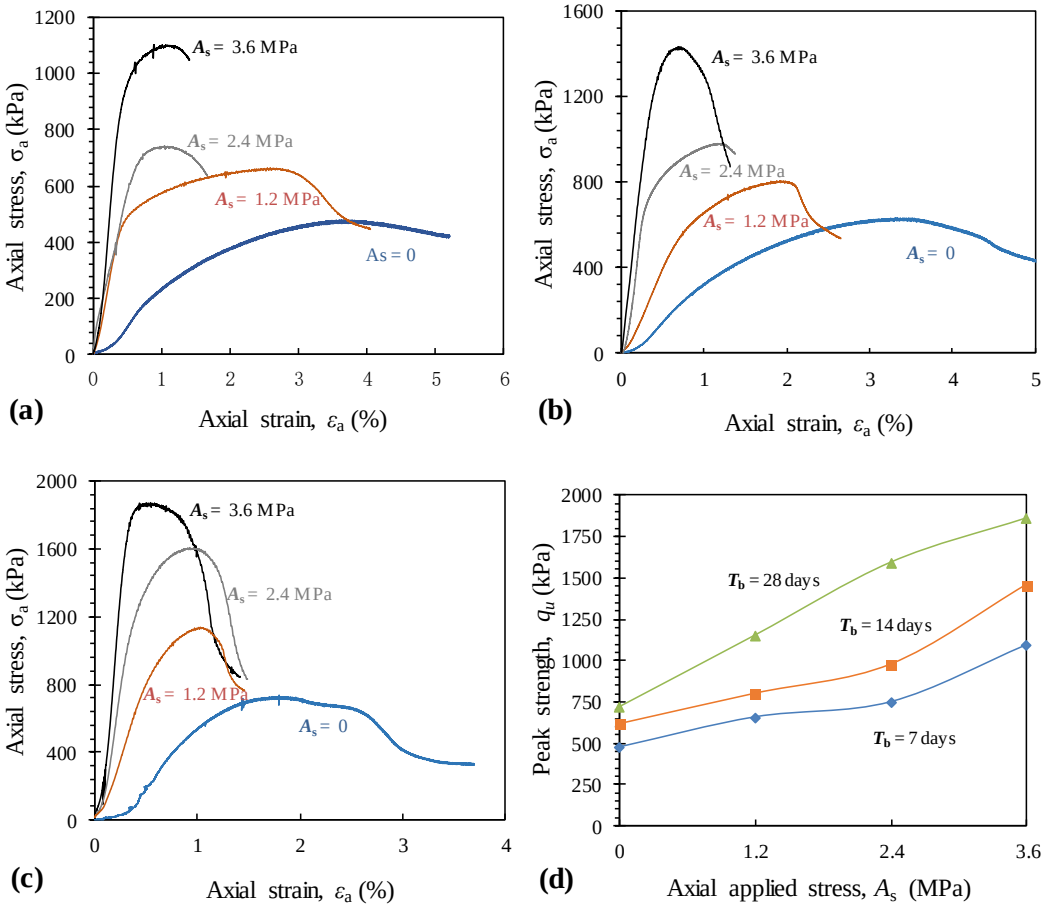

Figure 4. Uniaxial compression test results for 3% MC-CPB under the different depth of upper portion overburden for a) stress-strain relations for 7 days cured samples, b) stress-strain relations for 14 days cured samples, c) stress-strain relation for 28 days cured samples and d) peak strength vs axial applied stress.

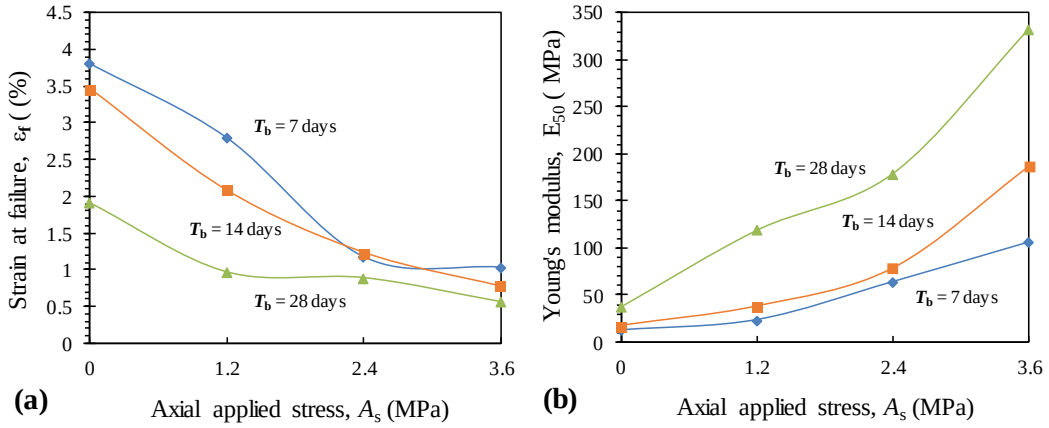

Figure 5. Uniaxial compression test results: a) Peak strain at failure b) Young's modulus for 3% MC-CPB under the different depth of upper portion overburden (axial applied stress)

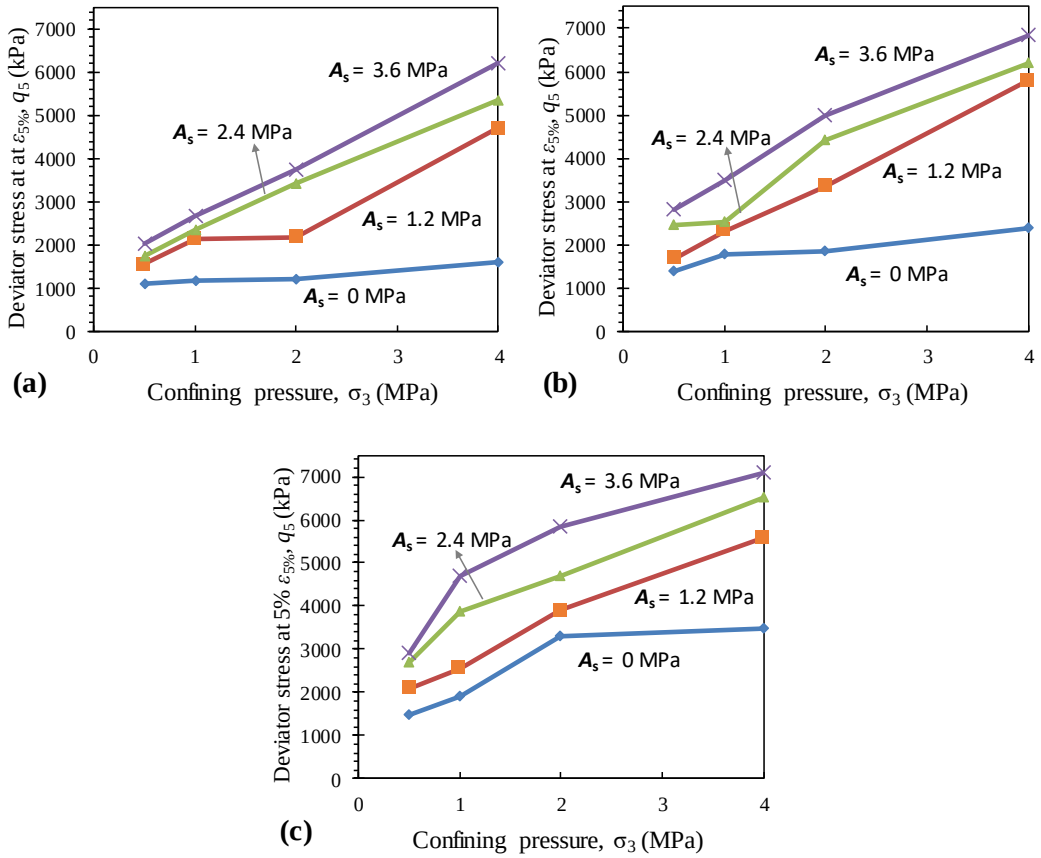

Figure 6. Deviator stress at ε_a= 5% for CPB under different axial applied stress a) 7 day-curing, b) 14 day-curing, c) 28 day-curing

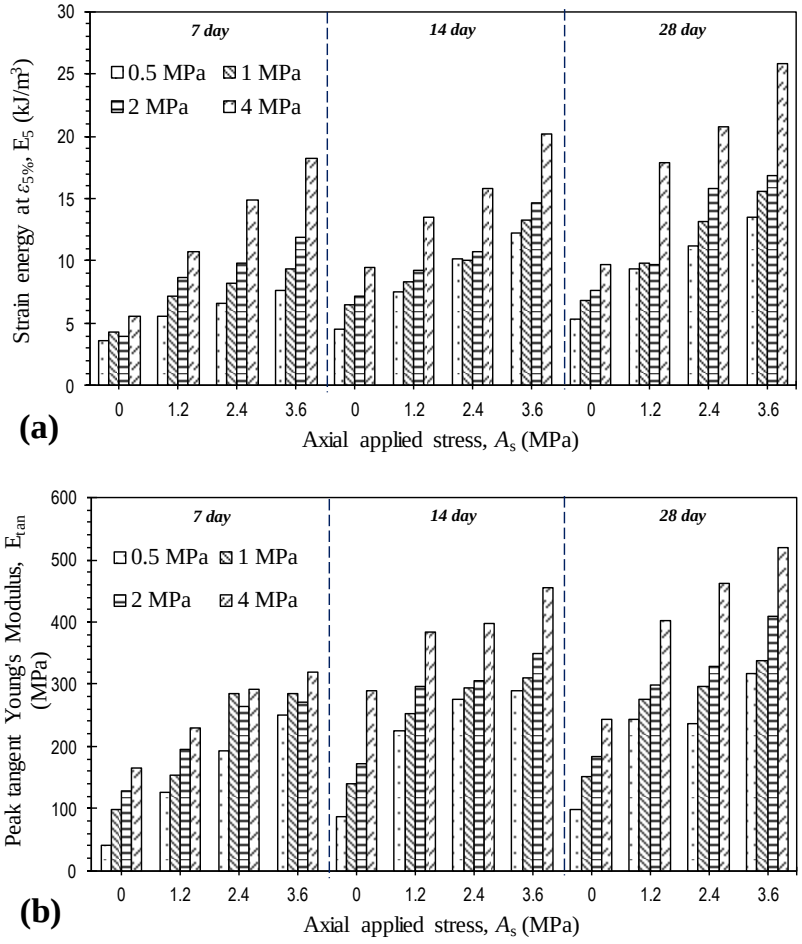

Figure 7. a) Strain energy at ε_a= 5% for CPB curing under different axial applied stress, b) Peak tangent Young's Modulus for CPB curing under different axial applied stress

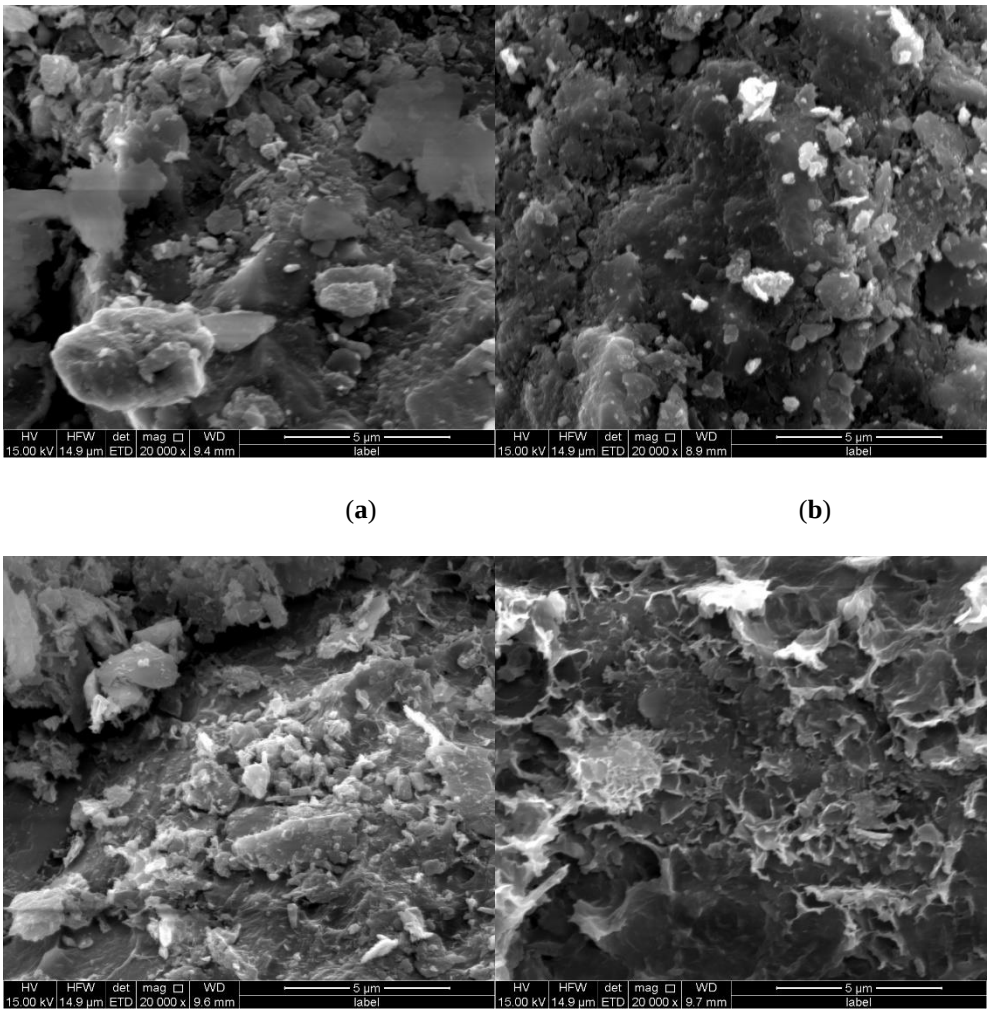

Figure 8. SEM micrographs for the tested samples cured for 28 days a) A_s = 0 MPa, b) A_s = 1.2 MPa, c) A_s = 2.4 MPa and d) A_s = 3.6 MPa

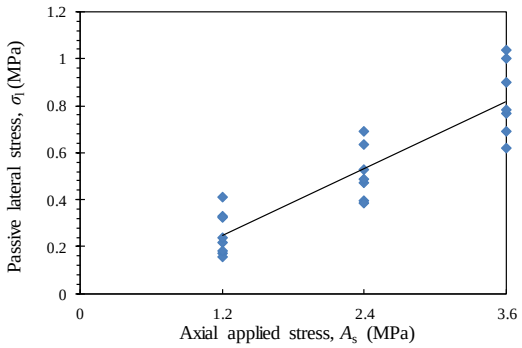

Figure 9. Axial applied stress vs. passive lateral stress

Appendix

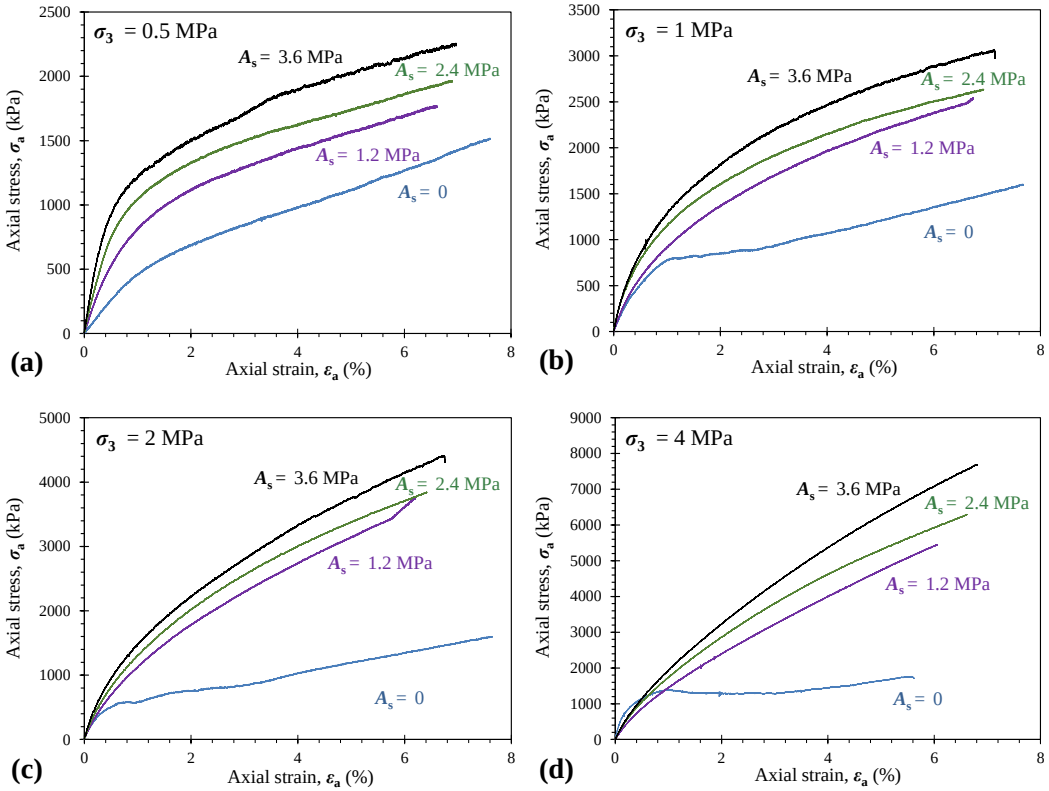

Figure A1. Triaxial tests for 7 days cured samples.

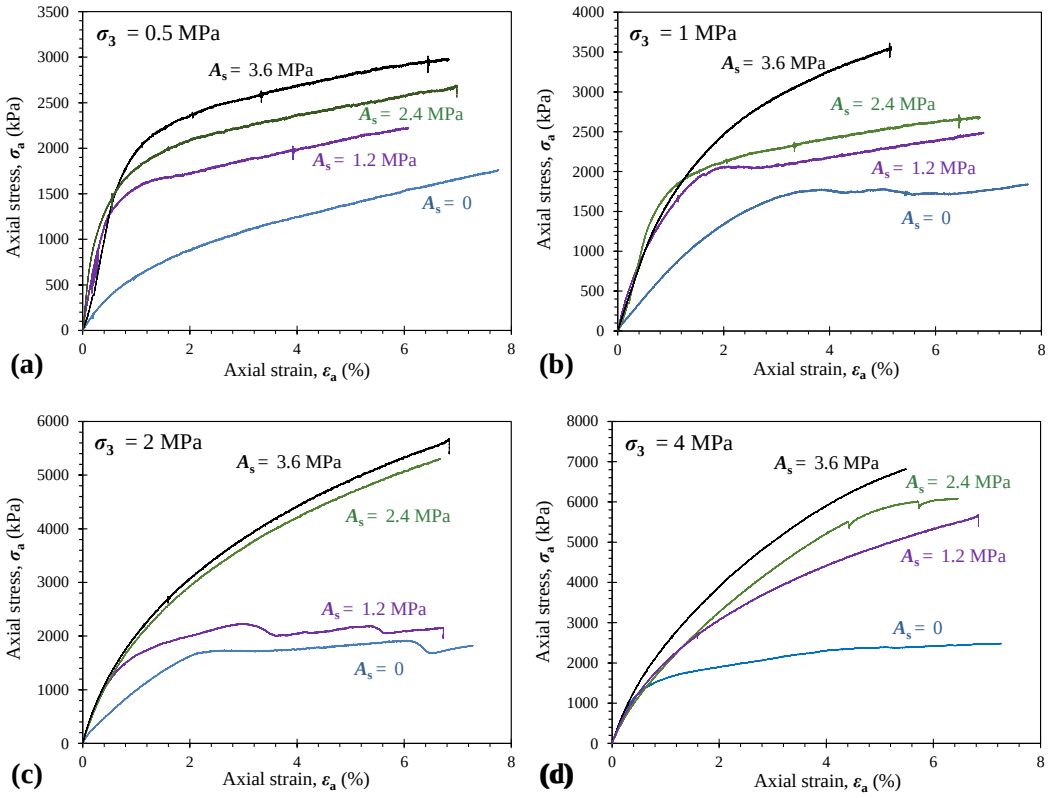

Figure A2. Triaxial tests for 14 days cured samples.

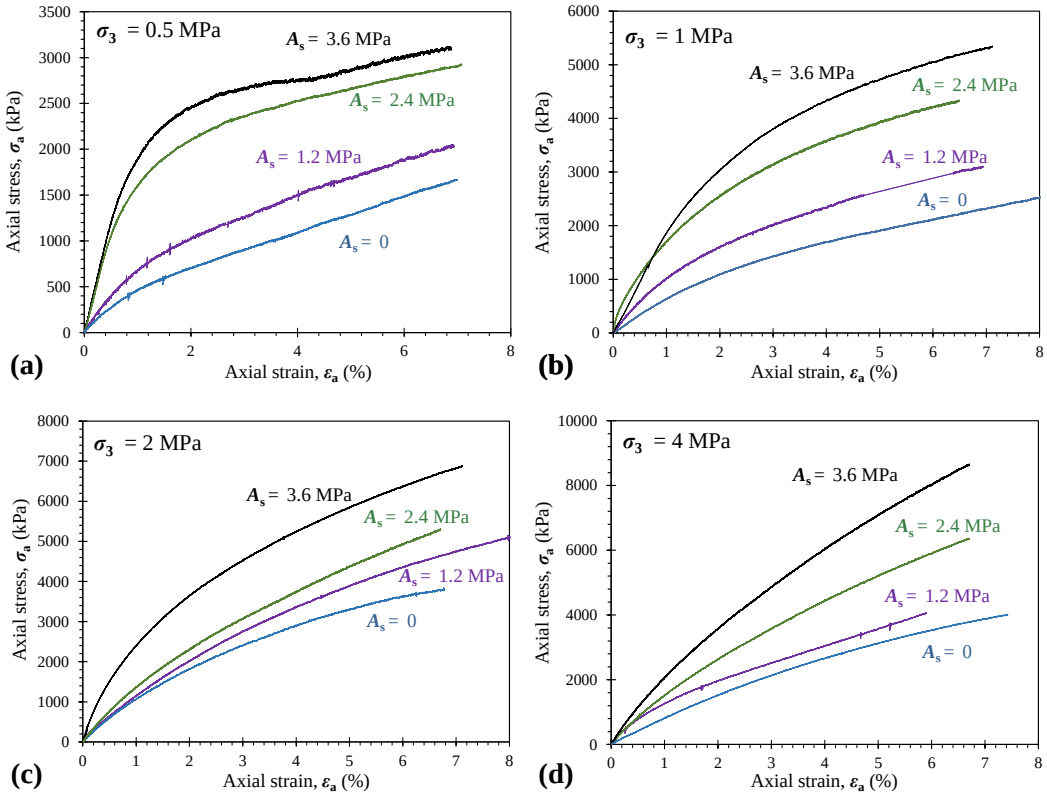

Figure A3. Triaxial tests for 28 days cured samples.

Chapter 6— The influence of saturation condition on the strength of Cement Paste Backfill

Statement of Authorship

Yue Zhao[a], Abbas Taheri[b], Murat Karakus[c] and An Deng[d]

[a] **PhD Student** - School of Civil, Environmental and Mining Engineering, The University of Adelaide, Adelaide 5005, Australia (Email: Yue.Zhao@adelaide.edu.au)

[b] **Senior Lecturer** - School of Civil, Environmental and Mining Engineering, The University of Adelaide, Adelaide 5005, Australia (Email: Abbas.Taheri@adelaide.edu.au)

[c] **Associate Professor** - School of Civil, Environmental and Mining Engineering, The University of Adelaide, Adelaide 5005, Australia (Email: Murat.Karakus@adelaide.edu.au)

[d] **Senior Lecturer** - School of Civil, Environmental and Mining Engineering, The University of Adelaide, Adelaide 5005, Australia (Email: An.Deng@adelaide.edu.au)

Publication Details:

Zhao, Y., Taheri, A., Karakus, M., & Deng, A. (2020). The influence of saturation condition on the strength of Cement Paste Backfill. (Unpublished and Unsubmitted work in manuscript)

Statement of Authorship

Title of Paper	The influence of saturation condition on the strength of Cement Paste Backfill
Publication Status	☐ Published ☐ Accepted for Publication ☐ Submitted for Publication ☑ Unpublished and Unsubmitted w ork w ritten in manuscript style
Publication Details	Zhao, Y., Taheri, A., Karakus, M., & Deng, A. (2020). The influence of saturation condition on the strength of Cement Paste Backfill.

Principal Author

Name of Principal Author (Candidate)	Yue Zhao		
Contribution to the Paper	Overall paper preparation		
Overall percentage (%)	70%		
Certification:	This paper reports on original research I conducted during the period of my Higher Degree by Research candidature and is not subject to any obligations or contractual agreements with a third party that would constrain its inclusion in this thesis. I am the primary author of this paper.		
Signature		Date	10/01/2020

Co-Author Contributions

By signing the Statement of Authorship, each author certifies that:

i. the candidate's stated contribution to the publication is accurate (as detailed above);
ii. permission is granted for the candidate in include the publication in the thesis; and
iii. the sum of all co-author contributions is equal to 100% less the candidate's stated contribution.

Name of Co-Author	Abbas Taheri Senior Lecturer, School of Civil, Environmental and Mining Engineering, The University of Adelaide		
Contribution to the Paper	Development of research idea, Supervised research, review and revision for the paper		
Signature		Date	06/01/2020

Name of Co-Author	Murat Karakus Associate Professor, School of Civil, Environmental and Mining Engineering, The University of Adelaide

Contribution to the Paper	Development of research idea, Paper review and revision		
Signature		Date	06/01/2020

Name of Co-Author	An Deng Senior Lecturer, School of Civil, Environmental and Mining Engineering, The University of Adelaide		
Contribution to the Paper	Development of research idea, Paper review and revision		
Signature		Date	10/01/2020

Please cut and paste additional co-author panels here as required.

Abstract

Cement paste backfill (CPB) has increasingly been used to fill the mined cavities in underground mine operations, to re-use tailings in underground mines. Strength performance of CPBs is well studied over the past few decades, to minimise its operating costs as well as a superior mechanical support for underground exploration. Additional work is, however, necessary to take into account more realistic conditions, such as the drainage of initially saturated backfill and the interference of surrounding underground water which lead to the variation of backfill saturation condition. A series of confined compression tests for compacted CPB sample with different binder content and curing time and various unsaturated confined compression tests for compacted tailing material were carried out. Four different matric suction values were used to simulate various saturation condition. The experimental data show that matric suction increases the peak deviator stress of the tailings sample in a non-linear trend. Overall, the greater the MC content, the longer the curing period and the higher the matric suction, the higher the friction angle of failure envelope. However, the difference between the friction angle obtained from MC-treated mixtures is considerably small (i.e. 4.4 °) compare to the difference between the friction angle obtained from pure tailing specimen under various saturation condition (i.e. 9.6 °).

Keywords: cemented paste backfill; Minecem; saturation condition; matric suction

1. Introduction

Mine tailings, deposited after minerals been extracted, are the largest source of waste in mine processing. Approximately 14 billion tons of tailings were produced globally by the mining industry in 2010 (Jones and Boger 2012; Zhao et al. 2018). Tailings have been traditionally deposited into tailings storage facilities which associated with severe environmental, geotechnical and economic concerns (Dold 2014; Franks et al. 2011; Liu et al. 2016). Cement paste backfill (CPB) has increasingly been used to fill the mined cavities in underground mine operations, to re-use tailings in underground mines (Belem and Benzaazoua 2007; Zhang et al. 2012; Fall et al. 2010; Sivakugan et al. 2006). Cemented Paste Backfill recycles processed tailings into underground mined voids, which reduces the volume that needs to be surface-disposed. Using CPB thus mitigates the potential environmental impacts associated with tailings disposal and assists waste management (Fall et al. 2010; Sivakugan et al. 2015; Yilmaz et al. 2014; Rankine and Sivakugan 2007). These refilled CPB can then performs as both the support system and working platform for further ore extraction. CPB is a high-density slurry composed of tailings, a low proportion of cementitious binders (3–7%) and processed mine water to meet the requirements of designed mechanical properties (Jones and Boger 2012; Rankine and Sivakugan 2007).

Over the past few decades, CPB technology has been increasingly applied to revive mined cavities in underground mine operations, owing to its low operating costs as well as its superior mechanical performance compared with other backfilling methods (Fall et al. 2010; Brackebusch 1994; Ouattara et al. 2017). Strength performance of CPBs is governed by physicochemical and mineralogical properties of the tailings, chemical composition of the mixing water, binder type (and it is content), the adopted mix design (or solids content), and in situ stress and curing conditions (Xu et al. 2018; Benzaazoua et al. 2004; Fall and Samb 2008; Taheri and Tatsuoka 2012 and 2015; Cao et al. 2018; Wu et al. 2018).

The information the laboratory cured specimens provides is limited; additional work is, however, necessary to take into account more realistic conditions, such as the drainage of initially saturated backfill and the interference of surrounding underground water which lead to the variation of backfill saturation condition. Under the influence of content binder, the mechanical property and hydraulic conductivity of CPB is highly time-dependent. The strength increases and hydraulic conductivity decreases as the curing time increase, especially at early ages (0- 14 days) (Taheri and Tatsuoka 2012 & 2015; Cao et al. 2018;

Belem et al. 2002; El Mkadmi et al. 2014; Fall et al. 2009). It leads to massive difficulty on the study of CPB mechanical performance under different saturation as it is time-consuming to change the saturation condition of CPB as well.

The objective of the study is to investigate the effect of various saturation condition on the strength characteristic of CPB. In this paper, the authors first recall the CPB samples for different binder content (0%, 1.5%, 3%, 6%) and curing time (7 days and 14 days) under complete dry condition. Then various saturation and unsaturation condition was applied to pure tailings material by providing different matric suction using a back pressure shear box to study the effect of saturation condition on the strength of CPB.

2. Materials

The tailings are from a copper-gold underground mine located in South Australia and used in the present study. The physical properties, including specific gravity, grain size data and Atterberg limits, are given in Table 1 as per relevant ASTM and Australian standards (AS).

The chemical composition of the tailings is provided in Table 1 as well. The chemical composition mainly consists of silicon dioxide (SiO_2) and iron oxide (Fe_2O_3), with mass fractions of 38.27% and 37.70%, respectively.

Commercially manufactured cementitious agent, commonly traded as Minecem in Australia (hereafter referred to as MC), was used as the binder. Minecem is a slag–blended cement specifically developed for underground, mine-backfilling applications. The chemical composition of MC, as supplied by the manufacturer, are given in Table 2.

The mixing water used was mine-processed water, which was sourced from the same mine. The chemical composition of the processed mine water is presented in Table 2 as well. The pH was found to be 7.5, from which the water was characterised as a neutral substance.

3. Experimental Program

3.1. Soil-water retention curve

Figure 1 shows the chilled mirror dew-point psychrometer (WP4C) as one type of psychrometer that effectively measures suctions. The WP4C device is placed in a temperature and humidity controlled room to minimise environmental influence for

measurement. Then saturated tailings were dried in a low-temperature oven (40^{o}C) for different times to measure the matric suction for different water content. For different water content, two samples were cut, trimmed and levelled with a knife and then measuring the suction in the WP4C chamber. After measuring the suction, the specimens were placed in an oven to determine the dry weight for actual water content (w) calculation. Figure 2 illustrates the water retention curve for pure tailings material using WP4C device.

3.2.Triaxial Compression Test for dry sample

In this study, a series of the sample with different binder content were prepared by standard compaction. A total of seven mixing and curing condition designs, as outlined in Table 3, were prepared in this study. For ease of presentation, the following coding system is used to designate the various curing condition designs:

$$MC_a T_b C_c \quad (1)$$

where MC_a = a% MC content; T_b = b days of curing; C_c = c kPa of confining pressure

An automated hydraulic triaxial testing system for the specimen of 50 mm in diameter and 100 mm in height was used to measure the deformation of the compacted cement paste backfill. Cured CPB samples were tested in dry condition. The absolute value of the axial strain rate during the triaxial compressive loading was equal to 1 mm/min in all the tests. Since the specimens were unsaturated as they were when they were compacted, it is very likely that the specimens were essentially under drained conditions at this relatively low strain rate (Taheri et al. 2012). Unconsolidated drained test (UD) program was used to investigate CPB at dry state. The tests were undertaken under four different confining pressures (i.e. 0 kPa, 50 kPa, 100 kPa, 150 kPa).

The tailings and binder were mixed in dry form. The required amount of processed mine water corresponding to an optimum moisture content was added to each blend, as shown in the compaction results in Figure 3. The optimum moisture content for pure tailing, 1.5% MC, 3% MC and 6% MC are 8.75%, 9.65%,10.2% and 11.35%, respectively. After thoroughly mixed by a mechanical mixer for approximately 5 minutes to obtain a uniform consistency. The resultant mix was compacted to the mold of 50 mm in diameter and 100 mm in height along with three compaction layers. The compacted samples were left in atmosphere condition where curing was allowed for periods of 7 and 14 days.

3.3.Unsaturated Triaxial Compression Test

For the study of CPB under unsaturated condition, no binders were added to the CPB sample. The tailings were mixed with the optimum content of water for pure tailing (8.75%) and compared using the same method as explained in section 3.1.

The unsaturated triaxial test was carried out with the same automated hydraulic triaxial testing system with an additional backpressure shear box and a high air-entry disk under the sample. The additional backpressure shear box provides and controls the pore-air pressure. Each sample was saturated before the consolidation stage. During consolidation, the sample was consolidated under a specific confining pressure and matric suction. The consolidation was completed when there was no more change in the volume of the confining pressure controller. Consolidated drained (CD) tests were carried out under constant confining pressure, and matric suctions.

A total of five various suction level (50 kPa, 200 kPa, 400 kPa and 600 kPa) and three confining pressure values (i.e. 200 kPa, 350 kPa and 500 kPa) were selected in this study. For ease of presentation, the following coding system is used to designate the various curing condition designs:

$$MC_0S_bC_c \tag{2}$$

where MC_0 = 0% MC content; S_b = b kPa of applied suction; C_c = c kPa of confining pressure

4. Results and Discussions

4.1.Effect of MC on Confined Compression Strength under dry condition

Stress-strain curves, obtained from the confined compression tests, for various MC-treated mixtures—$MC_aT_bC_c$ where a = {0,1.5, 3, 6}, b = {7, 14} and c = {0, 50, 100, 150 }—are provided in Figure 4 and 5 in the Appendix section. The stress-strain locus for all MC-treated mixtures exhibited a rise–fall behaviour with visually detectable peak points, thus signifying a strain-softening character accompanied by brittle sample failures. In general, the greater the MC content and the longer the curing period, the more pronounced the strain-softening effect, and hence, the more dramatic the sample failure.

Figure 6 a and b illustrate the variations of peak deviator stress q_u against MC content for the samples tested at various confining pressures. At any given curing time, the greater the

MC content, the higher the peak deviator stress, following a monotonically increasing trend. The sample $Mc_0T_7C_0$, for instance, exhibited a peak deviator stress of q_u = 565.3 kPa, while the inclusion of MC = 1.5%, 3% and 6%, with the same 7-day curing condition, resulted in q_u = 656.3 kPa, 1029.1 kPa and 1065.5 kPa, respectively. Similarly, for any given MC content, an increase in confining pressure promoted a major increase in the peak deviator stress up to Cc = 150 kPa, beyond of which the effect of curing was found to be rather marginal. The inclusion of 3% MC at Tc = 7 days, for instance, resulted in q_u = 1029.1 kPa, while higher values of 1477.3 kPa, 1898.3 kPa and 2061.7 kPa were noted for the same 3% MC inclusion at 0kPa, 50 kPa, 100 kPa and 150 kPa of confining pressure, respectively.

The axial strain at failure, denoted as ε_u, is an indication of the material's ductility, with higher values manifesting a more ductile/less brittle character. Figure 7a illustrates the variations of axial strain at failure against MC content for the samples tested at various confining pressures for seven days curing. The axial strain at failure demonstrated a trend similar to that observed for the peak deviator stress for seven days cured samples; however, adversely for 14 days cured samples. In general, the greater the MC content and the higher the applied confining pressure, the higher the sample's ductility for seven days cured samples. Moreover, the greater the MC content and the higher the applied confining pressure, the lower the sample's ductility for 14 days cured samples.

The area under a typical stress-strain curve up to the failure point, defined as peak strain energy (or energy adsorption capacity) and denoted as E_u, serves as a measure of the material's toughness. Figure 8 illustrates the variations of peak strain energy against MC content for the samples tested at various confining pressures for two different curing time (7 days and 14 days). The variations of peak strain energy followed a trend similar to that observed for the peak deviator stress, thus indicating that the greater the MC content, the higher the confining pressure and the longer the curing time, the higher the sample's degree of toughness. As typical cases, the samples $MC_{1.5}T_7C_0$, $MC_{1.5}T_7C_{150}$, $MC_{1.5}T_{14}C_{150}$ and $MC_3T_{14}C_{150}$ resulted in E_u = 5.9 kJ/m^3, 13.3 kPa,13.9 kPa and 20.6 kPa, respectively.

Table 4 illustrates the variations of the friction angle and the total cohesion against MC content for the samples tested at two different curing time (7 days and 14 days). The analysis of the failure envelope obtained at constant MC content and curing time shows at any given curing time, the greater the MC content, the higher the friction angle, following a monotonically increasing trend. Similarly, the cohesion increased with the increase of MC

content and curing time. The difference between the friction angle obtained from MC-treated mixtures is considerably small (4.4). Therefore, for the following analyses, the friction angle obtained from the unsaturated confined compression test of pure tailing may represent the unsaturated behaviour of MC-treated mixtures to a certain degree.

4.2.Effect of Saturation on Confined Compression Strength

The compacted tailings specimens were tested under three different confining pressures (200 kPa, 350 kPa and 500 kPa). For each confining pressure, the test was carried out individually with five different matric suction value (0 kPa, 50 kPa, 200 kPa, 400 kPa and 600 kPa) to obtain measure the stress-strain relations.

Figure 9 a-c shows the relationship between deviator stress and axial deformation for different suction values at a constant confining pressure. Figure 10 shows the relationship between deviator stress and axial deformation for different confining pressure at a fully saturated condition.

The behaviour of the tailings concerning the saturation condition is summarised as follows:

1. For fully saturated condition (0 kPa suction), despite the confining pressure, the deviator stress followed by a strain-hardening behaviour. For all matric suctions, the deviator stress show a strain-softening behaviour

2. For 50 kPa matric suction, the deviator stress curve shows a strain-hardening behaviour after peak value at all confining pressure. For all matric suction above 50 kPa, the deviator stress shows a peak value followed by a strain-softening behaviour.

3. Overall for all stress-strain curves, the peak deviator stress increases with an increase in the confining pressure. At a given confining pressure, a higher peak deviator stress can be observed for higher matric suction.

After calculation of initial moisture content, the inflow of water during saturation regime and outflow of water after apply matric suction the actual degree of saturation could be calculated. Figure 11 illustrates the relationship between saturation condition and matric suction under various confining pressures. In general, the greater the matric suction allpied, the lower the degree of saturation for the sample. The samples $MC_0S_{200}C_{200}$, $MC_0S_{200}C_{350}$

and $MC_0S_{200}C_{500}$ exhibited actual degree of saturation of 60.0 %, 62.9% and 61.6%. As such, the increase in confining pressure showed less or none effect on the degree of saturation.

The variation of deviator strength for matric suction under constant confining pressure show a slightly non-linear relationship with deviator stress being higher for higher confining pressure. In Figure 12 b), the failure envelop of shear strength obtained at constant matric suctions gives the slope and angle of friction for tested matric suction values.

Table 5 illustrates the variations of the friction angle and the total cohesion against matric suction for the samples. The friction angle increased from 22.1to 27.6 °, 29.0 °, 30.7 ° and 31.7 ° for matric suction equal to 0 kPa, 50 kPa, 200 kPa, 400 kPa and 600 kPa respectively. The cohesion dropped from 35.5 kPa to 7.7 kPa after applying 50 kPa matric suction and increased continuously to 10.8 kPa, 29.5 kPa and 33.1 kPa respectively for matric suction equal to 200 kPa, 400 kPa and 600 kPa.

5. Conclusions

This study investigated the effect of various saturation condition on the strength characteristic of CPB and compared the results with CPB under dry condition. There still some limitations for this study, the initial aim was to compare the unsaturated CPB strength and saturated CPB strength under the same confining pressure. With the limited loading capacity, some lower confining pressure had to apply for unsaturated CPB. To do some future investigation, appropriate confining pressures should be carefully selected. However, based on the results obtained, the following conclusions appear to be warranted:

- The greater the MC content and/or the longer the curing period, the higher the developed strength, toughness and stiffness
- As the confining stress increases the maximum deviator stress increases regardless of the state of specimens
- The greater the MC content and/or the longer the curing period, the higher the friction angle and cohesion of failure envelope. However, the difference between the friction angle obtained from MC-treated mixtures is considerably small (4.4 °) compare to the difference between the friction angle obtained from pure tailing specimen under various saturation condition (9.6 °).

- The tailing material shows a peak value followed by a softening behaviour at high matric suction and a strain hardening behaviour at zero matric suction
- For any given applied confining pressure, the wetted pure tailings specimens had a lower peak deviator stress than dry specimens.
- The friction angles show a linear relationship with respect to the matric suction. Where the cohesion decrease form from 35.5 kPa to 7.7 kPa after increasing matric suction from 0 kPa to 50 kPa and kept increase with the increase of matric suction. The increase in peak deviator stress shows a non-linear increment trend for the matric suction.

References

Belem, T., & Benzaazoua, M. (2007). Design and Application of Underground Mine Paste Backfill Technology. *Geotechnical and Geological Engineering, 26*(2), 175-175. doi:10.1007/s10706-007-9167-y

Belem, T., Bussière, B., & Benzaazoua, M. (2002). The Effect of Microstructural Evolution on the Physical Properties of Paste Backfill. *Tailings and Mine Waste'01*, January 16-19, Fort Collins, Colorado, Balkema: Rotterdam, 365-374.

Benzaazoua, M., Fall, M., & Belem, T. (2004). A contribution to understanding the hardening process of cemented pastefill. *Minerals Engineering, 17*(2), 141-152. doi:10.1016/j.mineng.2003.10.022

Brackebusch, F.W. (1994). Basics of paste backfill systems. *Mining Engineering*, 46(1), 1175–1178. doi: 10.1016/0148-9062(95)90153-V

Cao, S., Song, W., & Yilmaz, E. (2018). Influence of structural factors on uniaxial compressive strength of cemented tailings backfill. *Construction and Building Materials, 174*, 190-201. doi:10.1016/j.conbuildmat.2018.04.126

Dold, B. (2014). Submarine Tailings Disposal (STD)—A Review. *Minerals, 4*(3), 642-666. doi:10.3390/min4030642

El Mkadmi, N., Aubertin, M., & Li, L. (2014). Effect of drainage and sequential filling on the behaviour of backfill in mine stopes. *Canadian Geotechnical Journal, 51*(1), 1-15. doi:10.1139/cgj-2012-0462

Fall, M., & Samb, S. S. (2008). Pore structure of cemented tailings materials under natural or accidental thermal loads. *Materials Characterization, 59*(5), 598-605. doi:10.1016/j.matchar.2007.05.003

Fall, M., Adrien, D., Célestin, J. C., Pokharel, M., & Touré, M. (2009). Saturated hydraulic conductivity of cemented paste backfill. *Minerals Engineering, 22*(15), 1307-1317. doi:10.1016/j.mineng.2009.08.002

Fall, M., Célestin, J. C., Pokharel, M., & Touré, M. (2010). A contribution to understanding the effects of curing temperature on the mechanical properties of mine

cemented tailings backfill. *Engineering Geology, 114*(3-4), 397-413. doi:10.1016/j.enggeo.2010.05.016

Franks, D. M., Boger, D. V., Côte, C. M., & Mulligan, D. R. (2011). Sustainable development principles for the disposal of mining and mineral processing wastes. *Resources Policy, 36*(2), 114-122. doi:10.1016/j.resourpol.2010.12.001

Jones, H., & Boger, D. V. (2012). Sustainability and Waste Management in the Resource Industries. *Industrial & Engineering Chemistry Research, 51*(30), 10057-10065. doi:10.1021/ie202963z

Liu, Q., Liu, D., Liu, X., Gao, F., & Li, S. (2016). Research and application of surface paste disposal for clay-sized tailings in tropical rainy climate. *International Journal of Mineral Processing, 157*, 227-235. doi:10.1016/j.minpro.2016.11.014

Ouattara, D., Yahia, A., Mbonimpa, M., & Belem, T. (2017). Effects of superplasticizer on rheological properties of cemented paste backfills. International Journal of Mineral Processing, 161, 28-40. doi:10.1016/j.minpro.2017.02.003

Rankine, R. M., & Sivakugan, N. (2007). Geotechnical properties of cemented paste backfill from Cannington Mine, Australia. Geotechnical and Geological Engineering, 25(4), 383-393. doi:10.1007/s10706-006-9104-5

Sivakugan, N., Rankine, R. M., Rankine, K. J., & Rankine, K. S. (2006). Geotechnical considerations in mine backfilling in Australia. *Journal of Cleaner Production, 14*(12-13), 1168-1175. doi:10.1016/j.jclepro.2004.06.007

Sivakugan, N., Veenstra, R., & Naguleswaran, N. (2015). Underground Mine Backfilling in Australia Using Paste Fills and Hydraulic Fills. *International Journal of Geosynthetics and Ground Engineering, 1*(2). doi:10.1007/s40891-015-0020-8

Taheri, A., & Tatsuoka, F. (2012). Stress-strain relations of cement–mixed gravelly soil from multiple–step triaxial compression test results. *Soils Found*, 52, 748–766, doi:10.1016/j.sandf.2012.07.014.

Taheri, A., & Tatsuoka, F. (2015). Small- and large-strain behaviour of a cement-treated soil during various loading histories and testing conditions. *Acta Geotech*, 10, 131–155, doi:10.1007/s11440-014-0339-7.

Taheri, A., Sasaki, Y., Tatsuoka, F., &Watanabe, K. (2012). Strength and deformation characteristics of cemented-mixed gravelly soil in multiple-step triaxial compression. *Soils and Foundations*, 52(1): 126-145,

Wu, J., Feng, M., Chen, Z., Mao, X., Han, G., & Wang, Y. (2018). Particle Size Distribution Effects on the Strength Characteristic of Cemented Paste Backfill. *Minerals*, *8*(8). doi:10.3390/min8080322

Xu, W., Cao, P., & Tian, M. (2018). Strength Development and Microstructure Evolution of Cemented Tailings Backfill Containing Different Binder Types and Contents. Minerals, 8(4). doi:10.3390/min8040167

Yilmaz, T., Ercikdi, B., Karaman, K., & Kulekci, G. (2014). Assessment of strength properties of cemented paste backfill by ultrasonic pulse velocity test. Ultrasonics, 54(5), 1386-1394. doi:10.1016/j.ultras.2014.02.012

Zhang, Q., Zhang, J., Huang, Y., & Ju, F. (2012). Backfilling technology and strata behaviours in fully mechanized coal mining working face. *International Journal of Mining Science and Technology, 22*(2), 151-157. doi:10.1016/j.ijmst.2011.08.003

Zhao, Y., Soltani, A., Taheri, A., Karakus, M., & Deng, A. (2018). Application of Slag–Cement and Fly Ash for Strength Development in Cemented Paste Backfills. *Minerals*, *9*(1), 22. doi:10.3390/min9010022

List of Tables

Table 1. Physical and Chemical composition of the used tailings.

Physical Properties	Value	Chemical component	Mass percentage (%)
Specific gravity, G_s	2.4	SiO_2	38.27
Fines [< 75 μm] (%)	38.6	Fe_2O_3	37.70
Fine sand [0.075–0.425 mm] (%)	55.2	Al_2O_3	7.19
Medium sand [0.425–2 mm] (%)	6.2	K_2O	2.33
Liquid limit, w_L (%)	19.2	Ca	0.81
Plastic limit, w_P (%)	13.1	Mg	0.75
Plasticity index, I_P (%)	6.1	Ti	0.56
Optimum water content, w_{opt} (%)	8.7	Na_2O	0.07
Maximum dry unit weight, γ_{dmax} (kN/m^3)	20.2	Other	12.32

Table 2. Chemical composition of MC and mine-processed water.

Minecem Chemical Component	Mass percentage (%)	Processed water Component	Value (mg/L)
Granulated blast furnace slag	50	CL^-	5800
Portland cement clinker	20	SO_4^{2-}	2400
Cement kiln dust	< 15	NO_3^-	6
Natural gypsum	5–7	Na^+	3800
Chloride, Cl^-	< 8	Ca^{2+}	480
Limestone	< 7	K^+	380
Sulfur trioxide, SO_3	< 4	Mg^{2+}	280
Crystalline silica	< 1		

Table 3. Design of various curing scenarios with different dates and applied pressures

Designation	MC Content, M_c (%)	Confining Pressure, σ_3 (kPa)
MC_0T_7	0	0, 50, 100, 150
$MC_{1.5}T_{7,14}$	1.5	0, 50, 100, 150
$MC_3T_{7,14}$	3	0, 50, 100, 150
$MC_6T_{7,14}$	6	0, 50, 100, 150

Table 4. Summary of friction angle for tested MC contents and curing times

	7 days curing		14 days curing	
MC Content, M_c (%)	**Friction angle ϕ (°)**	**Cohesion C (kPa)**	**Friction angle ϕ (°)**	**Cohesion C (kPa)**
0	32.5	211.2		
1.5	32.9	240.9	34.8	256.4
3	35.2	298.2	35.8	318.1
6	36.1	274.3	36.9	350.6

Table 5. Summary of friction angle for tested matric suction values

Matric Suction (kPa)	Friction angle ϕ (°)	Cohesion C (kPa)
0	22.05	35.5
50	27.61	7.7
200	28.96	10.8
400	30.68	29.5
600	31.66	33.1

List of Figures

Figure 1. WP4 Dewpoint Potentiometer

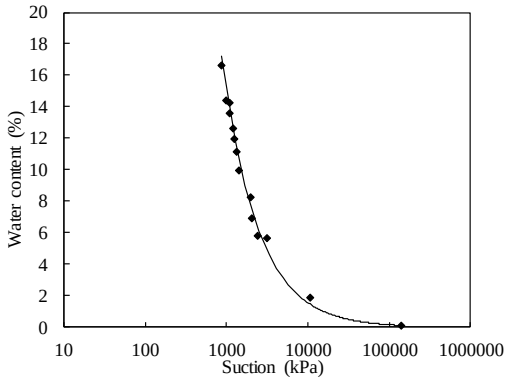

Figure 2. Water retention curve (WRC) of pure tailings

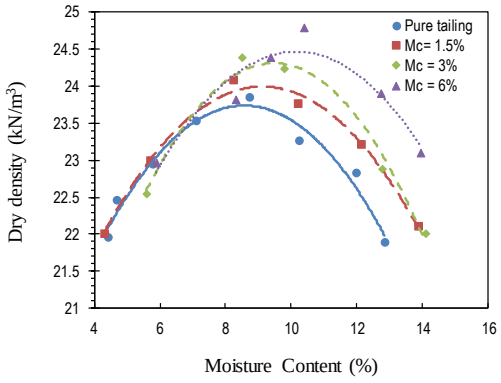

Figure 3. Compaction test results for various cement contents

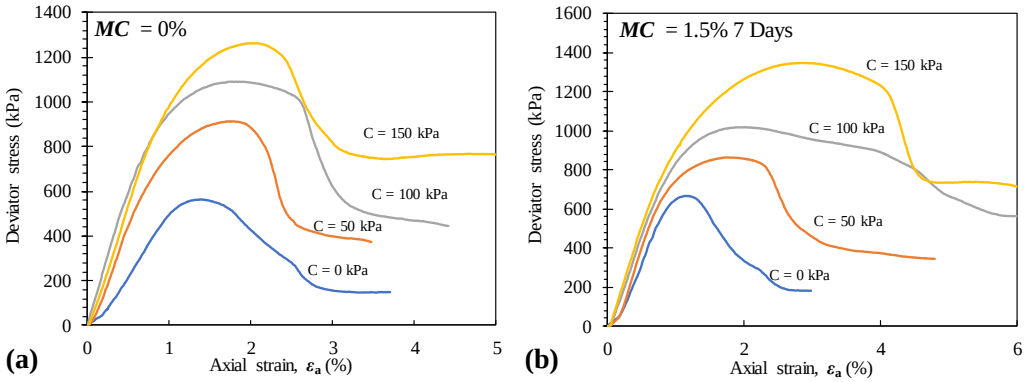

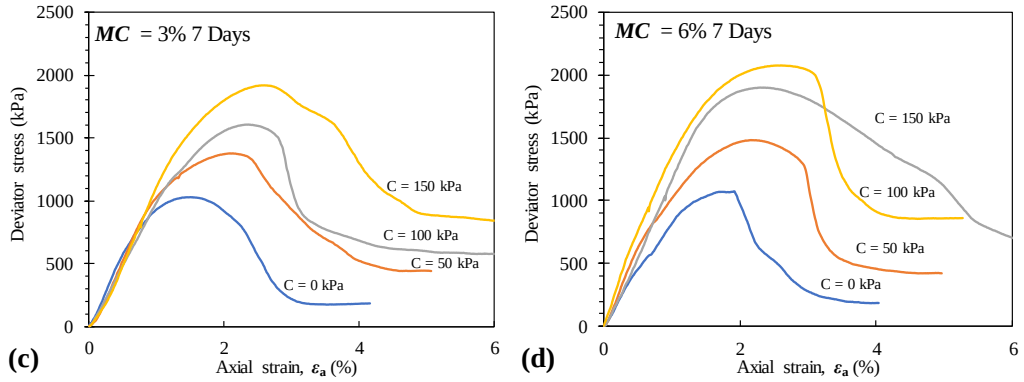

Figure 4. Stress–strain curves for compacted cement mixed tailings under complete dry condition (7 day curing), obtained by various confining pressure (a) MC content = 0% ; (b) MC content = 1.5%; (c) MC content = 3% ; (d) MC content = 6%

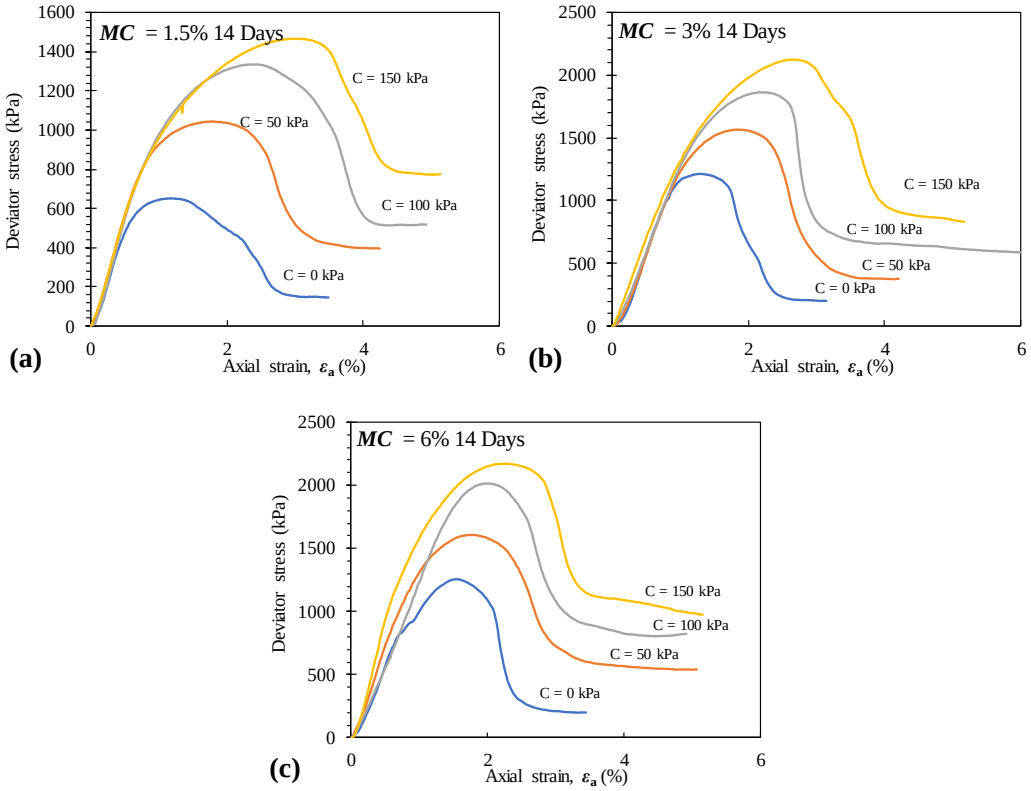

Figure 5. Stress–strain curves for compacted cement mixed tailings under complete dry condition (14 day curing), obtained by various confining pressure (a)MC content = 1.5% ; (b) MC content = 3%; (c) MC content = 6%

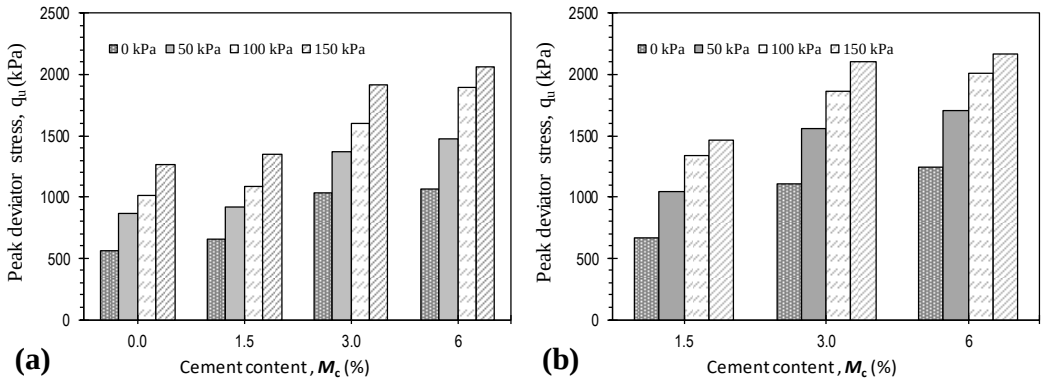

Figure 6. Variations of peak deviator stress at failure against MC content for the samples tested at various confining pressures (a) 7 days curing and (b) 14 days curing

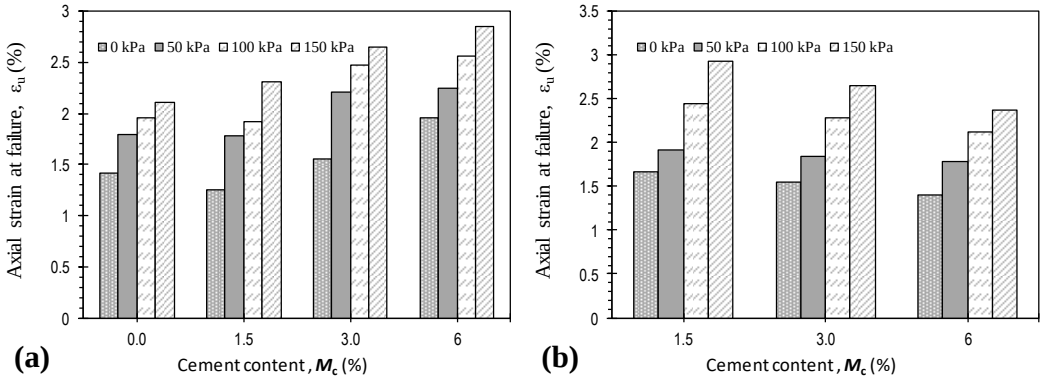

Figure 7. Variations of axial strain at failure ε_u against MC content for the samples tested at various confining pressures (a) 7 days curing and (b) 14 days curing

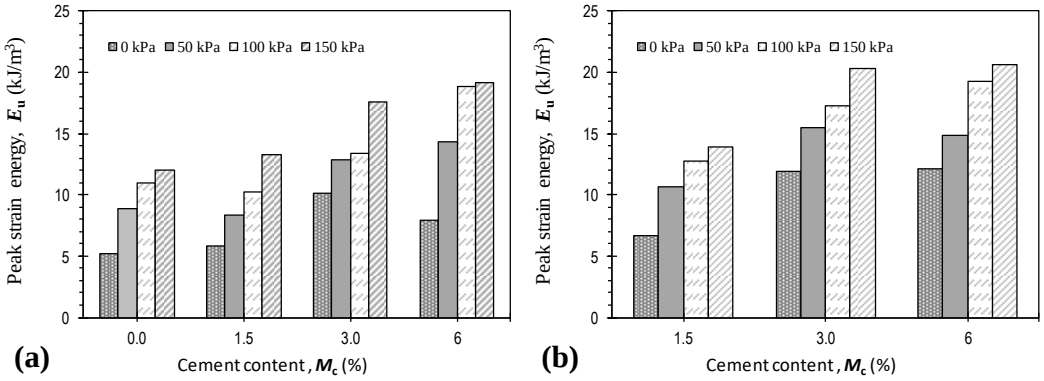

Figure 8. Variations of peak strain energy E_u against MC content for the samples tested at various confining pressures (a) 7 days curing and (b) 14 days curing

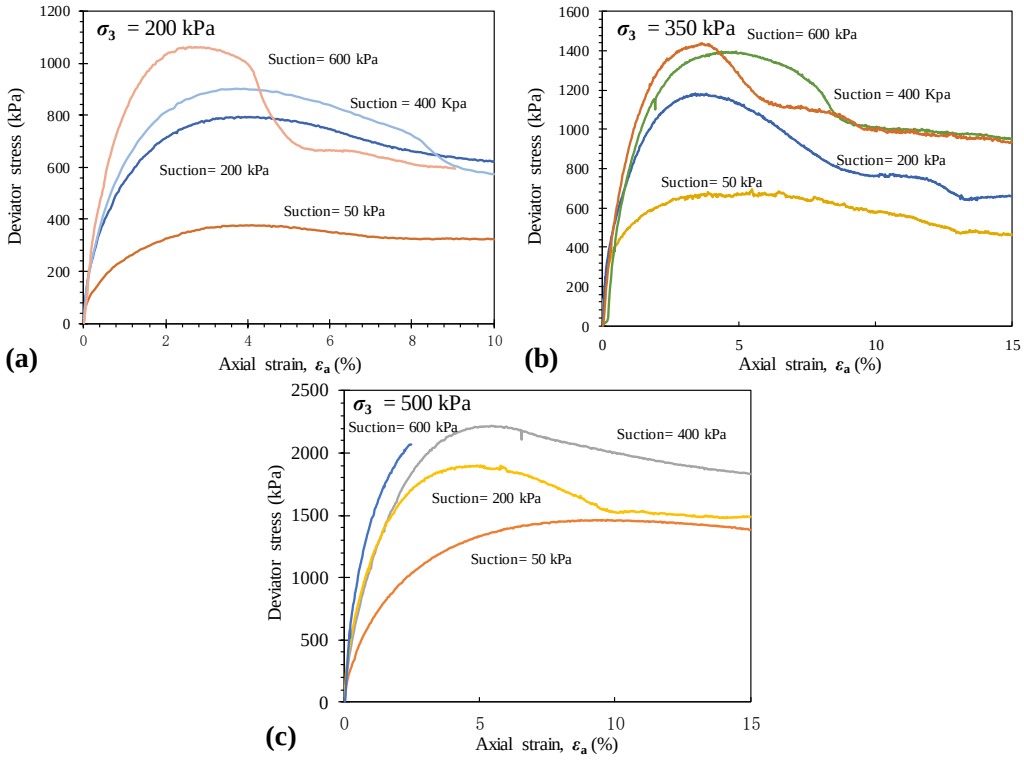

Figure 9. Stress-strain curves for compacted tailings, obtained by various suction level (a)confining pressure = 200 kPa; (b) confining pressure = 350 kPa; (c) confining pressure = 500 kPa

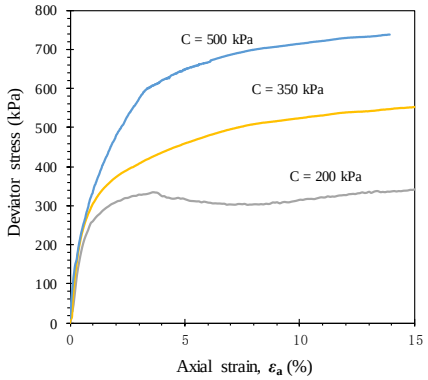

Figure 10. Stress-strain curves for compacted tailings at fully saturated condition obtained by various confining pressure.

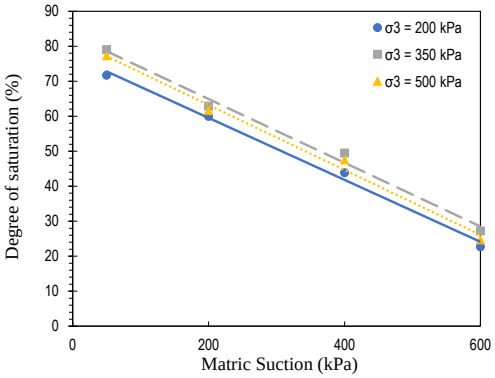

Figure 111. Variations of saturation condition against matric suction for the samples tested at various confining pressures.

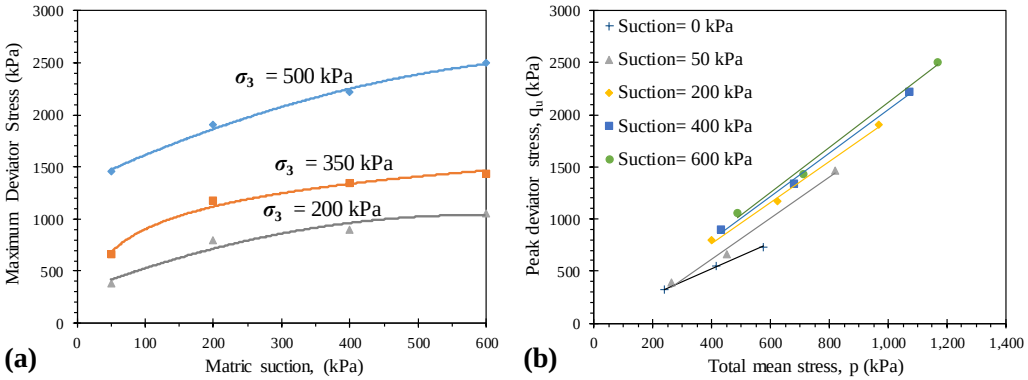

Figure 12. (a)Failure envelopes corresponding to different confining pressure, (b) Failure envelopes corresponding to different matric suction values